INVESTIGATION OF THE STRUCTURAL, OPTICAL AND ELECTRICAL PROPERTIES OF PLASMA POLYMERIZED N,N,3,5 TETRAMETHYLANILINE THIN FILMS

PhD Thesis

Hasina Akther

Bangladesh University of Engineering and Technology (BUET)
Dhaka-1000, Bangladesh.

June 2011

INVESTIGATION OF THE STRUCTURAL, OPTICAL AND ELECTRICAL PROPERTIES OF PLASMA POLYMERIZED N,N,3,5 TETRAMETHYLANILINE THIN FILMS

By
Hasina Akther
Roll: P 04041402 F
Session: April/2004

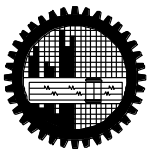

Department of Physics,
Bangladesh University of Engineering and Technology (BUET)
Dhaka 1000, Bangladesh.
June 2011

INVESTIGATION OF THE STRUCTURAL, OPTICAL AND ELECTRICAL PROPERTIES OF PLASMA POLYMERIZED N,N,3,5 TETRAMETHYLANILINE THIN FILMS

A dissertation submitted to the Department of Physics of Bangladesh University of Engineering and Technology in partial fulfillment of the requirements for the degree of DOCTOR OF PHILOSOPHY (Ph.D.) in Physics

by
Hasina Akther
Roll: P 04041402 F
Session: April/2004

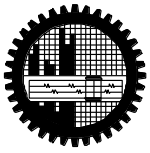

Department of Physics,
Bangladesh University of Engineering and Technology (BUET)
Dhaka 1000, Bangladesh.
June 2011

Declaration

It is hereby declared that this thesis or any part of it has not been submitted elsewhere for the award of any degree or diploma.

Signature of the candidate

_____

(Hasina Akther)

Dedicated

To

Contents

List of Figures

Chapter 4

List of Tables

Chapter 2

Chapter 4

Abbreviations and symbols used in this Thesis

ABS	Absorbance
ac	Alternating Current
Cr-Al	Chromel-Alumel
cc	Capacitively Coupled
d	Thickness
dc	Direct Current
DTA	Differential Thermal Analysis
EA	Elemental Analysis
F_L	Fermi Level
FTIR	Fourier Transform Infrared
I	Intensity of Radiation
IR	Infrared
J	Current Density
k	Boltzmann Constant
K	Extinction Co-efficient
LB	Langmuir-Blodgett
PECVD	Plasma Enhanced Chemical Vapour Deposition
PF	Poole Frenkel
PPDP	Plasma polymerized diphenyl
PPm-X	Plasma polymerized m-xylene
PPPANI	Plasma polymerized polyaniline
PPTMA	Plasma polymerized N,N,3,5 tetramethylaniline
PVD	Physical vapour deposition
PANI	Polyaniline
rf	Radio frequency
SCLC	Space charge limited conduction
σ_{ac}	ac electrical conductivity
SEM	Scanning electron microscopy
T_g	Glass transition temperature

T_m	Melting point
TMA	N,N,3,5 tetramethylaniline
TGA	Thermogravimetric analysis
TSDC	Thermally stimulated depolarization current
UV-Vis	Utraviolet-Visible
XPS	X-ray photoelectron spectroscopy
α	Absorption coefficient
λ	Wavelength
ΔE	Activation energy
σ	Electrical conductivity
ε'	Dielectric constant
$tan\partial$	Dielectric loss tangent
ε''	Dissipation factors
ε_o	Permittivity of free space
μ	Mobility of the charge carrier
θ	Trapping factor

Acknowledgements

I offer my heartiest gratitude and profound respect to my supervisor Professor Dr. Md. Abu Hashan Bhuiyan, Department of Physics, Bangladesh University of Engineering and Technology (BUET), Bangladesh for providing me the opportunity to work in such a dynamic field of research. I am indebted to him for his continuous guidance, suggestions, kind supervision of the research work and also for acquainting me with the world of advance research.

I am thankful to the Head, Department of Physics, Professor Dr. A. K. M. Akther Hossain, BUET for his keen interest and encouragement during my research work. The opportunity to work in the Department of Physics, BUET, was really a unique experience that was professionally and socially. I would also like to thank the members of the Doctoral Committee Professor Dr. M. Huq, Professor Dr. Jiban Podder, Professor Dr. Md. Feroz Alam Khan, and Professor Dr. Nazma Zaman of the Department of Physics, BUET and Professor Dr. A.B.M. Obaidul Islam of the Department of Physics, University of Dhaka for not only giving their valuable time but also for contributing to my technical knowledge and spirit during the progress of research work.

I am grateful to Prof. Dr. Md. Wahab Khan, Department of Chemistry, BUET for valuable discussion on various chemical reaction mechanisms and to help in drawing the chemical structures of the compounds used. I like to thank the Chairman, Department of Chemistry, University of Dhaka for allowing me to take the infrared spectra.

I am also thankful to Dr. M. A. Gafur, Senior Engineer, PP & PDC, Md Shahidul Islam, Chief Scientific Officer, Industrial Physics Division and the authority of the Bangladesh council for scientific and industrial research (BCSIR), Dhaka, for giving me the opportunity to do the elemental analysis, ultraviolet-visible spectroscopy differential thermal analysis and thermogravimetric analysis. I am thankful to Mr. S. Hossain Sarker of Semiconductor Technology Research Centre, University of Dhaka, for his help during modification of the polymerization system. I am grateful to all the persons in the faculty library and BUET

central reference library for providing me with the valuable journals and books during the work.

I would like to thank to Professor Dr. J.A. Syed, Department of Physics, Dhaka University of Engineering and Technology, Bangladesh, Professor Dr. R. Sumi, , Department of Crystalline Materials Science, Nagoya University, Japan and Professor Dr. S. Yagi, Department of Physical Science, Hiroshima University, Japan for doing X-ray photoelectron spectroscopy. Many thanks go to the thin films research group members of Department of Physics, BUET, past and present, for their advice, help and cooperation. I must appreciate the opportunity to learn and work in such a highly interactive, research environment. Mr. Sunirmal Mujumder, Mr. Masud Reza, Mr. Rama Bijoy Sarker, Dr. M.M. Kamal Ms. Rummana Matin, Ms. Tamanna Afroze, Md Jellur Rahman, Md. Ali Ashraf- thank you very much for making everyday unique and interesting along my research journey.

I am gratefully acknowledged the financial assistance during my Ph.D program by the authority of BUET. I am also thankful to the authority of Dutch Bangla-Bank for granting the Ph.D. fellowship and indebted to the authority of Bangladesh Jute Research Institute, Dhaka, for granting me study leave during the research work.

Profound gratitude to my mother, brothers, sisters, and my relatives for their cooperation and giving inspiration of this thesis work without which this work would not been possible. I am grateful to my husband, my sweet daughters and finally all praise to Almighty Allah for giving me strength and courage to complete the work.

Abstract

Plasma polymerized N, N, 3, 5 tetramethylaniline (PPTMA) thin films were deposited on to glass substrates at room temperature by a capacitively coupled parallel plate reactor. The structural and optical properties of as deposited, heat treated and iodine (I) doped PPTMA thin films of different thicknesses were characterized by scanning electron microscopy, elemental analysis (EA), infrared (IR) spectroscopy, X-ray photoelectron spectroscopy (XPS), and ultraviolet-visible (UV-Vis) spectroscopy. The surfaces of the PPTMA thin films were observed to be smooth and pinhole free. The energy dispersive x-ray observations indicate the presence of C, N, O in as deposited PPTMA and I doped PPTMA samples. The structural analyses by IR spectroscopy reveal that PPTMA thin films are formed with certain amount of conjugation, which modifies on heat treatment and iodine doping. The π–π^* transition in PPTMA thin film demonstrates the presence of an increased degree of conjugation in the resulting films. The XPS analyses show that C, N, and O are present on the surface of the PPTMA thin film and possible groups C-H, C=C, C-N, and C=O are found in the PPTMA structure. The atomic ratio N/C of the PPTMA thin film bulk and surface are found to be 0.12 and 0.20 by EA and XPS, respectively. Allowed direct transition (E_{qd}) and indirect transition (E_{qi}) energy gaps were determined from Tauc plots. The direct energy gap of as deposited PPTMA thin films is 2.8 eV and that of iodine doped PPTMA thin films is 2.6 eV. The change of energy gap indicates that there is a charge transfer complex arising between the host PPTMA and the iodine. It is observed that E_{qd} increases a little, E_{qi} decreases, on heat treatment of PPTMA.

The current density-voltage characteristics of as deposited PPTMA and iodine doped PPTMA thin films have been investigated at different temperatures. It is observed that space charge limited conduction is operative in the higher voltage region in iodine doped PPTMA thin films. From the experimental studies the carrier mobility, the free carrier density, and the total trap density of as deposited PPTMA are found to be about 1.3×10^{-13} $m^2 V^{-1}s^{-1}$, 2.0×10^{21} m^{-3} and 4.0×10^{30} m^{-3}, respectively and those of iodine doped PPTMA are about 1.5×10^{-12} $m^2 V^{-1}s^{-1}$, 3.7×10^{22} m^{-3} and 1.2×10^{27} m^{-3}, respectively . At lower temperatures, the available thermal energy is not sufficient to ionize the traps, so hopping mobility is

observed. While at higher temperatures, the higher values of activation energy indicate a transition from a hopping process to a distinct energy level process. The conductivity of iodine doped PPTMA thin film is higher than that of as deposited PPTMA thin film. The alternating current (ac) capacitance and electrical conductance of PPTMA thin films were measured as functions of frequency ($100 < f < 10^5$ Hz) and temperature ($300 < T < 450$ K). The ac electrical conductivity is more dependent on temperature in the low frequency region than that in the high frequency region. In PPTMA thin films the conduction may be dominated by hopping of carriers between the localized states at low temperatures and thermally excited at the high temperatures. The activation energies are estimated to be about 0.05 eV in the low temperature and 0.23 eV in the high temperature. Dielectric constant decreases with the increase of frequency but dielectric loss increases with increasing frequency with a minimum in the low frequency region. The temperature dependence of the Cole-Cole diagram shows the existence of distribution of dielectric relaxation times in the PPTMA thin films.

CHAPTER 1

Introduction

1.1 Introduction

The use of plasma polymerization for synthesis of novel thin film materials has become attractive and has been an active area of research in the recent past. Plasma polymerization is an efficient method for organic thin film deposition and surface modification. Thin Films of organic compounds have attracted a great deal of attention of the researchers for their applications such as in the fields of mechanics, electronics and optics etc. [1-2]. The plasma polymerization method is largely recommended because it enables the fabrication of very thin films and compounds that could not be obtained any other ways.

In a number of applications, both conductivity and transparency are required, for which metals, inorganic conductors and ion-conducting polymer can be used. In the strive for reduction in size, costs and weight of electronic equipment, the combination of polymeric properties and conductivity would be highly advantageous. This has long been recognized by the scientific and industrial community and has resulted in extensive research in this field. Due to often weak bonding between organic molecules in the solid state, they share many of the properties of both semiconductors and insulators, and hence their study has led to a deepening of fundamental understanding of the electronic and optical properties of polymers. Generally, thin polymer films can be formed in two ways: one is wet processing, such as the Langmuir-Blodgett (LB) film method, spin-coating, dip-coating and chemical vapor deposition (CVD). Although excellent results have been achieved this way, there are a number of problems that can arise such as pinholes, inclusion of solvents in different polymer layers, and contaminants. An alternative approach, which can avoid such difficulties, is plasma polymerization. This type of vapor deposition under vacuum provides a clean environment. It is solvent free and is well suited to sequential depositions [3-5].

Now a days, material preparation, processing and surface modification have become a prominent area of research in the development of science and technology. Among different kinds of polymerization techniques, plasma polymerization emerges as a most important technique for the preparation of organic thin films. In plasma polymerization the monomer is fragmented into reactive species, which subsequently recombine, forming a polymer. The advantages of plasma polymerization include; the environmental friendliness of the solvent-

free process; the deposition of ultra-thin films, pinhole-free films; the deposition of highly adherent films with substrate activation in the plasma environment; and the simplicity of the reactor [5-8]. Plasma polymerization has been dealt as an extension of polymerization from the academic view point and as a new technology to prepare thin films from a practical view point. The concept of plasma polymerization has been based on the application of polymers developed to the formation of organic material under plasma conditions. Plasma polymerization is an attractive technique, using which it is possible to modify the surface properties of a substrate, while retaining the transparency and bulk properties of the substrate materials. Furthermore, it is a solvent-free, fast and versatile process. In the thin film technology, plasma polymerization is accepted and is preferred owing to the desirable features of the thin films it yields, because the films produced in plasma have strong adhesion to the substrate surface [9-14].

In this thesis, preparation of plasma polymerized N,N,3,5 tetramethylaniline (PPTMA) thin films and study of structural, optical and electrical properties are described. The chemical structure of PPTMA observed to be little different than that of monomer keeping its aromatic ring structure. This film was found to be deficit in carbon and hydrogen and contained oxygen, which was not a part. The surfaces of PPTMA thin films were observed to be uniform, pinhole and fracture free. From the analyses, it was showed that C, N, and O were present on the surface of the thin film and possible groups C-H, C=C, C-N, C-O, and C=O were found in PPTMA structure. The current density-voltage (J-V) characteristics of as deposited PPTMA and iodine doped PPTMA thin film have been investigated. The conductivity of iodine doped PPTMA thin film is higher than that of as deposited PPTMA thin film. The space charge limited conduction is operative in the higher voltage region in iodine doped PPTMA thin films. The capacitance and ac electrical conductance of PPTMA thin films were measured as functions of frequency and temperature. Dielectric constant decreases with the increase of frequency and that decreases with the increase of temperature but dielectric loss increases with increasing frequency with a minimum in the low frequency region.

1.2 Review of Earlier Research Work

Glow discharge or plasma polymerization is widely used to prepare polymer thin films. The plasma polymerization as a plasma assisted deposition process is a well-known and efficient

method to produce organic thin films and offers good control over the film properties. The term plasma polymerization should not be limited to the formation of organic materials but should cover a wider area that includes metallic or inorganic elements. Thus plasma polymerization is gaining recognition as an important process for the formation of entirely new kinds of materials. The recent development of science and technology of thin films of organic compounds produced through plasma polymerization has drawn much attention of the scientists to investigate their various properties. In these developments, the concept of plasma polymerization has been based on the application of polymers developed to the formation of organic material under plasma conditions. Then the process has attracted the attention of scientists and engineers in different disciplines as an exotic method of polymerization. Today plasma polymerization is based on the molecular processes by which the size of molecules increases. The arrangement of the atoms that constitute the molecules of a monomer is accomplished during the organic synthesis of the monomer.

Polyaniline prepared from aniline, an amine aromatic, shows interesting combination of properties that make them very attractive. It seems to be a promising material, which exhibits a good electrical behavior and good environmental stability [15]. The optical and electrical characterization of plasma polymerized pyrrole (PPPy) films in the presence and absence of iodine were carried out by Kumar et al. [16]. From the current-voltage characteristics of the two types of polymer films they found that the conductivity of the doped PPPy was approximately two times greater than that of the undoped one. It was observed that the optical band gap energies of the undoped and iodine-doped PPPy film were 1.3 and 0.8 eV respectively. A comparison of the Infrared (IR) spectra of the two types of films revealed that almost the same bonds were present in both cases. These results suggest that iodine was not bonded in any manner to the polymer chain of PPPy due to the doping. The Scanning electron microscopy (SEM) photograph of the iodine-doped films shows that its surface is smoother with iodine resulting in an increase in the conductivity of the films. A detailed analysis of the conduction mechanism showed that the conduction mechanism in the undoped PPPy film is a schottky type mechanism.

Bhadra et al. [17] reviewed the synthesis, processing and applications of polyaniline (PANI). These paper provided of the different methods used for the synthesis of PANI along with a number of special methods used to obtain a nano structured PANI. They observed PANI can

be applied in different areas such as electrical, electronic, thermoelectric, electrochemical, electromagnetic, electromechanical, electro-luminescence, electrorheological, chemical, membrane, sensors, and so on because of its some special properties such as conductive in nature, the increase of viscosity in solution when under an electric field, its change in electrical conductivity or color when exposed to acidic, basic and some neutral vapors or liquids, its easy variation of oxidation states, very high capacitance values, volume changes at different oxidation state and its ability to emit color under various excitation.

Sajeev et al. [18] investigated the pristine and iodine doped PANI thin films prepared by radio frequency (rf) and ac plasma polymerization techniques separately for the comparison of their optical and electrical properties. Doping of iodine was done in situ. Analysis of the Fourier transform infrared (FTIR) spectra of monomer aniline and PANI prepared under ac and rf conditions indicate the presence of aromatic ring stretching (1600 cm^{-1}) and C-C stretched vibration (1500 cm^{-1}) even after polymerization. A quick comparison between the spectra of ac and rf thin films exhibit marked structural difference between the polymers evolved by both polymerization routs. They have observed that the optical band gap of the polyaniline thin films prepared by rf and ac plasma polymerization techniques differ considerably and the band gap is further reduced by in situ doping of iodine. The electrical conductivity measurements on this films show a higher value of electrical conductivity in the case of rf plasma polymerized thin films when compared to the ac plasma polymerized films. They have also found that the iodine doping enhanced conductivity of the polymer thin films considerably. This increase in conductivity can be attributed to the evolution of conjugated structure during rf plasma polymerization due to benzene ring opening in the presence of iodine. Typically the mechanism of conduction observed in these films is space charge limited conduction (SCLC). They reported that PANI is generally considered as a p-type conductor. The iodine like electron acceptor dopant reduces the binding energy of the polymer. This reduction of binding energy results in an enhanced mobility of the carriers and the conductivity is enhanced further.

Elashmawi et al. [19] studied polyvinyldene fluoride (PVDF) and different concentrations of iodine were prepared by casting method using dimethyl sulfoxide as a common solvent. Their crystalline structure, optical and dielectric properties were examined. Ultraviolet-visible (UV-Vis) spectra revealed that the PVDF films filled with iodine show new broad bands at 286 and

353 nm which are attributed to the formation of charge transfer complex. The conductivity of the new composites is lower at lower frequency and showed higher conductivity at higher frequencies. The high values of dielectric constant may be due to the interfacial effects with in the bulk of the sample and electrode effects.

Chowdhury et al. [20] studied on the chemical analysis of the plasma-polymerized diphenyl (PPDP) thin films. The PPDP films were characterized by SEM, elemental analysis (EA), IR spectroscopy, Auger electron microscopy (AES) and X-ray photoelectron spectroscopy (XPS). The SEM micrograph shows that there are clear grain boundaries of irregular shapes and the surface morphology of the PPDP film is observed to be and pinhole and fracture free. The elemental analysis reveals that PPDP film is mainly composed carbon, hydrogen and oxygen atoms with a small amount of nitrogen atom. It is observed that carbon and hydrogen replacements occur with the inclusion of oxygen and nitrogen. The IR analysis reveals that the structure of PPDP thin film is different from that of the monomer diphenyl. From the AES and XPS investigations, it is observed that plasma polymer of diphenyl prepared by glow discharge technique is elementally different from the monomer and is seen that there is no significant variation in the concentration of carbon, oxygen and nitrogen calculated from XPS and AES spectra. It is found that the surface and bulk atomic concentrations of the constituent elements are not identical. The bulk atomic concentration determined from elemental analysis is different in comparison to that obtained by XPS and AES analyses of the film surface.

Nakamura et al. [21] prepared thin films from cobalt tetraphenylporphyin (CoTPP) by plasma polymerization at different rf power ranging from 10 to 100W. They observed that the plasma polymerized CoTPP thin films has cross- linked structure in which the original structure porphyin in CoTPP was retained to some extent depending on the rf power. Then the chemical structure of the vacuum deposited and plasma polymerized thin film have been analyzed by Uv-vis, XPS, Atomic force microscopy (AFM) and their hardness, adhesive force to a glass substrate and current–voltage characteristics were measured. Investigation of a sandwich type device of Au/ CoTPP/ ITO (Indium Tin Oxide) glass revealed that the plasma polymerized CoTPP thin film has p–type semi-conducting characteristics.

Bazaka and Jacob [22] studied and examined the fabrication and characterization of polymer thin films from non-synthetic Terpinen-4-ol monomer using radio frequency plasma polymerization. The optical properties, thickness and roughness of the thin films were studied

in the wavelength range 200–1000 nm using ellipsometry. The polymer thin films of thickness from 100 nm to 1000 nm were fabricated and the films exhibited smooth and defect-free surfaces. The energy gap was estimated to be 2.67 eV, the value falling into the semiconducting region. The obtained optical and surface properties of Terpinen-4-ol based films substantiate their candidacy as a promising low-cost material with potential applications in electronics, optics, and biomedical industries.

Bae et al.[23] deposited plasma polymerized organic thin films on Si and glass substrates by plasma-enhanced chemical vapor deposition (PECVD) method using methylcyclohexane and ethyl-cyclohexane as organic precursors. The optical properties of the polymerized thin films were investigated by FTIR and UV-Vis spectroscopy. It was observed that as the plasma power was increased, the main IR absorption peak intensity of thin films was increased while the transmittance of the UV-Vis spectra was decreased. The later result suggests that with increasing RF power, high degree cross-linking density of the electrons could be overlapped, resulting in formation of more stable polymers. The increase of absorption peak intensity with increasing the rf power can be explained with either the increase of carbon contents or the scattered reflection caused by plasma bombardment. The optical band gap of the films also has a decreasing tendency with increasing rf power. Thus the above review studies it is observed that among many methods of depositing thin films of organic compounds plasma polymerization can be considered as an attractive one for the formation of new kinds of material. Thin films prepared by plasma polymerization technique have extensive application as chemical, physical, and biological sensors, microelectronic devices, nonlinear optical devices, etc. Therefore high quality polymer thin films should be developed for a variety of industrial applications.

Bhuiyan et al. [24] described the XPS observations on plasma-polymerized acrylonitrile (PPAN) thin films and PPAN films pyrolysed at 573 and 773 K. The C (Carbon) 1s, N (Nitrogen) 1s and O (Oxygen)1s spectra of as deposited PPAN indicated that PPAN films are cross-linked and pyrolysis caused extensive unsaturation and inclusion of O in PPAN structure. The angle –resolved XPS reveals that PPAN thin film may be a two-layer system i.e. the surface of the film may have slightly different composition than that of the bulk.

Mitu et al. [25] deposited parylene-like thin films of di-para-xylylene by plasma decomposition instead of conventional thermal decomposition. Growth rates within the range

4-250 nm/min were achieved with plasma polymerization, comparing favorably with the low deposition rates of 5-10 nm min^{-1} for the conventional CVD process. Depending on the rf power and precursor mass flow values, thin films with various morphology and composition were obtained, ranging from rough semi-crystalline to smooth amorphous and from polymer-like to hydrogenated carbon-like films. The electrical properties of the thin films studied by means of dielectric spectroscopy and charge stability measurements correlated to structural properties of the films. Films deposited under low applied power/ mass flow rate conditions showed good charge stability, making plasma deposited films interesting for electrostatic micro-electromechanical systems applications.

Xiao Hu et al. [26] prepared plasma polymerized 4-cyanopyridine (PPCPD) thin films of desired thickness through plama polymerization under different glow discharge conditions. The effect of the discharge power on this film was investigated by FTIR, UV-Vis and XPS measurements. A high retention of aromatic ring structure of the starting monomer in the deposited plasma films was obtained when a low discharge power was used. A red shift in the maximum absorption wavelength for the films was observed as compared with the monomer absorption spectrum. The AFM showed that the PPCPD film with quite smooth surface could be grown under a relatively low discharge power.

Tamirisa et al. [27] synthesized polyaniline thin films on several substrates position at various distance from the center of the coil of an inductively coupled pulsed-plasma reactor. FTIR spectroscopy results revealed that the chemical composition and structure of the films were very dependent on the substrate's position with respect to the rf coil. SEM studies indicated that as the films became thicker they developed nodules at somewhat smoother under layer. The impendence measurements were consistent with relatively rough films possibly containing pinholes.

Zhao et al. [28] studied a novel conjugated polymer, poly 4-biphenylcarbonitrile (PBPCN) thin film using a plasma polymerization technique and investigated the effect of the discharge power on the chemical structure and surface compositions using FTIR spectroscopy, UV-Vis spectroscopies, and XPS. The results showed that a large π conjugation system can be formed in the PBPCN thin films at low plasma discharge power of 30 W, and the plasma polymerization of PBPCN monomer took place mainly through the opening of the π bonds of

the C≡N functional groups. A high discharge power of 50 W brought about more severe molecular (aromatic ring) fragmentation and thus the conjugation length of PBPCN films decreases due to the formation of non-conjugated polymer.

Hosono et al. [29] reported the effect of the discharge conditions on the structure and electrical conductivity of the PPPy films. Comparative studies of the IR, EA and UV-Vis observations showed that some pyrrole rings were remained in the PPPy films prepared with 10 and 20 W discharge power, whereas almost all the pyrrole rings were cleaved in the PPPy films prepared with 50 and 100 W discharge power. Silverstein et al. [30] investigated on the synthesis, the dependence of molecular structure and properties on the polymerization conditions of plasma polymerized thiophene (PPTh). They found that the transparent polymerized thiophene films depend on the carrier gas used (if any) and on the plasma power.

Valaski et al. [31] investigated on the influence of electrode material and film thickness on charge transport properties of electrodeposited polypyrrole (PPy) thin films. They found that the film morphology, roughness and electrical conductivity are strongly influenced by the choice of substrate and the choice of electrode materials played a quite important role in specifying the resistivity as well as the conductivity. The selection of metals with high work function values imposes an increase in the mobility and the positive free carrier concentration of semiconductor at thermodynamic equilibrium and consequently, in its electrical conductivity. They also observed that the films with different electrode materials show different properties. Au/PPy/Al configuration showed only ohmic conduction behavior; on the other hand, TO/PPy/Ni and Au/PPy/Al configuration showed ohmic behavior in the lower voltage region but SCL conduction mechanism in higher voltages. In the study on the influence of the film thickness on the conductivity, they found that different conduction mechanisms were shown by the films of different thickness. When PPy film thickness was increased (~above 300 nm) the charge transport tends to be space charge limited, but for smaller thickness ($d \leq 300$ nm) of the films, the charge transport was limited by thermoionic emission. The charge mobility was also found to be increased for the smaller thickness. It was also reported that the film morphology was highly thickness dependent. The morphology was found to be better (lower roughness) for smaller thickness.

Luo et al. [32] investigated on the plasma polymerization of styrene with carbondioxide under glow discharge conditions. Polystyrene thin films have been successfully prepared by

plasma polymerization technique by using carbondioxide, as carrier gas and styrene vapor, as monomer. The structure and composition of the plasma polymerized films were characterized by XPS, FTIR and compared with the film prepared by conventional thermal polymerization. The morphology information of the films was recorded by optical microscopy. XPS and FTIR results reveal that chemical composition of the plasma polymerized films is different from that of the thermal polymerized films and that oxygen content of in the plasma polymerized films increases with the flow rate of CO_2. XPS analysis further confirms that the content of these oxygen-containing groups increases with CO_2 flow rate.

The plasma polymerized tetraethylorthosilicate (PPTEOS) thin films were deposited by Zaman and Bhuiyan [33] on to glass substrates at room temperature by a parallel plate capacitively coupled glow discharge reactor. The J-V characteristics of PPTEOS thin films of different thickness have been studied at different temperatures in the voltage region from 0.2 to 15 V. In the J-V curves two slopes were observed, one in the lower voltage region and another in the higher voltage region. The voltage dependence of current density at the higher voltage region indicates that the mechanism of conduction in PPTEOS thin films is space charge limited conduction. The carrier mobility, the free carrier density and the total trap density were calculated from the observed data. The activation energies are estimated to be about (0.13 ± 0.05) and (0.46 ± 0.07) eV in the lower and higher temperature regions respectively for an applied voltage of 2 V and (0.09 ± 0.03) and (0.43 ± 0.10) eV in the lower and higher temperature regions respectively for an applied voltage of 14 V. The conduction in PPTEOS may be dominated by hopping of carriers between the localized states at the low temperature and thermally excited carriers from energy levels within the band gap in the vicinity of high temperature.

The preparation and characterization of ac PPPy thin films has been studied by Joseph John et al. [34]. The electrical conductivity studies of the aluminium/ polymer/ aluminium structure have been carried out and SCLC mechanism is identified as the most probable conduction mechanism in those polymer films. The electrical conductivity showed an enhanced value in the iodine doped sample. The reduction of optical band gap by iodine doping is correlated with observed conductivity results.

Sajeev et al. [35] studied on the carrier transport mechanism of polyaniline (PA) thin films prepared by rf plasma polymerization. The mechanism of electrical conduction and carrier

mobility of PA thin films for different temperatures were examined using the Al-PA-Al structure. It was found that the mechanism of carrier transport in these films was space charge limited conduction. The J-V studies on an asymmetric electrode configuration using indium tin oxide (ITO) as the base electrode and Al as the upper electrode (ITO-PA-Al structure) showed a diode-like behavior with a considerable rectification ratio.

Kumar et al. [36] worked on PPPy in the presence and absence of iodine, and characterized it's optical and electrical properties. They studied of IR and SEM revealed that iodine was not bonded in any manner to the polymer chain of PPPy but that it made the surface morphology of the PPPy film smoother. An analysis of the electronic spectra gave band gap energies of 1.3 and 0.8 eV for the undoped and doped PPPy films respectively. The current-voltage characteristics of the two types of polymer films revealed that the conductivity of the doped PPPy film was approximately two times greater than that of the undoped one.

Hegemann and Schutz [37] determines the activation energy in the active plasma zone to obtain stable, functional coatings, especially, asymmetrical radio frequency discharges enable a high conversion of monomer flow into film deposition. They compared the unconfined asymmetrical set up to a symmetrical reactor with confined geometry supporting the described concept for the up-scaling of plasma processes.

Mathai et al. [38] prepared PANI thin films of different thickness by ac plasma polymerization technique. The study of asymmetric electrode configuration showed that barrier heights play a significant role in the conduction process. An activated process with activation energy decreased from 0.73 to 0.65 eV as the bias voltage increased. From their observations, they inferred that electrode limited Schottky-type conduction was dominant in plasma polymerized PANI thin films.

Bae et al. [39] deposited organic polymer thin films onto glass and Si (100) substrates at room temperature by plasma-enhanced CVD (PECVD) method. They compared the surface and optical properties of plasma polymerized organic thin films prepared at various rf power. They found that the contact angle, refractive index, and the intensity of the main absorption peak of thin films were increased as the plasma power increased, while the optical transmittance was decreased, signifying that the plasma polymerized organic films have lower surface energy with increasing rf power.

Many researchers have devoted in studying the direct current (dc) electrical conduction mechanisms in various plasma–polymerized organic compounds. Shah Jalal et al. [40] studied dc electric conduction mechanism in plasma polymerized m-xylene (PPm-X) thin films. They found (Poole–Frenkel) PF mechanism to be operative in PPm-X thin films. Measurements of the temperature dependence of ohmic and SCLC currents on thin films of polycrystalline particles of B-magnesium phthalocyanine (MgPc) dispersed in a polymer binder in Schottky junction cells have been carried out by Riad et al. [41]. The square power dependence in SCLC indicated that current conduction was limited by a discrete trapping level above the valence band edge. They also determined that the conduction process was Schottky emission in the lower voltage range and the PF effect for higher voltage levels.

Silva and Amaratunga [42] characterized diamond-like carbon thin films using the SCLC under electron and hole injection. They showed that the mid gap states were similar to those in a-Si:H with a large dangling-bond density. Pradhan Dilip et al. [43] studied the effect of plasicizer (PEG_{200}) on dielectric and electrical properties of plasticized polymer nanocomposite electrolytes. They reported that at low frequency, the variation of relative dielectric constant with frequency shows the presence of material electrode interface polarization processes. The loss tangent peaks appearing at a characteristic frequency suggest the presence of relaxing dipoles in all the samples. The frequency dependence of ac conductivity follows the universal power law with a small deviation in the low frequency region due to the electrode polarization effect. The conductivity increases with increase in plasticizer concentration. Analysis of electrical modulus and dielectric permittivity functions suggest that ionic and polymer segmental motions are strongly coupled.

Gong et al. [44] synthesized PANI thin films of various chemical compositions by rf plasma-polymerization technique and they showed a correlation between the C/N ratio and their different properties. The plasma-polyaniline films have been characterized by UV-Vis spectroscopy, FTIR spectroscopy, electron spin resonance, XPS, SEM and contact angle measurements, which indicated that the contents of quinoid sequences and aliphatic cross linking moieties increase with increasing plasma power input and discharge duration.

The electrical conductivity, activation energy and morphology of polythiophene synthesized by rf resistive plasmas were studied by Olayo et al. [45]. It was reported that the continuous collisions of particles in the plasma had induced the polymerization of thiophene but also

broke some of the monomer molecules producing complex polymers with thiophene rings and aliphatic hydrocarbon segments. These multidirectional chemical reactions were more marked at longer reaction times in which the morphology of the polymers evolved from smooth surfaces, at low exposure time, to spherical particles with diameter in the 300-1000 nm interval. Between both morphologies, some bubbles were observed to be formed on the surface. The intrinsic conductivity of plasma polymers of thiophene synthesized in this way varied in the range of 10^{-10} to 10^{-8} S/m. However, the conductivity resulted very sensitive to the water content in the polymers, which produced variations of up to 5 magnitude orders. The activation energy of the intrinsic conductivity was between 0.56 and 1.41 eV, increasing with the reaction time.

Semiconductor-like thin films were grown using metallic phthalocyanines (MPc) (M=Fe, Pb, Co) and 1,8 dihydroxiantraquinone by Sanchez et al. [46]. The effect of temperature on conductivity was measured of the films and it was found that the temperature-dependent electric current in all cases showed a semiconductor behavior with conductivities in the order of $10^{-6}\Omega^{-1}cm^{-1}$. The calculated optical band gap values of these materials as well as the magnitude of their electrical conductivities of the thin films suggest the possibility of considering them for use in the preparation of electronic devices.

Pandey et al. [47] fabricated Schottky device by thermal evaporation of indium on chemically synthesized polyaniline, poly(o-anisidine), and poly(aniline-co-orthoanisidine) co-polymer. They performed electrical characterization of each of these devices using current (I)-voltage (V) and capacitance (C)- voltage(V) measurements. Good rectification (0.6 V) was found in the case of In/Poly (aniline-co-o-anisidine) junction.

Ram et al. [48] studied aluminium-polyaniline-aluminium(Al-PANI-Al) capacitor configurations and found that the moment of charge carriers under the influence of an electric field gives rise to the space charge phenomenon, leading to the interfacial polarization. The relaxation phenomenon seen in this configuration has been attributed to the damping of dipole oscillators originating due to the application of external electric field. The increase in the value of mobility both with increasing temperature and thickness observed in the case of Al-PANI-Al configuration support the formation of space charge in doped polyaniline.

Yamada et al. [49] investigated poly (vinylsulfonic acid) chains having cation-exchangeable groups introduced onto a surface of polyaniline film by means of plasma-graft polymerization. The redox reaction mechanism of the plasma grafted polyaniline film has been examined with a combination of electrochemical and microgravimetric techniques. The development of the graft layer of which the thickness was uniformed by increased polymerization time. Plasma-grafting has effective on cation migration which take place in order to maintain electrioneutrality of the polyanline film during redox process in the electrolyte.

Valaski et al. [50] reported their investigation of charge transport properties of thin electrodeposited polypyrrole (PPy) films. The positive charge carrier mobility was estimated and demonstrated that its value was higher for thinner films. Yamada et. al. [51] investigated poly(vinylsulfonic acid) chains having cation-exchangeable groups introduced onto a surface of polyaniline film by means of plasma-graft polymerization. The redox reaction mechanism of the plasma grafted polyaniline film has been examined with a combination of electrochemical and microgravimetric techniques. The development of the graft layer of which the thickness was ununiformed was realized by increased polymerization time. Plasma-grafting has effective on cation migration which take place in order to maintain electrioneutrality of the polyanline film during redox process in the electrolyte.

The dc and ac electrical properties were investigated for thermally evaporated ZnPc thin films with aluminium(Al)/gold electrical contacts by Saleh et al. [52]. The current density-voltage (J-V) measurements at room temperature indicated that an ohmic conduction was dominant at lower applied voltages, while at higher applied voltages a space charge limited conduction (SCLC) was observed. Bhuiyan and Bhoraskar [53] studied the electrical, optical and ESR measurements of plasma polymerized acrylonitrile thin film. The electrical resistivity and optical band gap show a drastic decrease as a result of these structural changes. They found that the electrical conduction in the thin film and pyrolysed film is dominated by the hopping mechanism resulting from the thermally activated charge carriers having low mobility.

An electrical study of aging of conductivity of polyaniline-polystyrene (PANI-PSt) blend has been demonstrated by Jousseaume et al. [54]. Their study showed that the electrical

conductivity decreased with time following a first order or a non first order kinetic depending principally on the nature of the dopant.

Han et al. [55] analyzed the dielectric spectra of PANI salt films by changing the dopants and film-formation methods. In the film-doping method the increase in dopant size resulted in subsequent displacement of the dielectric relaxation peak toward lower frequency which was found to be the result of an increased inter-chain distance on the PANI surface leading to lower carrier hopping.

The ac measurements on organic materials have been used to understand conduction process in these materials in the presence of ac electric field. Dielectric relaxation studies are important to understand the nature and the origin of dielectric losses, which in turn may be useful in the determination of electronic structure in solids. Dielectric constant (ε') and dielectric loss of N-P-nitroaniline thin films were studied by El-Nahass et al. [56] and found that both these parameters were decreased with increasing frequency while increased with increasing temperature. They also reported the estimated values of the maximum barrier height. These values were in good agreement with the theory of hopping of charge carriers over a potential barrier between charge defect states. Saravanan et al. [57] studied plasma polymerized aniline and found low dielectric constant values, which were stable over a wide range of frequencies. Dielectric constant and ac conductivity were measured in the frequency range 100 Hz-1 MHz and in the temperature range 300-373 K. It has been observed that capacitance and dielectric loss decrease with increase of frequency and increase with increase of temperature. The ac conductivity increases with increase in temperature and frequency. The conductivity increases rapidly at higher frequencies rather than at the lower frequencies. The variation of ac conductivity with temperature as a function of different frequencies is also studied and activation energies were calculated and are found to be in the range 0.366-0.1435 eV, which is very low. The low activation energies of these films indicate that a hopping conduction mechanism occurs in rf plasma-polymerized aniline thin films. The IR spectrum shows that the peaks in the plasma-polymerized aniline are not sharp when compared with the monomer aniline and most of the IR absorption features of the monomer aniline are noticeable in the spectrum of polyaniline with the shift in wave numbers. IR studies also reveal that the aromatic ring is retained in the polyaniline, thereby increasing the thermal stability.

The dielectric properties from a set of molybdenum (Mo) containing diamond like carbon (DLC) films deposited using electron cyclotron resonance chemical vapor deposition (ECR-CVD) were investigated by Huang et al [58]. It is shown that the film permittivity can be greatly increased by the introduction of Mo. There is a drastic reduction in the permittivity at frequencies of up to 10 kHz. The ac conductivity exhibits three characteristic regions in the frequency range investigated: constant, liner and super liner regions. The high ε'' and tanδ at low frequencies resulted from the high dc conductivity of the films. The relaxation polarizations in the film are responsible for the peaks of ε'' and tanδ. For the film with high Mo content, the permittivity is frequency dependent at low temperature. However, for the high frequency of 1 MHz, the film permittivity is weakly Mo dependent at the temperature below 145 K. The relaxation time was observed to decrease with increasing Mo content in the films at room temperature. The effect of voltage on the permittivity of the films is insignificant at frequencies above 10 kHz. Finally, it was concluded that the films have a potential application in microwave devices.

Zhao et al. [59] studied plasma polymerized 1- cyanoisoquinoline (PPCIQ) thin film of desired thickness was prepared by plasma polymerization under different glow discharge conditions. The effect of discharge power on the chemical structure, surface composition and morphology of the PPCIQ thin films were investigated by FTIR, XPS, Atomic force microscopy (AFM) and deposition rate measurements. A high retention of the aromatic ring structure of the starting monomer in the deposited plasma films is obtained at a low discharge power. The dielectric measurement shows that a low dielectric constant of 2.62 has been obtained for the PPCIQ thin films for the first time.

Dielectric properties of poly (butylenes succinate) crystalline under different conditions have been reported in the temperature range of 163-383 K and in the frequency range of 0.01-105 Hz by Tai [60]. Both the dipolar α and β processes have been identified at low temperatures; the α process is associated with the amorphous fraction while the β with the relaxations in both the amorphous and crystalline fractions. The space charge effect dominates the high temperature dielectric spectra. These spectra have been analyzed in the light of an equivalent circuit model. The Maxwell-Wagner-Sillars polarization, electrode polarization and free charge motion are well resolved.

It has been reported by various researchers [15, 17, 35, 48] that polyaniline, an amine aromatic $C_6H_5(NH_2)$ as shown in Fig 1.1(a), is a useful and interesting material in its bulk and thin film form for many applications in electrical, electronic, optical, etc. devices. Ab initio quantum mechanical investigations have been carried out by Mhin and Park [15] to examine the effects of constituents on structural deformations and electronic properties. Using a superposition approximation, they obtained good structural parameter to describe the electrical properties of push-pull para-disubstituted benzene derivatives. The amount of charge transfer and the length of the path were important parameters explaining the behavior of the electronic properties and these two structural parameters have no relationship. They also predicted that the substitution of electron donor groups like $-N(CH_3)_2$ in aniline might effect the electronic property.

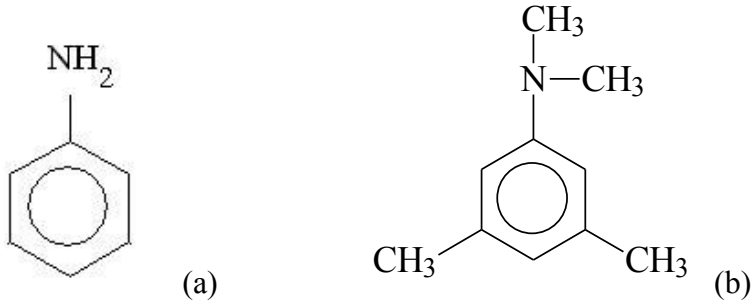

Fig 1.1 The structure of (a) polyaniline and (b) N,N,3,5 tetramethylaniline

In such case it is proposed to investigate experimentally the optical, electrical, etc. properties of plasma polymerized N,N,3,5 tetramethylaniline (TMA) thin films. From these points of view, TMA is selected as a monomer for the preparation of thin film by plasma polymerization technique and to study its structural, optical and electrical properties.

1.3 Objectives of the Thesis

The advantageous and typical characteristics make the plasma polymerized thin films to be utilized in various disciplines such as, in dielectrics, in electronics, optical, biomedical devices, etc. TMA, may emerge as a promising material because it contains aniline and the substitution of electron donor groups in those thin films of TMA might effect the optical and electrical properties. This work is aimed at preparing thin films of TMA by plasma polymerization technique. Then the structural, optical and electrical properties of the as-deposited and modified PPTMA thin films are investigated as follows.

(a) **Film Characterization**: The structural information and identification of functional groups and surface morphology of as deposited and heat treated PPTMA thin films are investigated.

(b) **Thermal Analysis**: Thermal decomposition and stability of PPTMA thin films are studied.

(c) **Optical properties**: The optical energy gaps and the allowed direct transitions, and allowed indirect transitions and forbidden transitions of PPTMA thin films are determined from the UV-Visible spectroscopic study.

(d) **Electrical properties**:

(i) Direct Current measurements: The current density- voltage (J-V) and thermally activated current is measured for metal/thin film/metal sandwiched structure samples of different thicknesses as a function of temperature. The carrier mobility, the free carrier density, and the total trap density are calculated in PPTMA thin films from these data. The dc electrical investigation is felicitate to understand the electrical conduction mechanism and thermally activated conduction mechanism in PPTMA.

(ii) Alternating Current measurements: The ac electrical conductivity, dielectric constant and loss tangent of PPTMA will be determined at different temperature as a function of frequency. The results obtained from the ac electrical investigation will be analyzed with the existing theories to elucidate the relaxation behavior and dielectric loss mechanism in these materials.

The results observed in electrical investigations in conjunction with the structural, thermal and optical analyses may help understanding the reasons for the change of the optical and electrical properties due to modification of PPTMA by heat treatment and iodine doping. This understanding may indicate some suitable application of these materials.

1.4 Thesis Layout

Organization of this thesis is divided into five chapters.

Chapter 1 gives general introduction followed by a review of earlier research work, the objectives of the study and the thesis layout.

Chapter 2 illustrates briefly polymers and their general properties, different polymerization processes, overview of gas discharge plasma, plasma polymerization mechanism, application

of plasma polymerized organic thin films. Theories on EA, IR, SEM, XPS, DTA/TGA , UV-Visible, electrical properties are focused at the end of the chapter.

The experimental techniques are briefly explained in chapter 3 along with description of the plasma polymerization set up, generation of glow discharge, deposition parameters, film thickness measurements, sample formation etc. The monomer, substrate materials and its cleaning process are also described here. The experimental procedure on EA, IR, SEM, DTA/TGA, UV-Visible, electrical formation and electrode deposition of PPTMA thin films are also described in this chapter.

Chapter 4 begins with results of elemental analysis followed by IR, SEM, XPS, DTA/TGA spectroscopy. The details of UV-Vis absorption measurement and calculated values of direct and indirect transition energy gaps are discussed at the end of the chapter and lastly a brief account of the existing theories on dc and ac conduction mechanism followed by the current voltage measurements and temperature dependence of current, the analyses of J-V characteristics and temperature dependence of current data.

Chapter 5 is arranged with conclusions and suggestions for future work. And finally the thesis is folded up with references and Appendix at the end.

CHAPTER 2

Theories on characterization Techniques and Electrical properties

2.1 Introduction

A literature survey on polymers and their general properties, different polymerization processes is presented in this chapter. The details of plasma, overview of polymer, plasma polymerization, different types of glow discharge reactors, plasma polymerization mechanism of plasma polymerized thin films are illustrated in this chapter. Application of plasma polymerized organic thin films is focused in the chapter. Description of the theory of different techniques is described in this chapter.

2.2 An Overview of Polymers

2.2.1 Polymer

A polymer is a material whose molecules contain a very large number of atoms linked by covalent bonds, which makes polymers macromolecules. Polymers consist mainly of identical or similar units joined together. The unit forming the repetitive pattern is called a "mer" or "monomer. In some cases the repetition is linear, such as a chain is built up from its links and in other cases the chains are branched or interconnected to form a three dimensional network. The repeat unit of the polymer is usually equivalent or nearly equivalent to the monomer, or starting material from which the polymer is formed. The length of the polymer chain is specified by the number of repeat units in the chain, which is known as the degree of polymerization. Polymers are thought to be colloidal substance i.e. glue-like materials. From chemical point, the colloidal substances are in fact large molecules and that their behavior could be explained interns of the size of the individual molecules. Polymer materials, some of which are naturally occurring are in use from historical time, some are new and of recent products.

Usually the biggest differences in polymer properties result from how the atoms and chains are linked together in space. Polymers that have a 1-D structure will have different properties than those that have either a 2-D or 3-D structure.

One-dimensional Polymers

One dimensional polymer is most common. They can occur whenever reacting two chains join to make a chain. If the long-chains pack regularly, side-by-side, they tend to form crystalline polymers. If the long chain molecules are irregularly tangled, the polymer is amorphous since there is no long range order. Sometimes this type of polymer is called glassy.

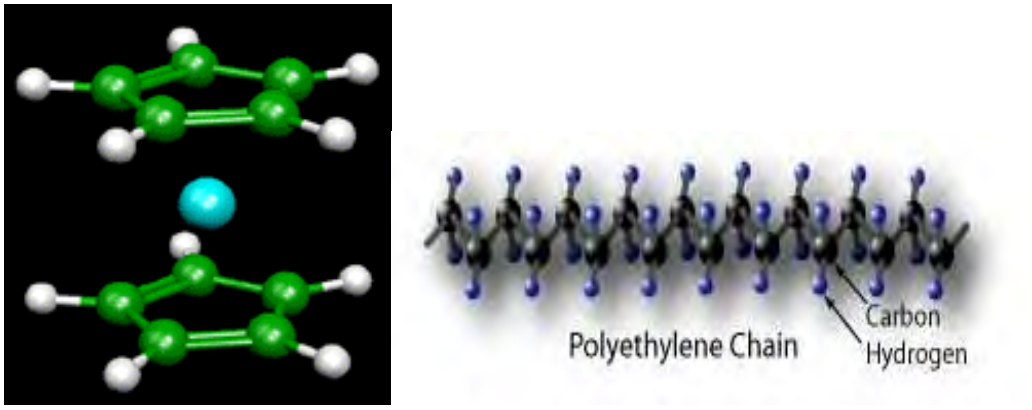

Fig 2.1 Structure of polymer and polyethylene chain.

Two-dimensional Polymers

Two dimensional polymers are rare; the best example of one would be graphite. It is the structure of graphite which provides its great lubricating capability. The condition to form this planar structure is to have three or more active groups all directed in the same plane and capable of forming a planar network. This structure offers low shear strength and good lubricating properties.

Three-dimensional Polymers

Crystalline Diamond is an example of the three-dimensional crystalline polymer in which carbon is linked to four corners of the tetrahedra and these are packed with long range order in space to form a lattice. Diamond has properties which are much more like ceramics than polymers in terms of mechanical behavior (high melting point, modulus, hardness, strength, and fracture behavior).

Highly cross-linked structure is the most significant property of plasma polymers to distinguish it from the conventional polymers. Cross-linking in polymer means, in addition to the bonds which hold monomers together in a polymer chain, many polymers form bonds between neighboring chains. These bonds can be formed directly between the neighboring chains, or two chains may bond to a third common molecule. Though not as strong or rigid as the bonds within the chain, these cross-links have an important effect on the polymer. Polymers with a high enough degree of cross-linking have “memory”. When the polymer is stretched, the cross-links prevent the individual chains from sliding past each other. The

chains may straighten out, but once the stress is removed they return to their original position and the object returns to its original shape [61-63].

2.2.2 Classification of polymers

Depending on the different functional groups and structures in the field of macromolecules, polymers are classified in various ways listed in table 2.1.

Table 2.1 Classification of polymer

Basic Classification	**Polymer types**
Origin	Natural, Semisynthetic, Synthetic
Thermal response	Thermoplastic, Thermosetting
Mode structure	Addition, Condensation
Line structure	Linear, Branched, Cross–linked
Tacticity	Isotactic, Syndiotactic, Atactic
Crystallinity	Non-crystalline(amorphous),Semi-crystalline, Crystalline.

A polymer may be completely amorphous in the solid state, which means that the chains in the specimen are arranged in a totally random fashion. In the region the polymer is a glass, but as the sample is heated it passes through a temperature, called the glass transition temperature beyond which it softens and becomes rubberlike. A continuing increase in temperature leads to a change of the rubbery polymer to a viscous liquid. The crystalline polymer on heating would become a viscous liquid.

2.3 Plasma Polymerization

2.3.1 Plasma

Plasma is described as an electrically neutral medium of positive and negative particles. It is highly reactive making it useful for a number of chemical processing applications. Plasma is created when a neutral gas is given sufficient energy from an electronic discharge source to create new product ions and radicals. The source of free electrons is generally a high energy glow discharge such as a high voltage electrode. This resulting collision of electrons and gas molecules result in a net energy transfer to the molecules producing metastable fragments and energized ions. The resulting product is a mixture of highly excited ions consisting of

fragmented portions of the parent molecule. Plasma generated from oxygen (O_2) carrier gas typically consists of O^+, O^-, O_2^+ and O_3^+ ions for example. The plasma particles are extremely unstable and their energetic states cause them to be highly reactive with particles or surfaces that they contact. Plasma is generally produced in a low pressure environment using a high vacuum system to promote stability of ionic radicals formed. This low pressure stability is achieved by effectively increasing the mean free path between the active components. Plasma may also be produced in an environment near atmospheric pressure without the need for maintaining an expensive vacuum system. The physics definition of plasma is an ionized gas with an essentially equal density of positive and negative charges. A gas into which sufficient energy is provided to free electrons from atoms or molecules and to allow both species, ions and electrons, to coexist. Plasmas are described as the fourth state of matter and although they are not perceived as very common in our everyday surrounding, plasma are the most abundant form of matter in the universe. Gases can become plasmas in several ways, but all include pumping the gas with energy. A spark in a gas will create a plasma. A hot gas passing through a big spark will turn the gas stream into a plasma that can be useful. The ionization degree can vary from 100% (fully ionized gases) to very low values (partially ionized gases). When the temperatures greater than 10,000K all molecules and atoms tend to become ionized. Plasma is considered as being a state of materials, and the state is more highly activated than in the solid liquid, or gas state.

Besides the astroplasmas there are two main groups of laboratory plasmas, i.e. the high-temperature or fusion plasma and the so-called low temperature plasma or gas discharge [64-65]. Ionized refers to presence of one or more free electrons, which are not bound to an atom or molecule. The free electric charges make the plasma electrically conductive so that it responds strongly to electromagnetic fields. The classical definition of plasma limits the term, to an appreciably ionized gas or vapor that conducts neutral fluids *hot* and viscous. The modern definition is less restrictive, plasma simply connoting a more or less ionized gas.

2.3.2 Glow Discharge Plasma

2.3.2.1 Capacitively Coupled Radio-Frequency Discharge

If an ac voltage (Up to kHz) is used, the discharge is still basically of a dc type and each electrode really acts as a cathode and anode alternatively. The frequencies generally used for the alternating voltages are typically in the radiofrequency (rf) range. Capacitively coupled

(cc) discharge can also be generated by alternating voltages in another frequency range. Therefore, the term „alternating current (ac)" discharges as opposed to dc discharges might be more appropriate. The term „capacitively coupled" refers to the way of coupling the input power into the discharges ie by means of two electrodes and their sheaths forming a kind of capacitor. The rf discharges which also results from the differences in mass between electrons and ions, is the phenomenon of self bias. The self-bias or dc-bias is formed i) when both electrodes differ in size and ii) when a coupling capacitor is present between the rf power supply and the electrode or when the electrode is non conductive (because it then acts as a capacitor). When a certain voltage is applied over the capacitor formed by the electrodes, the voltage over the plasma will initially have the same value as the applied voltage. Capacitively coupled plasma is similar to glow discharge plasmas, but generated with high frequency RF electric fields, typically 13.56 MHz. These differ from glow discharges in that the sheaths are much less intense. These are widely used in the microfabrication and integrated circuit manufacturing industries for plasma etching and plasma enhanced chemical vapor deposition.

When the applied voltage is initially positive the electrons will be accelerated toward the electrode. Hence the capacitor will be rapidly charged up by the electron current and the voltage over the plasma will drop. When the applied potential changes polarity after one half-cycle, the voltage over the plasma changes with the same amount. The capacitor will now be charged up by the ion current and the voltage over the plasma will, therefore drop as well, but this second drop is less pronounced, because of the much lower mobility of the ions and hence the lower ion flux. At the next half-cycle, the applied potential, and hence also the voltage over the plasma, again changes polarity. The voltage over the plasma drops again more rapidly, because the capacitor is again charged up by the electron flux. This process repeats itself, until the capacitor is finally sufficiently negatively charged so that the ion and electron fluxes integrated over one rf-cycle, are equal to each other. This results in a time-averaged negative d.c. bias at the rf-powered electrode.

Because of the negative dc bias, the ions continue to be accelerated toward the rf-powered electrode, and they can, therefore cause sputtering of the rf-electrode material. In fact, the cc rf discharge often resembles a dc glow discharge with a similar subdivision in different regions, similar operating conditions, and with similar processes occurring in the plasma.

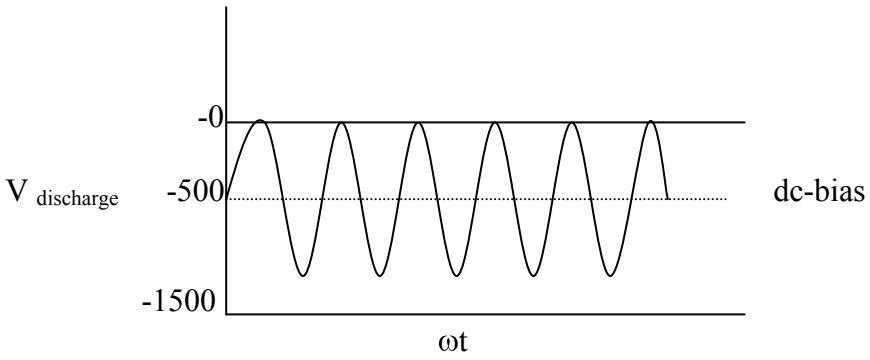

Fig.2.2 Typical sinusoidal voltage in a cc-rf discharge in the case of a large negative dc bias.

2.3.2.2 Inductively Coupled Glow Discharges

In the inductively coupled source, the plasma chamber is mostly also surrounded by a coil. Simply speaking, the rf currents in the coil (inductive element) generate an rf magnetic flux, which penetrates the plasma region. Inductively coupled plasma is similar to a CCP and with similar applications but the electrode consists of a coil wrapped around the discharge volume which inductively excites the plasma.

Following Faraday"s law:

$$\Delta \times E = -\partial B / \partial t$$

the time-varing magnetic flux density induces a solenoidal rf electric field, which accelerates the free electrons and sustains the discharge. Basically, two different coil configurations can be distinguished in inductive discharges for processing applications, i.e. cylindrical and planar. In the first configuration, a coil is wound around the discharge chamber, as a helix. In the second configuration, which is more commonly used for materials processing, a flat helix or spiral is wound from near the axis to near the outer radius of the discharge chamber, separated from the discharge region by a dielectric. Advantages of the latter are reduced plasma loss and better ion generation efficiency; disadvantage is the higher sputter-contamination, UV-damage and heating of neutrals at the substrate. Multipole permanent magnets can be used around the process chamber circumference to increase radial plasma uniformity. The planar coil can also be moved close to the wafer surface, resulting in near-planar source geometry, having good uniformity properties, even in the absence of multipole confinement.

It should be mentioned that the coupling in IC plasma is generally not purely inductive, but has a capacitive component as well, through the wall of the reactor. Indeed, when an inductive

coupling is used, deposition on the wall is often observed to follow a pattern matching the shape of the coil. This is an indication of localized stronger electric fields on the walls, showing that the coupling is at least partly capacitive through the walls of the reactor. It is mentioned that inductively coupled plasma are not only used as materials processing discharges, but they are also applied in other fields, albeit in totally different operating regimes. So IC plasmas are the most popular plasma sources in plasma spectrochemistry.

2.3.2.3 Direct Current Glow Discharge

Plasma polymerization process takes place usually in a low temperature generated by glow discharge. The space between the electrodes becomes visible when a glow discharge is established, the actual distribution of light in the glow discharge is significant and is dependent on the current-voltage characteristics of the discharge [66-67].

When a constant potential difference is applied between the cathode and anode, a continuous current will flow through the discharge; giving rise to a direct current (dc) glow discharge. In a dc glow discharge the electrodes play an essential role for sustaining the plasma by secondary electron emission. The potential difference applied between the two electrodes is generally not equally distributed between cathode and anode, but it drops almost completely in the first millimeters in front of the cathode. However, for most of the other applications of dc glow discharges (sputtering, deposition, chemical etching, analytical chemistry etc.), the distance between cathode and anode is generally short. So normally a short anode zone is present beside cathode dark space and negative glow, where the slightly positive plasma potential returns back to zero at the anode.

A dc glow can operate over a wide range of discharge conditions. The pressure can vary from below 1 pa to atmospheric pressure. The product of pressure and distance between the electrode is a better parameter to characterize the discharge. For instance, at lower pressure, the distance between cathode and anode should be longer to create a discharge with properties comparable to these of high pressure with small distance. The discharge can operate in a rare gas (most often argon or helium) or in a reactive gas (N_2, O_2, H_2, CH_4, SiH_4, SiF_4, etc.), as well as in a mixture of these gases.

2.3.2.4 Alternating Current Glow Discharge

The mechanism of glow discharge generation will basically depend on the frequency of the alternation. At low frequencies (60 Hz), the effect is simply to form dc glow discharges of

alternating polarity. However the frequency is higher than 60 Hz the motion of ions can no longer follow the periodic changes in field polarity. But above 500 KHz the electrode never maintains its polarity long enough to sweep all electrons or ions, originating at the opposite electrode, out of the inter-electrode volume. In this case the regeneration of electrons and ions that are lost to the walls and the electrodes takes place within the body of the plasma. The mechanism by which electrons pick up sufficient energy to cause bond dissociation or ionization involves random collisions of electrons with gas molecules, the electron picking up an increment of energy with each collision. A free electron in a vacuum under the action of an alternating electric field oscillates with its velocity 90 out of phase with the field, which obtains no energy, on the average, from the applied field. The electron can gain energy from the field only as a consequence of elastic collisions with the gas atoms, as the electric field converts the electron‟s resulting random motion back to ordered oscillatory motion. Because of its interaction with the oscillating electric field, the electron gains energy on each collision until it acquires enough energy to be able to make an inelastic collision with a gas atom. In that case the process of these inelastic collisions is termed volume ionization.

Thus the transfer of energy from the electric field to electrons at high frequencies is generally accepted as that operative in microwave discharges. It has also been put forward as that applicable to the widely used rf of 13.56 MHz.

2.3.3 Plasma Reactors

A plasma reactor was constructed for the purpose of ionizing gases above a polymer substrate placed on a grounded sample holder. Different kinds of reactors including capacitatively and inductively coupled rf reactors, microwave and electron cyclotron reactors can be used for plasma polymerization. In the current research, capacitatively coupled rf plasma (glow discharge plasma) system was used. Glow discharge reactor is the important part of plasma polymerization system. Because reactor geometry influences the extent of charge particle bombardment on the growing films which affects the potential distribution in the system. Different kinds of reactors including capacitively coupled and inductively coupled rf reactors, microwave, dual-mode (MV/rf), etc. can be used for plasma polymerization processes. The presence of insulating layers on the electrodes deflects plasma current into any surrounding conducting areas and thus leads to gross plasma non-uniformity or plasma extinction.

Therefore, when insulating materials are involved, ac power is usually employed so that power may pass through the insulator by capacitive coupling.

Reactors with internal electrodes have different names, e.g. flat bed, parallel plates, planar, diode etc. Their main features are power supply, coupling system, vacuum chamber, rf driver electrode, grounded electrode, and eventually one or most substrate holders. Among the internal electrode arrangements a bell-jar-type reactor with parallel plate metal electrodes is most frequently used by using ac(1-50 kHz) and rf fields for plasma excitation.

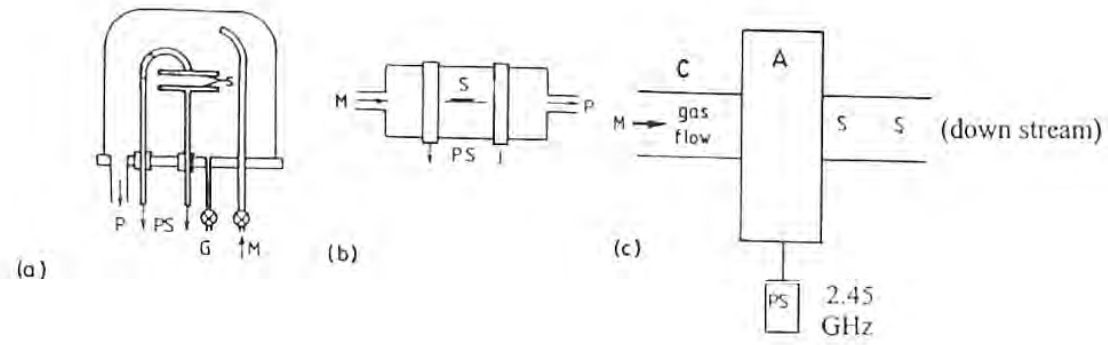

Fig.2.3 Different types of reactor configuration used for plasma polymerization (a) internal electrode reactor, (b) external electrode reactor, (c) electrode less microwave reactors.

The vacuum chambers can be made either of glass or of conductive materials, such as metal. In the case of bell-jar reactors, no particular care is taken for the grounded electrode apart from its area. On the contrary, the design and arrangement of the cathode require special attention: a metallic shield surrounding the electrode highly improves the glow confinement inside interelectrodic space; electrode material and area greatly affect the extend of sputtering on the target. In the current research, capacitively coupled reactor (glow discharge plasma) system was used for the formation of thin films.

2.3.4 Plasma Polymerization

Plasma polymerization is a process in which organic materials are reacted in an ionizing gas environment to form cross-linked polymer films. An ultra thin film can be formed by this process where thin films deposit directly on surfaces as comprising the vacuum deposition of covalently bonded materials. In this process, the growth of low-molecular-weight molecules (Polymer) occurs with the assistance of the plasma energy, which involves activated electrons, ions and radicals. Condition for this process is the presence of chain-producing atoms, such as carbon, silicium or sulfur, in the working gas.

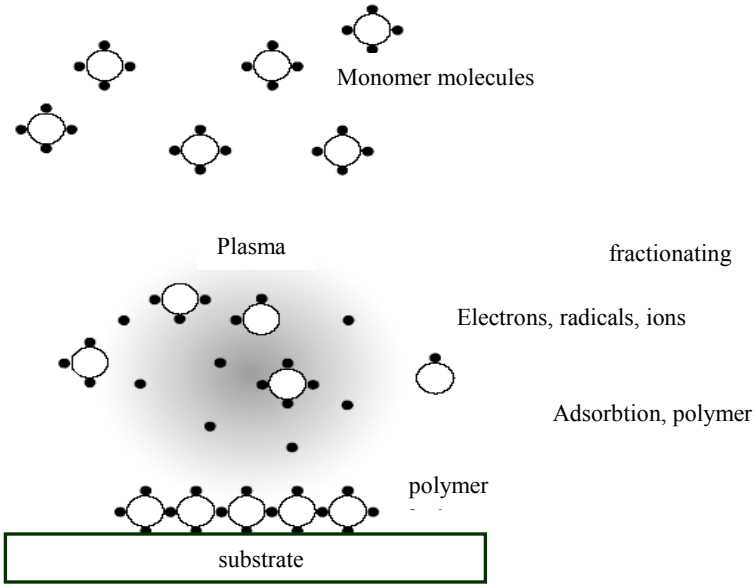

Fig.2.4 A schematic plasma polymerization configuration

The mechanisms of plasma polymerization and that of free radical polymerization have some similarity but the fundamental processes are vastly different. The materials obtained by plasma polymerization are significantly different from conventional polymers and also different from most inorganic materials. Hence plasma polymerization should be considered as a method of forming new types of materials rather than a method of preparing conventional polymers. This polymerization process covers a wide interdisciplinary area of physics, chemistry, science of interfaces and materials science and so on [68-70]. Thus plasma polymerization is a versatile technique for the deposition of films with functional properties suitable for a wide range of modern applications.

Plasma Polymerization process usually takes place in low temperature plasma, which is generated by glow electrical discharges operated in a molecular gas under low pressure. The energy transfer from electrons to gas molecules leads to the formation of a host of chemically reactive species such as radicals and ions, which along with photons cause a variety of plasma-chemical reactions. Plasma polymerization is an ultra-thin film processing technology and covers very important subject area that can be recognized as comprising the vacuum deposition of covalently bonded materials.

2.3.5 Plasma Polymerization Mechanism

The process by which a polymer is formed from its corresponding monomer can be categorized into two major groups.

1) Steps growth polymerization

In this process the polymer is formed from the monomer by the stepwise repetition of particular reaction. This involves the condensation of two poly functional molecules to produce a larger molecule during which small molecules like water are eliminated.

2) Chain growth polymerization

This is a very rapid process where a series of consecutive steps results in a long chain of molecules. Contrary to the step growth process, here the growth is completed within a very short time and also intermediate size molecules are not eliminated.

In these reactions the chain is carried by an ion or a free radical. Free radical is a reactive substance with a unpaired electron formed by the decomposition of an unstable molecule called initiator. The chain growth is initiated by initiators which initially undergo decomposition to form free radicals.

Studies on plasma polymerization mechanisms suggest that free radical are the most likely reactive species involved in polymer formation under plasma conditions. Here the whole process consists of three steps namely initiation, propagation and termination. In the first step an initiator radical is formed the decomposition of the initiator.

$$I \xrightarrow{K_d} I*$$

Where K_d is the constant of decomposition rate. The initiator radical formed now acts on the monomer molecules forming monomer radicals.

$$Z* + M \xrightarrow{K_i} M_1^*$$

Where M is the monomer, K_i is the initiating rate and M_1^* is the monomer radical. The first monomer radical can react with a monomer molecule to produce a dimer radical.

$$M_1^* + M \xrightarrow{Kp} M_2^*$$

K_p is the rate of polymerization and M_2^* is the dimer radical formed in the first process of polymerization.

This polymerization process proceeds as

$$M_2^* + M \xrightarrow{Kp} M_3^*$$

$$M_{x-1}^* + M \xrightarrow{Kp} M_x^*$$

Two termination processes are identified.

(1) Combination (2) Disproportionation. Combination can be represented as

$$M_x^* + M_y^* \xrightarrow{Kt'} M_{x+y}$$

Disproportion can be represented as

$$M_x^* + M_1^* \xrightarrow{Kt''} M_x + M_y$$

$K_{t'}$ and $K_{t''}$ are the termination rates of polymerization process and they depend on the external conditions of the process. In radical polymerization, the termination is a second order reaction in M^* and the radical can be terminated by collision with the initiator radical. But this may be ignored due to the low concentration of the initiator. Radical polymerization is the dominant process in plasma-polymerization. The initiators here are the accelerated positive ions and the electrons formed by the high electric field. These collide with monomer molecules and produce radicals. The initiator concentration in such a process is very high. In this kind of plasma-polymerization the termination reaction can occur as a result of a collision.

2.3.6 The Effect of Plasma Process Parameters on Film Properties

The deposition rate of plasma polymerization and the physical and chemical properties of these films depend upon following process parameters. Generally, when the other parameters are kept constant (power, pressure, etc), deposition rate rises monotonically with increasing flow rate at first because the polymerization rate is limited by the supply of fresh feed gases. At high flow rates, the deposition rate decreases because the residence time of the feed gases decreases and even activated species may be prevented from reaching the substrate by being drawn away and pumped out.

Effect of power

Increase of power will result in an increased density of energetic electrons and in an increased bombardment of the electrodes by energetic ions. With pressure and flow rate held constant, the deposition rate increases with power at first and then becomes independent of power at high power values.

Effect of pressure

The pressure of the system affects

a) Residence time of the gases.

b) Average electron energy in the system.

c) Mean free path of the molecule inside the reactor.

2.3.7 Comparison between Conventional Polymerization and Plasma Polymerization

In contrast to conventional polymerization, polymer formation in glow discharge sometimes may be characterized as elemental or atomic polymerization. That is, in glow discharge polymerization, the molecular structure of a monomer is not retained, and the original monomer molecules serves as the sources of elements from which large molecules are constructed. A polymer formed by plasma polymerization cannot usually be identified from the starting material, i.e., plasma polymerization is a system-dependent process. However, it is possible to predict the breakdown of monomer molecules, based on the bond strength of their chemical bonds. Then, the polymerization mechanism of these fragments may be deduced. Another important point is that characterization techniques of the final film need to be developed for the plasma polymer film, which is different from polymers in conventional sense. In conventional polymerization, the properties of the polymer are determined by the monomer being used, but the properties of the plasma polymer are not determined by the monomer being used but rather by the plasma parameters. The surface energies of plasma polymers of hydrocarbons are generally higher than those of conventional hydrocarbon polymers containing groups.

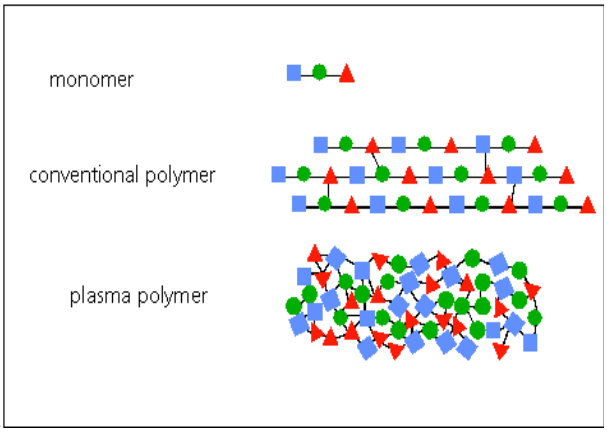

Fig. 2.5 Structure of conventional polymerization and plasma polymerization.

Unlike conventional polymerization, most of the reactions in plasma polymerization are one-step reactions between two reactive species. Some other reactions are between an activated species and a molecule, which are essentially the same as the propagation reaction of the conventional addition polymerization. Such reactions can proceed in a chain mechanism if the reacting molecule has the appropriate molecular structure. Thus plasma polymerization is vastly different from conventional polymerization.

2.3.8 Applications of Plasma polymerized Thin Films

Research and development of plasma and plasma-polymerized organic thin films have been undertaken very actively in the last few years and some of the products have been applied in a variety of technologies. Surface modification is probably the most important application field, plasma processes appear to have some distinct advantages compared to conventional processes. Plasma polymers are used as dielectric and optical coating to inhibit corrosion. A number of different plasma technologies are essential to different steps in the fabrication of ICs. The use of plasmas as lamps, more specifically fluorescent lamps is probably the oldest application. Nowadays, new types of so-called electrode less lamps are being developed, and the use of low temperature plasmas for displays as large and flat television screens. Applications of plasma-polymerized films are associated with biomedical uses, the textile industry, electronics, optical applications, chemical processing and surface modification [3,5,71-74]. The main advantage of plasma polymerization is that it can occur at moderate temperatures compared to conventional chemical reactions because of cracking of monomers and the formation of radicals occurs by electron impact reactions in the plasma. Segui described two applications and the problems that prevent their industrial application, ie the reactor geometry and neutralization of free radicals in the case of microcapacitors and contact openings and mobile charge quantity reduction in the case of component passivation. The chemical reactions in low temperature plasma have been studied extensively over the past few decades. A large number of applications have been proposed in terms of plasma modification of polymers and thin film deposition. Typical uses of plasma-polymerized films are listed in Table.2.2.

Table 2.2 Potential applications of plasma-polymerized films.

Electronics	Integrated ckt, amorphous semiconductor, amorphous fine ceramic etching.
Electrics	Insulator, thin film dielectrics, separation membrane for batteries.
Chemical processing	Reverse osmosis membrane, permselective membrane, gas separation membrane-lubrication insolubilization.
Surface modification	Adhesive improvement, protective coating, abrasion-resistant coating, anti-crazing and scratching.
Optical	Anti-reflection coating, anti-dimming coating, improvement of transparency, optical fiber, optical wave-guide laser and optical window, contact lens.
Textile	Anti-flammability, anti-electrostatic treatment, dying affinity, hydrophilic improvement, water repellence, shrink-proofing.
Biomedical	Immobilized enzymes, organelles and cells, sustained release of drugs and pesticides, sterilization and pasteurization, artificial kidney, blood vessel, blood bag, anti-coating.

2.4 Techniques for Structural and Thermal Analyses

2.4.1 Differential Thermal Analysis and Thermogravimetric analysis

The thermal properties of plasma polymerized thin films are important from the technological point of view. The term thermal analysis is frequently used to describe analytical experimental techniques, which is used to investigate the behavior of a sample as a function of temperature [83, 84].

Differential Thermal Analysis (DTA)

Differential thermal analysis (DTA) is the simplest and most widely used thermal analysis technique. The difference in temperature, T, between the sample and a reference material is recorded while both are subjected to the same heating programme. The technique of DTA is used to study the structural and phase changes occurring both in solid and in liquid materials during heat treatment. These changes may be due to dehydration, transition from one crystalline form to another, destruction of crystalline structure, oxidation, decomposition etc.

The principle of DTA consists of measuring heat changes associated with the physical or chemical changes occurring when any substance is gradually heated. The thermocouple(platinum-platinum rhodium 13%) for DTA measurement is incorporated at the end of each of the balance beam ceramic tubes, and the temperature difference between the

holder on the sample side and the holder on the reference side is detected. This signal is amplified and becomes the temperature difference signal used to measure the thermal change of the sample.

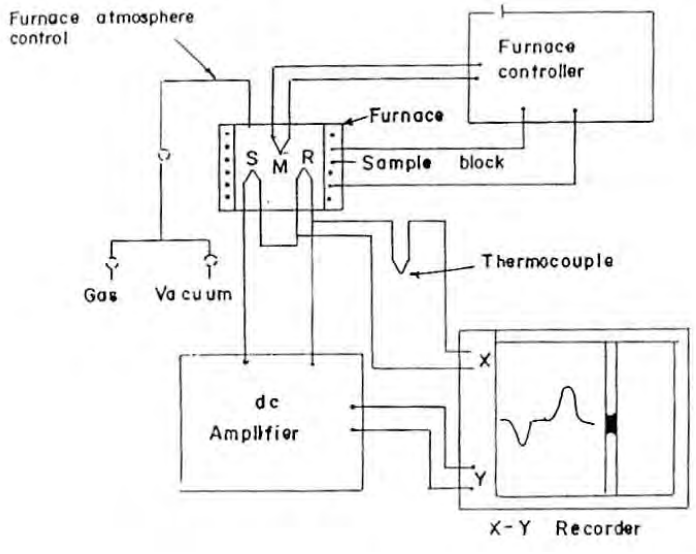

Fig 2.6 A schematic diagram showing different parts of a DTA apparatus

Thermogravimetric Analysis (TGA)

Measurements of changes in sample mass with temperature (thermogravimetry) are made using a thermobalance (sometimes referred to as a thermogravimetric analyzer). The TGA is a branch of thermal analysis, which examines the mass change of a sample as a function of temperature in the scanning mode or as a function of time in the isothermal mode under a variety of conditions, and to examine the kinetics of the physico-chemical processes occurring in the sample. Sample weight changes are measured as described below in Fig. 2.7.

Figure shows the sample balance beam and reference balance beam are independently supported by a driving coil/pivot. When a weight change occurs at the beam end, the movement is conveyed to the opposite end of the beam via the driving coil/pivot, when optical position sensors detect changes in the position of a slit. The signal from the optical position sensor is sent to the balance circuit. The TGA is used to characterize the decomposition and thermal stability of materials. The balance circuit supplies sufficient feedback current to the driving coil so that the slit returns to the balance position. The current running to the driving coils on the sample side and the current running to the driving coil on the reference side is detected and converted into weight signals.

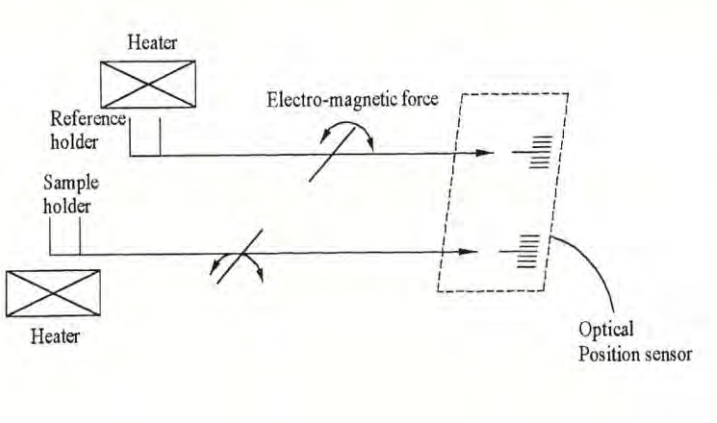

Fig 2.7 TGA measurement Principle.

2.4.2 Scanning Electron Microscopy

2.4.2.1 Principal

A scanning electron microscope (SEM) is a powerful microscope that uses electrons rather than light to form an image of objects such as fractured metal components, foreign particles and residues, polymers, electronic components, biological samples, and countless others. The shorter wavelength of electrons permits image magnifications of up to 100,000×, as compared to about 2,000× for conventional light microscopy. An SEM also provides a greater depth of field than a light microscope, allowing complex, three-dimensional objects to remain sharp and in focus. This capability reveals details that cannot be resolved by light microscopy. SEM is a very versatile technique employed for the examination and analysis of the micro structural characteristics of solid objects. SEM is capable of high resolution (values of the order of 10 nm), and its greater depth of focus allows more three-dimensional information to be gathered than optical microscopy. The technique uses a electron beam (typically 2 to 30kV) to strike a solid sample and cause secondary electrons, back-scattered electrons, x-rays and Auger electrons to be emitted. The intensities of the emitted secondary electrons vary with topography and may be detected and displayed using a cathode ray tube screen, producing a detailed image of the surface.

Small samples up to several millimeters and sometimes even larger can be investigated directly in the SEM if the sample material has a sufficiently high electric conductivity to prevent charging produced. For insulating samples, it needs to be coated with an extremely thin layer of an electrically conducting material (Ag, Au etc).

(a) Working Function of an Electron Microscope [75,76]

Electron Microscopes function exactly as their optical counterparts except that they use a focused beam of electrons instead of light to "image" the specimen and gain information as to its structure and composition.

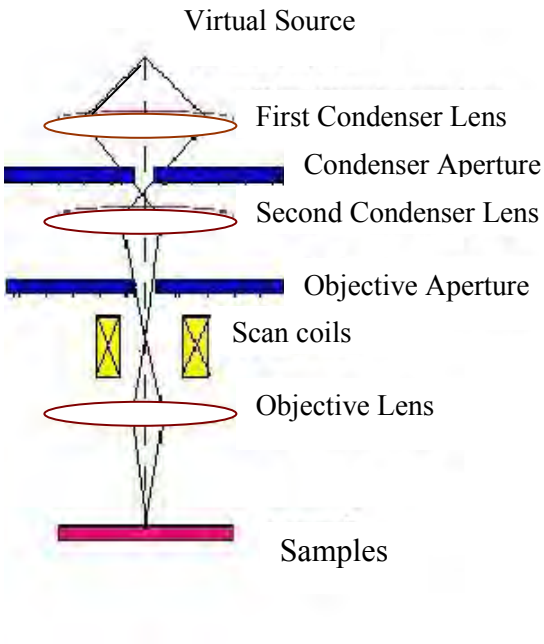

Fig. 2.8 Schematic diagram of a scanning electron microscope.

The basic steps involved in all Electron Microscopes are:

1. A stream of electrons is formed (by the Electron Source) and accelerated toward the specimen using a positive electrical potential.
2. This stream is confined and focused using metal apertures and magnetic lenses into a thin, focused, monochromatic beam.
3. This beam is focused onto the sample using a magnetic lens.
4. Interactions occur inside the irradiated sample, affecting the electron beam .These interactions and effects are detected and transformed into an image. The above steps are carried out in all EMS regardless of type.

2.4.2.2 Energy Dispersive X-ray (EDX) analysis

EDX Analysis stands for energy Dispersive X-ray analysis. It is sometimes referred to also as EDS or EDAX analysis. It is a technique used for identifying the elemental composition of the specimen, or an area of interest therefore. The EDX analysis system works as an

integrated feature of a scanning electron microscope, and can not operate on its own without the latter. During EDX analysis, the specimen is bombarded with an electron beam inside the scanning electron microscope. The bombarding electrons collide with the specimen atoms‟ own electrons, knocking some of them off in the process. A position vacated by an ejected inner shell electron is eventually occupied by a higher-energy electron from an outer shell. To be able to do so, however, the transferring outer electron must give up some of its energy by emitting an X-ray.

The amount of energy released by the transferring electron depends on which shell it is transferring from, as well as which shell it is transferring to. Furthermore, the atom of every element releases X-rays with unique amounts of energy during the transferring process. Thus, by measuring the amounts of energy present in the X-rays being released by a specimen during electron beam bombardment, the identity of the atom from which the X-ray was emitted can be established. The EDX spectrum is just a plot of how frequently an X-ray is ejected for each energy level. An EDX spectrum normally displays peaks corresponding to the energy levels for which the most X-rays had been received. Each of these peaks is unique to an atom, and therefore corresponds to a single element. The higher a peak in a spectrum, the more concentrated the element is in the specimen.

2.4.3 Elemental Analysis

The chemical compositions of plasma-polymerized materials can be characterized by elemental analyses technique. The elemental composition of plasma-polymerized materials generally differs substantially from that of monomer, which does not usually happen in case of conventional polymers. The technique used for the determination of CHN is based on the quantitative “dynamic Flash Combustion” method as shown in Fig.2.9. The samples are held in a tin container, placed inside the auto samples drum where they are purged with a continuous flow of helium and then dropped at certain intervals into a vertical quartz tube maintained 1293K (Combustion reactor). When the sample dropped inside the furnace, the helium stream is temporarily enriched with pure oxygen and the sample and its container melt and the tin promotes a violent reaction (Flash Combustion) in a temporary enriched atmosphere of oxygen.

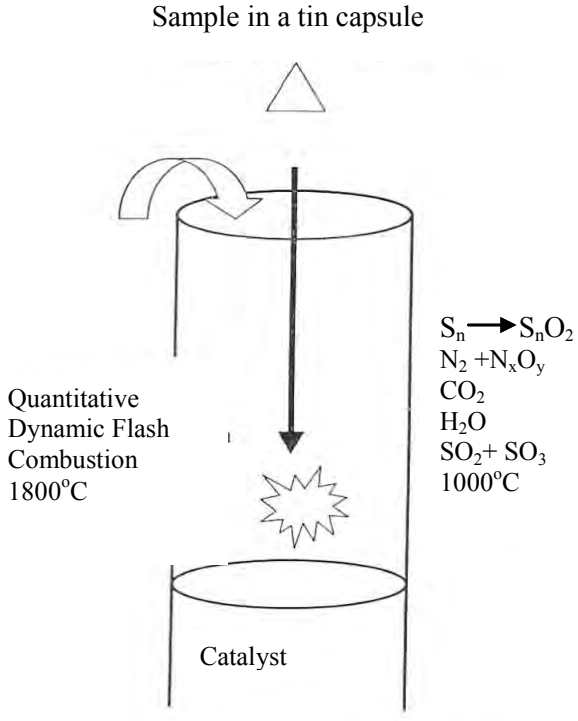

Fig. 2.9 The principle of operation of elemental analyzer.

Under these favorable conditions even thermally resistant substances are completely oxidized. The resulting combustion gases are separated and detected by a thermal conductivity detector, which gives an output signal proportional to the concentration of the individual components of the mixture.

2.4.4 Infrared Spectroscopy

Infrared (IR) spectroscopy is used to obtain information on the molecular structure of virtual all type of samples in any physical state (solid, liquid or gas). Infrared spectroscopy is based on the fact that all molecules vibrate and can absorb energy in the infrared region. Most of the vibrational absorption states correspond to the wavelength in the order of 2.5 to 25 μm (4000-400 cm^{-1}). When a beam of electromagnetic radiation of intensity is passed through a substance, it can either be absorbed or transmitted, depending upon its frequency, and the structure of the molecules. If a transition exists which is related to the frequency of the incident radiation by Planck‟s law, then the radiation can be absorbed. The type of absorption spectroscopy depends upon the type of transition involved and accordingly the frequency range of the electromagnetic radiation absorbed. If the transition is from one vibrational energy level to another, then the radiation is from the infrared portion of the electromagnetic spectrum and the technique is known as infrared spectroscopy [77, 78].

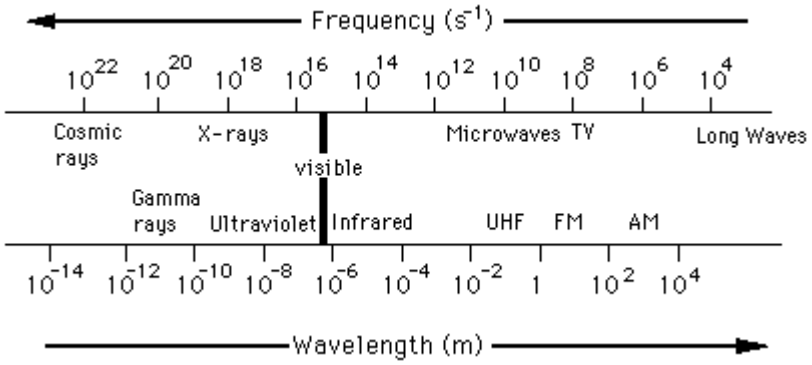

Fig. 2.10 The electromagnetic spectrum

Atoms and molecules can absorb electromagnetic radiation, but only at certain energies (wavelengths). The diagram in Fig. 2.10 illustrates the relationships between different energy levels within a molecule. The three groups of lines correspond to different electronic configurations. The lowest energy, most stable electron configuration is the ground state electron configuration. Certain energies in the visible and UV regions of the spectrum can cause electrons to be excited into higher energy orbitals; some of the possible absorption transitions are indicated by the vertical arrows. Very energetic photons (UV to x-ray region of the spectrum) may cause an electron to be ejected from the molecule (ionization). Photons in the infrared region of the spectrum have much less energy than photons in the visible or uv regions of the electromagnetic spectrum. They can excite vibrations in molecules. There are many possible vibrational levels within each electronic state. Transitions between the vibrational levels are indicated by the vertical arrows on the left side of the diagram. Microwave radiation is even less energetic than infrared radiation. It cannot excite electrons in molecules, nor can it excite vibrations; it can only cause molecules to rotate. Microwave ovens are tuned to the frequency that causes molecules of water to rotate, and the ensuing friction causes heating of water-containing substances. Fig 2.11 illustrates these three types of molecular responses to radiation.

A molecule absorbs infrared radiation when the vibration of the atoms in the molecule produces an oscillating electric field with the same frequency as the frequency of incident IR "light". All of the motions can be described in terms of two types of molecular vibrations. One type of the vibration, a stretch, produces a change of bond length. A stretch is a rhythmic

movement along the line between the atoms so that the interatomic distance is either increasing or decreasing.

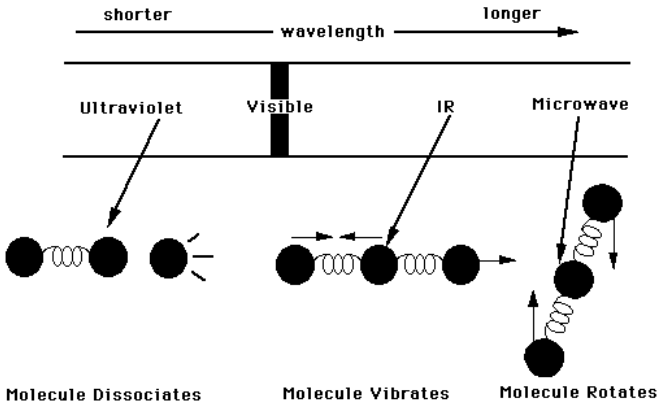

Fig 2.11 Molecular responses to radiation

The second type of vibration, a bend, results in a change in bond angle. These are also sometimes called scissoring, rocking, etc. motions. Each of these two main types of vibration can have variations. A stretch can be symmetric or asymmetric. Bending can occur in the plane of the molecule or out of the plane; it can be scissoring, like blades of a pair of scissors, or rocking, where two atoms move in the same direction.

A molecule absorbs only those frequencies of IR light that match vibrations that cause a change in the dipole moment of the molecule. In a complicated molecule many fundamental vibrations are possible, but not all are observed. Some motions do not change the dipole moment for the molecule; some are so much alike that they coalesce into one band. Even though an IR spectrum is characteristic for an entire molecule, there are certain groups of atoms in a molecule that gives rise to absorption bands at or near the same wave number, ν,(frequency) regardless of the rest of the structure of the molecule. These persistent characteristic bands enable to identify major structural features of the molecule.

There are no rigid rules for interpreting an IR spectrum. Certain requirements, however, must be meet before an attempt is made to interpret a spectrum.

i.) The spectrum must be adequately resolved and of adequate intensity.

i) The spectrum should be that of a reasonable pure compound.

ii) The spectrophotometer should be calibrated so that the bands are observed at their proper frequencies or wavelengths. Proper calibration can be made with reliable standards, such as polystyrene film.

iii) The methods of sample handling must be specified. If a solvent is employed, the solvent, concentration, and the cell thickness should be indicated.

2.4.5 X-ray Photoelectron Spectroscopy

X-ray photoelectron spectroscopy (XPS) is a surface analytical technique, which is based upon the photoelectric effect. Each atom in the surface has core electron with the characteristic binding energy that is conceptually, not strictly, equal to the ionization energy of that electron. When an X-ray beam directs to the sample surface, the energy of the X-ray photon is adsorbed completely by the core electron of an atom. If the photon energy, $h\nu$, is large enough, the core electron will then escape from the atom and emit out of the surface. The emitted electron with the kinetic energy of E_k is referred to as the photoelectron. The binding energy of the core electron is give by the Einstein relationship:

$$E_b = h\nu - E_k - \varphi$$

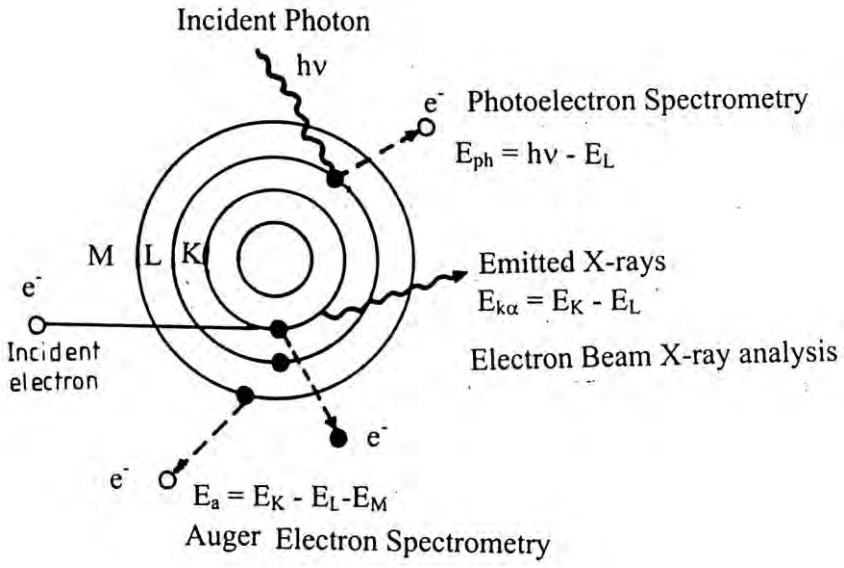

Fig.2.12 A typical atomic model with a scheme of emission of photoelectrons and of X-ray.

Where $h\nu$ is the X-ray photon energy (for monochromatic Al Kα, $h\nu$ = 1486.6eV); E_k is the kinetic energy of photoelectron, which can be measured by the energy analyzer; and ϕ is the work function induced by the analyzer, about 4~5eV. Since the work function, ϕ, can be compensated artificially, it is eliminated, giving the binding energy as follows:

$$E_b = h\nu - E_k$$

For insulating samples, once the photoelectrons are emitted out of the sample surface, a positive charge zone will establish quickly in the sample surface. As a result, the sample surface acquires a positive potential (varying typically from several volts to tens of volts) and the kinetic energies of core electrons are reduced by the same amount, *C*.

$$E_b = h\nu - (E_k - C)$$

It can be seen that the surface charging results in the shift of the XPS peaks to higher binding energy. In this case, the binding energy has to be calibrated with an internal reference peak. The C 1s peak from the adventitious carbon-based contaminant, with the binding energy of 285 eV, is commonly used as the reference for calibration. In order to neutralize the surface charge during data acquisition, a low-energy electron flood gun is used to deliver the electrons to the sample surface. The electron flood gun can be tuned to provide the right current to push the XPS peaks back to the real position.

The core electron of an element has a unique binding energy, which seems like a "fingerprint". Thus almost all elements except for hydrogen and helium can be identified *via* measuring the binding energy of its core electron. Furthermore, the binding energy of core electron is very sensitive to the chemical environment of element. The same atom is bonded to the different chemical species, leading to the change in the binding energy of its core electron. The variation of binding energy results in the shift of the corresponding XPS peak, ranging from 0.1eV to 10eV. This effect is termed as "chemical shift", which can be applied to studying the chemical status of element in the surface. Therefore, XPS is also known as electron spectroscopy for chemical analysis (ESCA). Since the number of photoelectron of an element is dependent upon the atomic concentration of that element in the sample, XPS is used to not only identify the elements but also quantify the chemical composition. When the monoenergetic soft x-rays (normally Mg Kα(1253.6 eV) or Al Kα (1486.6 eV) x-rays are used) reach the surface of sample, they interact with atoms in the surface region, cause electrons to be emitted by the photoelectric effect. The photons of soft x-rays have limited penetrating power in a solid on the order of 1-10 micrometers. The emitted electrons have measured kinetic energies given by:

$$KE = h\nu$$

Where hv is the energy of the photons, BE is the binding energy of the orbital from which the electron originates, and is the spectrometer work function [79-82].

The binding energy may be regarded as the energy difference between the initial and final states after the photoelectron has left the atom. Because there is a variety of possible final states of the ions from each type of atom, there is a corresponding variety of kinetic energies of the emitted electrons. The spectrum is obtained as a plot of the number of detected electrons per energy interval versus their kinetic energy. Each element has a unique set of binding energies, so XPS can be used to identify the elements and determine their concentration in the surface. Quantitative data can be obtained from peak heights or peak areas. Variations in the elemental binding energies (the chemical shifts) arise from differences in the chemical potential and polarizability of compounds. These chemical shifts can be used to identify the chemical state of the materials being analyzed.

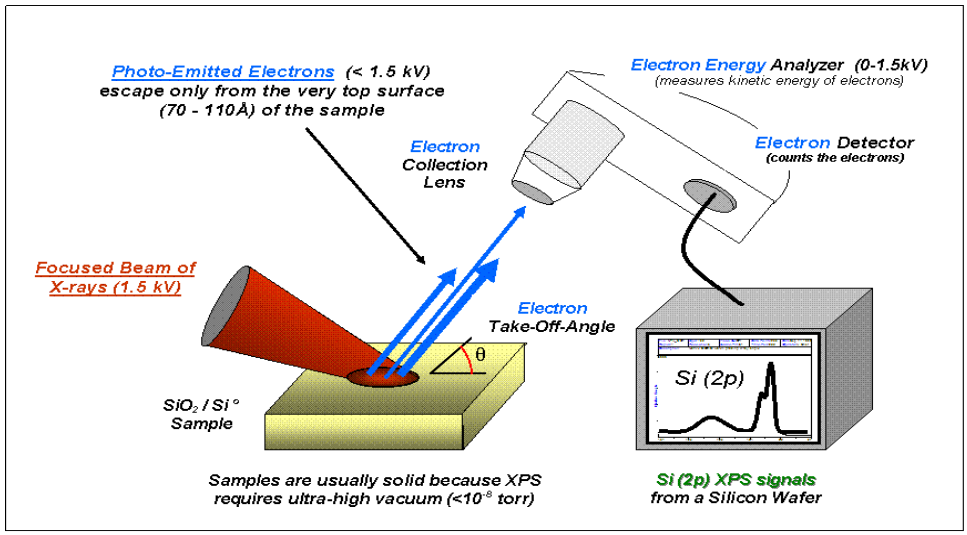

Fig.2.13 Basic components of a monochromic XPS system.

Fig.2.13 shows the basic components of a monochromic XPS system. XPS is a quantitative spectroscopic technique that measures the elemental composition, empirical formula, chemical state and electronic state of the elements that exist within a material. XPS spectra are obtained by irradiating a material with a beam of aluminium or magnesium X-rays while simultaneously measuring the kinetic energy (KE) and number of electrons that escape from the top 1 to 10 nm of the material being analyzed. XPS requires ultra-high vacuum (UHV) conditions. XPS is a surface chemical analysis technique that can be used to analyze the

surface chemistry of a material in its "as received" state, or after some treatment such as: fracturing, cutting or scraping in air or UHV to expose the bulk chemistry, ion beam etching to clean off some of the surface contamination, exposure to heat to study the changes due to heating, exposure to reactive gases or solutions, exposure to ion beam implant, exposure to ultraviolet light, for example.

2.3.9 Ultraviolet-Visible Optical Absorption Technique

Ultraviolet/visible (UV-Vis) spectroscopy is useful as an analytical technique for two reasons. First it can be used to identify some functional groups in molecules and secondly, it can be used for assaying. This second role - determining the content and strength of a substance is extremely useful. The UV-Vis spectroscopy is being widely to study the optical properties of plasma polymerized thin films. Using UV-Vis spectroscopy, the precise information about atomic and molecular structure obtained by investigating the interactions between ultraviolet or visible electromagnetic radiation and matter, some functional groups in molecules can be identified. Moreover, the impurity states, optical absorption coefficients, refractive index, extinction coefficients, optical energy gaps, the allowed direct and indirect forbidden transitions of optically active substances can also be evaluated by using this spectroscopic method. These properties refers to the potential applications such as light guide materials, optical fibers, photo diodes, optical coating to inhibit corrosion, etc. The optical energy gaps and the allowed direct transitions and allowed indirect transitions and forbidden transitions of optically active substances can be determined from the UV-Vis spectroscopic studies for the potential applications such as light guide material, optical fibers, optical coating to inhibit corrosion, etc. [85]. The most important application of UV-Vis spectroscopy is to determine the presence, nature and extent of conjugation present in the material. Increasing conjugation length generally moves the absorption spectrum to longer wavelengths and finally into the visible region.

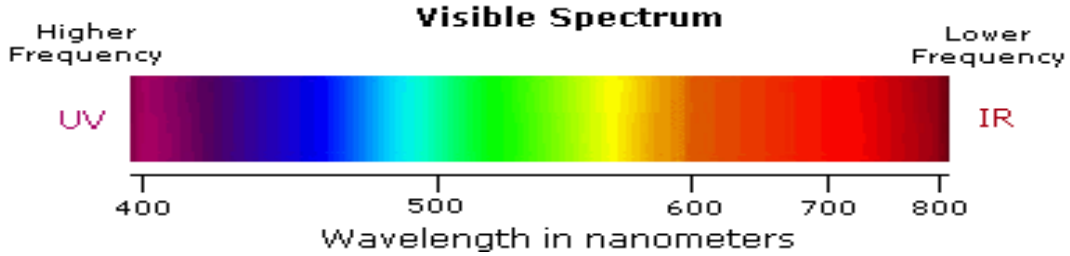

Fig 2.14 The visible region of light in an electromagnetic spectrum

Spectral lines observed in the UV-Visible region correspond to the energy difference between two well-defined electronic energy levels of the absorbing atom or molecule. As the direct relationship between energy and frequency shows that light of lower frequency will carry fewer energetic photons than light of a higher frequency. Therefore, when an atom or molecule absorbs energy in that region, its electrons are promoted from a state of lowest energy, i.e. the ground state, to states, or orbitals, of higher energy. When light either visible or ultraviolet is absorbed by valence electrons these electrons are promoted from their ground states to higher energy states. The energies of the orbital involved in electronic transitions have fixed values. Because energy is quantized, it seems safe to assume that absorption peaks in an UV/Vis spectrum will be sharp peaks. This is because there are also vibrational and rotational energy levels available to absorbing materials, shown in Fig.2.15. These vibrations and rotations also have discrete energy levels, which can be considered as being packed on top of each electronic level.

The absorption of UV-Visible radiation corresponds to the excitation of outer electrons. There are three types of electronic transition, which can be considered;

i) Transitions involving π, σ, and *n* electrons

ii) Transitions involving charge-transfer electrons

iii) Transitions involving *d* and *f* electrons

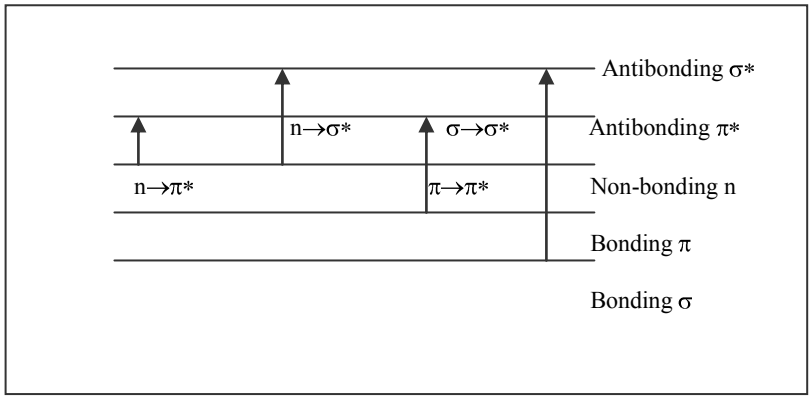

Fig 2.15 Summery of electronic energy levels.

Absorption of UV-Visible radiation in organic molecules is restricted to certain functional groups(chromophores) that contain valence electrons of low excitation energy. The spectrum of a molecule containing these chromophores is complex. This is because the superposition of

rotational and vibrational transitions on the electronic transitions gives a combination of overlapping lines. This appears as a continuous absorption band. Possible electronic transitions of π, σ, and *n* electrons are

$\sigma \rightarrow \sigma^*$ Transitions

An electron in a bonding σ orbital is excited to the corresponding antibonding orbital. The energy required is large. Absorption maxima due to $\sigma \rightarrow \sigma^*$ transitions are not seen in typical UV-Vis spectra (200-800 nm).

n **$\rightarrow \sigma^*$ Transitions**

This transition needs less energy than $\sigma \rightarrow \sigma^*$ transitions. They can be initiated by light whose wavelength is in the range 150-250 nm. The number of organic functional groups with $n \rightarrow \sigma^*$ peaks in the UV region is small.

n **$\rightarrow \pi^*$** and **$\pi \rightarrow \pi^*$ Transitions**

Most absorption spectroscopy of organic compounds is based on transitions of *n* or π electrons to the π^*excited state. This is because the absorption peaks for these transitions fall in an experimentally convenient region of the spectrum (200-800 nm). These transitions need an unsaturated group in the molecule to provide the π electrons.

Molar absorbtivities from $n \rightarrow \pi^*$ are relatively low, and range from 10 to 100 L mol^{-1} cm^{-1}. $\pi \rightarrow \pi^*$ transitions normally give molar absorption. Spectral lines observed in the UV-Visible region lies between 1000 and 10,000 L mol^{-1} cm^{-1}.

The solvent in which the absorbing species is dissolved also has an effect on the spectrum of the species. Peaks resulting from $n \rightarrow \pi^*$ transitions are shifted to shorter wavelength (**blue shift**) with increasing solvent polarity. The reverse (**red shift**) is seen for $\pi \rightarrow \pi^*$ transitions. This effect is greater for the excited state, and so the energy difference between the excited and unexcited states is slightly reduced resulting in a small red shift. This effect also influences transitions but is overshadowed by the blue shift resulting from salvation of lone pairs [86, 87].

Many inorganic species show charge-transfer absorption and are called charge-transfer complexes. For a complex to demonstrate charge-transfer behavior one of its components must have electron-donating properties and another component must be able to accept electrons. Molar absorption from charge transfer absorption are large(greater that 10,000 L mol^{-1} cm^{-1}).

2.3.9.1 Beer-Lambert Law

For most spectra the solution obeys Beer‟s Law. This states that the light absorbed is proportional to the number of absorbing molecules. This is only true for dilute solutions.

A second law- Lambert‟s law tells us that the fraction of radiation absorbed is independent of the intensity of the radiation. Combing these two laws gives the Beer-Lambert law:

$$I = I_o e^{-\alpha d} \qquad 2.1$$

$$\log_e\left(\frac{I_o}{I}\right) = \alpha d \qquad 2.2$$

where is I_o the intensity of the incident radiation, I is the intensity of the transmitted radiation, d is the path length of the absorbing species and α is the absorption co-efficient. The absorption spectrum can be analyzed by Beer-Lambert law which governs the absorption of light by the molecules and states that, “When a beam of monochromatic radiation passes through a homogeneous absorbing medium the rate of decrease in intensity of electromagnetic radiation in UV-Vis region with thickness of the absorbing medium is proportional to the intensity of incident radiation”.

The intensity of transmittance is expressed as the inverse of intensity of absorbance. The absorption co-efficient α, can be calculated from the absorption data using the upper relation

$$\alpha = \frac{2.303A}{d} \qquad 2.3$$

where $A = \log_{10}\left(\frac{I_o}{I}\right)$ is the Absorbance.

2.3.9.2 Direct and Indirect Optical Transitions

In solid state physics and related applied fields, the band gap, also called an energy gap or stop band, is a region where a particle or quasiparticle is forbidden from propagating. For insulators and semiconductors, the band gap generally refers to the energy difference between the top of the valence band and the bottom of the conduction band. Fundamental absorption refers to the annihilation or absorption of photons by the excitation of an electron from the valence band up into the conduction band, leaving a hole in the valence band. Both energy and momentum must be conserved in such a transition.

In the case of an indirect-band gap semiconductor, the minimum energy in the conduction band and the maximum energy in the valence band occur at different values of crystal momentum. Photon energies much larger than the forbidden gap are required to give direct transitions of electrons from the valence to the conduction band. However, transitions can occur at lower energies by a two-step process involving not only photons and electrons but also a third particle, a phonon.

To estimate the nature of absorption a random phase model is used where the k momentum selection rate is completely relaxed. The integrated density of states *N(E)* has been used and defined by

$$N(E) = \int_{-\infty}^{+\infty} g(E)dE \qquad 2.4$$

The density of states per unit energy interval may be represented by

$$g(E) = \frac{1}{V}\sum \delta(E - E_n) \qquad 2.5$$

where V is the volume, E is the energy at which $g(E)$ is to be evaluated and E_n is the energy of the nth state.

If $g_v \propto E^p$ and $g_c \propto (E\text{-}E_{opt})$, where energies are measured from the valance band mobility edge in the conduction band (mobility gap), and substituting these values into an expression for the random phase approximation, the relationship obtained

$v^2 I_2(v) \propto (h\,v\text{-}E_0)^{p+q+1}$, where $I_2(v)$ is the imaginary part of the complex permittivity. If the density of states of both band edges is parabolic, then the photon energy dependence of the absorption becomes

$$\alpha h\nu \propto \nu^2 I_2(\nu) \propto (h\,\nu\text{-}E_{opt})^2. \qquad 2.6$$

So for higher photon energies the simplified general equation which is known as Tauc relation is,

$$\alpha h\nu = B(h\nu - E_{\text{opt}})^n \qquad 2.7$$

where $h\nu$ is the energy of absorbed light, n is the parameter connected with distribution of the density of states and B, a constant or Tauc parameter and here $n = 1/2$ for direct and $n = 2$ for indirect transitions [88].

The above equation can be written as

$$\frac{d[\ln(\alpha h\nu)]}{d[h\nu]} = \frac{n}{h\nu - E_{opt}}$$

When finding the n, type of transition can be obtained from the absorption spectrum. A discontinuity in the d[ln(αhv)]/d(hv) versus hv plot at the band gap energy (E_{opt} or E_g), i.e. at $hv = E_g$ can be observed. The discontinuity at a particular energy value gives the band gap E_g, Thus from the straight-line plots of $(\alpha hv)^2$ versus hv and $(\alpha hv)^{1/2}$ versus hv the direct and indirect energy gaps of PPTMA thin films can be determined.

There are two kinds of optical transition at the fundamental edge of crystalline and non crystalline semiconductors, direct transitions and indirect transition, both of which involve the interaction of an electromagnetic wave with an electron in the valance band, which is then raised across the fundamental gap to the conduction band. For the direct optical transition from the valence band to the conduction band, it is essential that the wave vector for the electron be unchanged. In the case of indirect transition the interactions with lattice vibrations (phonons) take place; thus the wave vector of the electron can change in the optical transition and the momentum change will be taken or given up by photons. In other words, if the minimum of the conduction band lies in a different part of *k*-space from the maximum of the valence band, a direct optical transition from the top of the valence band to the bottom of the conduction band is forbidden.

2.6 Theories on Electrical Conduction Mechanism

2.6.1 Direct Current Electrical Conduction Mechanism

In the dc electrical conduction in plasma-polymerized materials, the carriers may either be electronic or ionic in nature and conduction is considered through the film, rather than along the plane of the film. The low field properties, which are usually ohmic in nature, but the high field electrical properties cannot describe by a single conduction process; usually the various field strength ranges manifest different electrical conduction phenomena. The materials, which have energy gaps more than 2 eV or above, the electrical properties may bear no resemblance to what is intrinsically expected of such an insulating material. So this is clear that the electrical properties of thin film insulators are determined not only by the intrinsic properties of the insulator but also by other properties, such as the nature of the electrical-insulator contact. The dc conduction mechanisms in different plasma-polymerized thin films have reported is the following :

i) **Schottky mechanism:** In this mechanism, the injection of carriers from electrode is performed by means of thermal or field-assisted emission.

ii) **PF mechanism:** If the carriers are produced by the dissociation of donor-acceptor centers in the bulk of the material, the process of conduction is then called PF mechanism.

iii) **SCL conduction mechanism:** In case of SCL conduction the transport by the carriers is slower than the generation and it constitutes a rate-determining step.

In general, if the carrier generation process is slower than transport of the carriers through a dielectric, the conduction is controlled either by Schottky or PF mechanism.[89-92].

At reasonable applied fields there will normally be a sufficient supply of carriers available to enter the insulator from the cathode(negatively biased electrode) to replenish the carriers drawn out of the bulk of the insulator. Under these conditions the J-V characteristics of the sample will be controlled primarily by conditions existing at the cathode-insulator interface; this conduction process is referred to as being emission-limited or contact-limited.

A power law can express the variation of current density with voltage in a material generally:

$$J \propto V^n \qquad 2.10$$

where, *n* is a power factor. When n is unity, the conduction is ohmic. If the value of n is more than unity, then the conduction process is other than ohmic. These are described in the following sections.

2.6.1.1.Schottky mechanism

The Schottky effect is the image force induced lowering potential energy for charge carrier emission when an electric field is applied. The image force effect plays an important role in the conduction process. The potential step at a neutral barrier in the presence of image force as a function of distance (x) from the metal-insulator interface is given by

$$\varphi(x) = \varphi_0 + \varphi(x) = \varphi_0 - \frac{e^2}{16\pi\varepsilon_0\ \varepsilon' x} \qquad 2.11$$

where, $\varphi_{im}(x) = -\frac{e^2}{16\pi\varepsilon_o\varepsilon' x}$ is the potential energy of electron due to image force. The barrier $\varphi(x)$ in the presence of image forces is illustrated by the line AB in Fig. 2.16 is not valid at the electrode surface.

The potential energy with respect to the Fermi level of the electrode is now given by

$$\varphi(x) = \varphi_o - \frac{e^2}{16\pi\varepsilon_o\varepsilon' x} - eFx \qquad 2.12$$

The change $\Delta\varphi_s = \varphi_o - \varphi(x)$ in the barrier height due to the interaction of the applied field with the image potential is given by

$$\Delta\varphi_s = -\left(\frac{e^3}{4\pi\varepsilon_o\varepsilon'}\right)^{1/2} F^{1/2} = \beta_s F^{1/2} \qquad 2.13$$

where $\beta_s = \left(\frac{e^3}{4\pi\varepsilon_o\varepsilon'}\right)^{1/2}$ 2.14

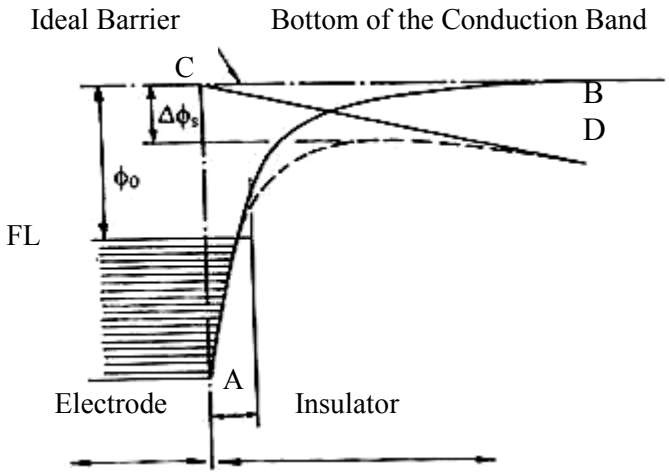

Fig 2.16 Schottky effect at a neutral contact.

is Schottky coefficient. Because of the image force lowering of the barrier, the electrode-limited current obeys the Richardson-Schottky law

$$J = AT^2 \exp[-(\varphi_o - \Delta\varphi_s)/kT] \qquad 2.15$$

This equation was first applied successfully to metal-vacuum interfaces.

2.6.1.2 Poole-Frenkel mechanism

The PF effect is the bulk analog of the Schottky effect at an interfacial barrier. This effect is also known as field-assisted thermal ionization process. As the potential energy of an electron in a Coulombic field $-e^2/4\pi\varepsilon' x$ is four times that due to the image force effects, the Poole-Frenkel attenuation of a Coulombic barrier $\Delta\varphi_{PF}$, uniform electric field is twice that due to the Schottky effect at a neutral barrier:

$$\Delta\varphi_{PF} = 2\Delta\varphi_s = 2\left(\frac{e^3}{4\pi\varepsilon_o\varepsilon'}\right)^{1/2} F^{1/2} = \beta_{PF}F^{1/2} \qquad 2.16$$

With the applied field, the Coulombic barrier height between electrode and the film is lowered, and the carrier can escape more easily giving rise to field assisted conductivity:

$$\sigma = \sigma_o \exp\left[\frac{\beta_{PF}F^{1/2}}{2kT}\right] \qquad 2.17$$

where F = V/d, is the dc applied field, k is Boltzmann constant, T is the absolute temperature, σ_o is the low field conductivity, β_{PF} is the Poole-Frenkel co-efficient and is given by

$$\beta_{PF} = 2\left[\frac{e^3}{4\pi\varepsilon_o\varepsilon'}\right]^{1/2} = 2\beta_s \qquad 2.18$$

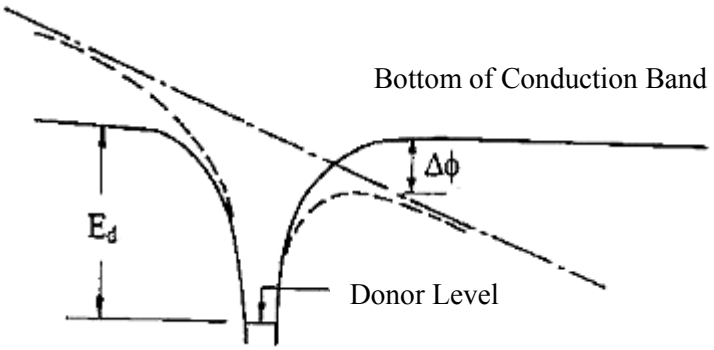

Fig 2.17 Poole-Frenkel effect at a donor center.

The general expression for J that is equally valid for both the PF and Schottky mechanisms is of the form

$$J = J_o \exp\left[\frac{\beta F^{1/2} - \varphi}{kT}\right] \qquad 2.19$$

where J_o is the low field current density; β is the coefficient: F is the static electric field and φ is the ionization energy of the localized centers in Poole-Frenkel conduction (it involves the emission of trapped electrons (holes) from localized centers or potential wells within the dielectric) and Coulomic barrier height of the electrode-polymer interface in Schottky conduction (it results from injection of electrons or holes from the electrodes into the conduction band of the dielectric.

2.6.1.3 Space charge limited conduction mechanism

Space charge is a concept in which excess electric charge is treated as a continuum of charge distributed over a region of space (either a volume or an area) rather than distinct point-like charges. This model typically applies when charge carriers have been emitted from some region of a solid the cloud of emitted carriers can form a space charge region if they are sufficiently spread out, or the charged atoms or molecules left behind in the solid can form a space charge region. Space charge usually only occurs in dielectric media (including vacuum) because in a conductive medium the charge tends to be rapidly neutralized or screened. The sign of the space charge can be either negative or positive. This situation is perhaps most familiar in the area near a metal object when it is heated to incandescence in a vacuum. This effect was first observed by Thomas Edison in light bulb filaments, where it is sometimes called the Edison effect, but space charge is a significant phenomenon in many vacuum and solid-state electronic devices.

The mechanism of electrical conduction in thin insulating films has been discussed by Lamb and several important theoretical modes have been put forwarded. Dielectric materials, which are basically insulators, are capable of carrying electric currents by virtue of carriers injected at one or both the electrodes. According to the basic assumptions, if an ohmic contact is made at the surface of an insulator, electrons flow from the metal to the conduction band of the insulator.

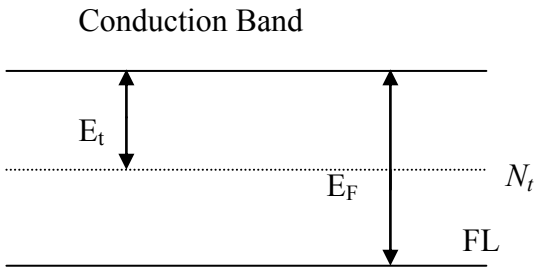

Fig 2.18 Energy diagram showing shallow traps in an insulator.

Due to the injected charges near the electrodes, there is a generation of space charge near the electrodes, which affect the conduction mechanism. As an effect, ohmic conduction changes into SCL conduction as the applied electric field is increased. When a bias is applied to the system, an insulator having two ohmic contacts on its surface. The result of the applied bias is

to add positive charge to the anode and negative charge to the cathode. As the voltage bias increases, the net positive charge on the anode increases and that on the cathode decreases then the current density would be

$$J = \frac{9}{8}\varepsilon'\varepsilon_o\mu\frac{V^2}{d^3} \qquad 2.20$$

Where μ is the mobility of charge carriers, ε′ is dielectric constant, ε_o is the permittivity of free space, V is the applied voltage, d is the thickness. Eqn 2.20 predicts that SCL current is directly proportional to V^2 and inversely proportional to d^3.

Practically, the character and the magnitude of SCL conduction are modified due to the presence of localized trapping centers which try to immobilize the injected charge carriers. If the insulator contains N_t shallow traps positioned an energy E_t below the conduction band and N_o is the number of charge carriers, shown in Fig.2.18 then the free component of the space charge

$$p_f = eN_c \exp\left(\frac{-E_F}{kT}\right) \qquad 2.21$$

and trapped component of the space charge

$$p_t = eN_t \exp\left[-\frac{E_F - E_t}{kT}\right] \qquad 2.22$$

thus the trapping factor, θ is defined as

$$\theta \equiv \frac{p_f}{p_t} = \frac{N_c}{N_t}\exp\left(\frac{-E_t}{kT}\right) \qquad 2.23$$

The SCL current density with traps is defined by:

$$J = \frac{9}{8}\varepsilon'\varepsilon_o\mu\frac{V^2}{d^3}\theta \qquad 2.24$$

For a shallow trap SCLC and trap-free SCLC, θ =1. According to eqn 2.24 J varies as d^{-1} in the ohmic region and as d^{-3} in the SCLC region except for the trap-filled SCLC part. In eqn 2.24 it can be seen that for a fixed V, the dependence of ln J on ln d should be linear with slope $l \geq -3$.

The voltage at which transition from the ohmic region to the shallow trap SCLC region (V_{tr}) occurs is given by

$$V_{tr} = \frac{8}{9} n_0 \frac{ed^2}{\varepsilon'} \qquad 2.25$$

where n_o is independent of both μ and J. This value will be defined from the extrapolated parts of the respective current region in the lnJ - lnV curves.

Traps are locations that arise from disorders, dangling bonds, impurity etc. Very often, the traps capture free charge carriers and thus play a very significant role in the conduction process. However, generally in amorphous and polycrystalline organic material, electrical charge transport is always accompanied by more or less frequent capture of charge carriers in these localized states. Such trapped carriers may be released after specific retention period or may recombine with opposite charge carriers. Traps may be classified into two types: electron traps and hole traps.

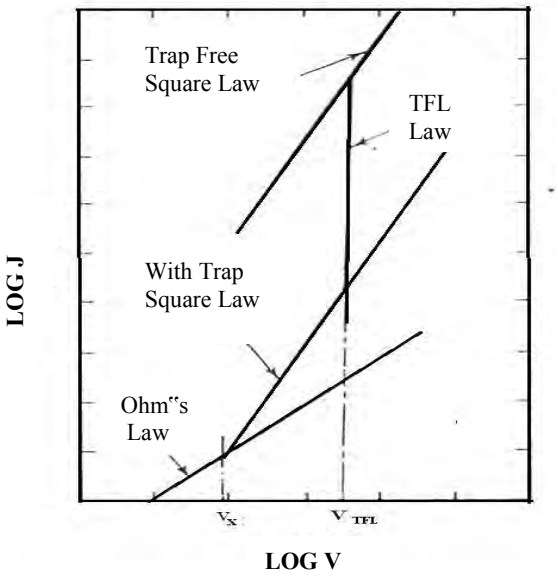

Fig.2.19 Trap process in space charge limited conduction mechanism.

There are several experimental methods for the detection of trap state, but most of them allowing only for an indirect conclusion on the energy distribution. Some of the most common methods are optically simulated current (OSC), thermally stimulated current (TSC), thermally stimulated luminescence (TSL) and J-V characteristics. Among them J-V characteristics method is widely used (Fig.2.19). In this method, space charge limited current with traps model is applied on experimentally observed electrical properties of the sample. By applying analytical method to this model, both information on the charge carrier mobility and the trap energy distribution are determined. Therefore a J-V characteristics method is used to

determine the trap depth as well as trap distribution. It gives very precise information related to the trap energy distribution and depth as compared with other experimental trap detection techniques.

2.6.2 Thermally Activated Conduction Process

2.4.2.1 Electronic conduction

Electrical conduction is the movement of electrically charged particles through a transmission medium. The band theory of solids has been applied to understand the electrical behavior of polymers. An important featured of the band system is that electrons are delocalized or spread over the lattice. Some delocalization is expected when an atomic orbital or any atom overlaps appreciably with those of more than one of its neighbors, but delocalization reaches an extreme form in the case of a regular 3-D lattice. The band theory assumes that the electrons are delocalized and can extend over the lattice. When electronic conduction is considered in polymers, band theory is not totally suitable because the atoms are covalently bonded to one another, forming polymeric chains that experience weak intermolecular interactions. But macroscopic conduction will require electron movement, not only along the chains but also from one chain to another.

The carrier mobility in organic molecules is usually very low. This is due to the fact that electrons, while jumping from one molecule to another, lose some energy. But the nobilities of electrons are found to increase with molecular size in such type of compounds. In polymer system, the conductivity is influenced by the factors such as dopant level, morphology of polymer, concentration of conducting species, temperature, etc. The temperature dependence of conductivity can be described by an Arrhenius type of eqn.

$$\sigma = \sigma_o \exp[-\Delta E/kT] \qquad 2.26$$

where ΔE is the activation energy for carrier generation. The plot of logσ vs 1/T must be linear for thermally activated conduction.

2.6.2.2 Hopping Conduction

Disorder in a lattice affects both the energetic and spatial distribution of electronic states. For a random distribution of atoms the density of electronic energy states tails into what is the electrons in these tails are localized. When the electrons are excited to higher energy,

conduction via localized electron implies discrete jumps across an energy barrier from one site to the next as shown in Fig.2.20.

An electron may either "hop" over or "tunnel" through the top of the barrier; the relative importance of these two mechanism depending on the shape of the barrier and the availability of the thermal energy.

For variable range hopping the electrical conductivity is given by

$$\sigma = \sigma_o \, exp - \left(\frac{T_o}{T} \right)^{\frac{1}{d+1}} \qquad 2.27$$

Where "d" is the dimensionality of transport, σ is the conductivity, σ_o is the initial value of conductivity, T is the absolute temperature and T_o is the activation energy in terms of temperature.

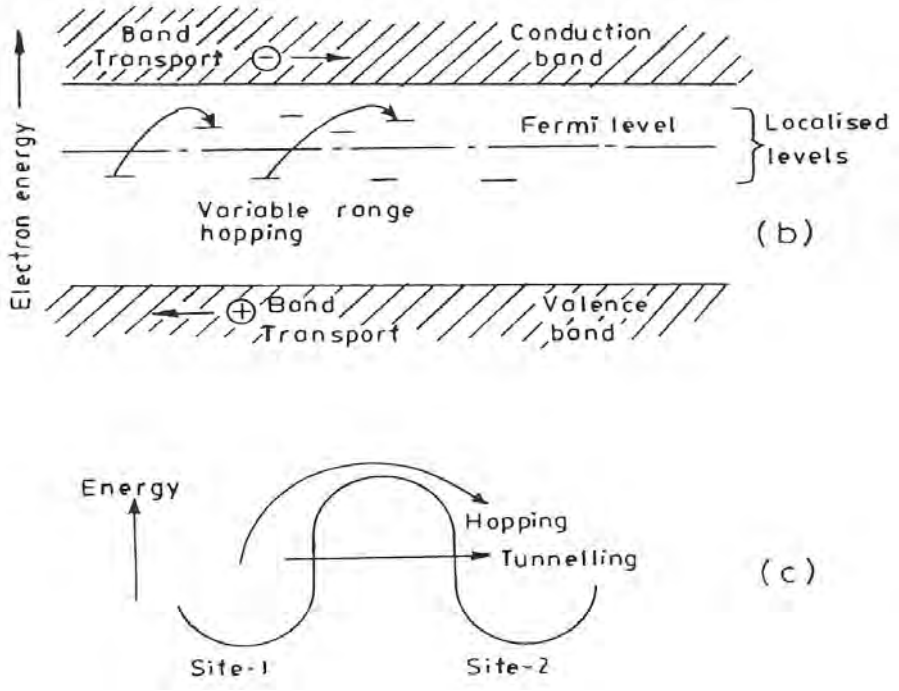

Fig 2.20 Diagram of electron-transfer mechanisms between adjacent sites separated by a potential-energy barrier.

2.6.3 Alternating Current Electrical Properties

2.6.3.1 Theory of Dielectrics

A dielectric is an electrical insulator that can be polarized by an applied electric field. When a dielectric is placed in an electric field, electric charges do not flow through the material, as in

a conductor, but only slightly shift from their average equilibrium positions causing dielectric polarization. Because of dielectric polarization, positive charges are displaced toward the field and negative charges shift in the opposite direction. This creates an internal electric field that partly compensates the external field inside the dielectric. If a dielectric is composed of weakly bonded molecules, those molecules not only become polarized, but also reorient so that their symmetry axis aligns to the field [92-95]

Thin films produced through glow discharge are known to have free radicals or polar groups independent of the nature of monomers. Owing to this reason, these polymers are good candidates for the investigation of dielectric properties. The ac conductivity and dielectric properties of plasma polymerized thin films provide information about the conduction process, dielectric constant, relaxation process, etc. which are dependent on the frequency and temperature. The capacitance of a parallel plate capacitor having a dielectric medium is expressed as

$$C = \frac{\varepsilon_0 \varepsilon^{/} A}{d} \qquad 2.28$$

where ε_0 is the permittivity of free space, $\varepsilon^{/}$ is the dielectric constant of the medium, A is the surface area of each of the plates/electrodes and d is the thickness of the dielectric. The parameters such as angular frequency (ω) of the applied field, the parallel resistance R_p, parallel capacitance C_p and the series resistance R_s and series capacitance C_s are related to the $\varepsilon^{/}$, dielectric dissipation factor ε'' and loss tangent as

$$\varepsilon^{/} = \frac{C_p}{C_0} \qquad 2.29$$

$$\varepsilon^{//} = \frac{1}{R_p C_p \omega} \qquad 2.30$$

$$\text{and} \quad \tan\delta = \frac{\varepsilon^{//}}{\varepsilon^{/}} = \frac{1}{R_p C_p \omega} \qquad 2.31$$

The conductivity of σ_{ac}, was calculated using equation

$$\sigma_{ac}(\omega) = G_p d/A \qquad 2.32$$

The dependence of ac conductivity, σ_{ac}, on frequency may be described by the power law,

$$\sigma_{ac}(\omega)=A\omega^{n} \qquad 2.33$$

where A is a proportionality constant and ω *(=2πf, f* is the linear frequency) is the angular frequency and n is the exponent which generally takes the valve less than unity for Debye type mechanism and is used to understand the conduction/relaxation mechanism in amorphous materals.

The dielectric behavior of a material is usually decribed by Debye dispersion equation $\varepsilon^{*}(\omega,T)=\varepsilon'-i\varepsilon''$ where ε is the complex dielectric permittibity, ε' (energy dissipated per cycle) is the real part of complex dielectric permittivity and ε'' (energy stored per cycle) is the imaginary part of the complex dielectric permittivity,

$$\varepsilon' = \varepsilon_{\infty} + \frac{\varepsilon_o - \varepsilon_{\infty}}{1+\omega^2\,\tau^2} \qquad 2.34$$

$$\varepsilon'' = \frac{(\varepsilon_o - \varepsilon_{\infty})\omega\tau}{1+\varepsilon^2\tau^2} \qquad 2.35$$

where ε_o is the static or relaxed dielectric constant at *(ω=0)*. Dielectric relaxation is the momentary delay (or lag) in the dielectric constant of a material. This is usually caused by the delay in molecular polarization with respect to a changing electric field in a dielectric medium (e.g. inside capacitors or between two large conducting surfaces). Dielectric relaxation in changing electric fields could be considered analogous to hysteresis in changing magnetic fields (for inductors or transformers). Relaxation in general is a delay or lag in the response of a linear system, and therefore dielectric relaxation is measured relative to the expected linear steady state (equilibrium) dielectric values. The time lag between electrical field and polarization implies an irreversible degradation of free energy.

In physics, dielectric relaxation refers to the relaxation response of a dielectric medium to an external electric field of microwave frequencies. This relaxation is often described in terms of permittivity as a function of frequency, which can, for ideal systems, be described by the Debye equation. On the other hand, the distortion related to ionic and electronic polarization shows behavior of the resonance or oscillator type. The character of the distortion process depends on the structure, composition, and surroundings of the sample.

2.6.3.2 The Cole-Cole Function

The difference in dielectric constant measured al low and high frequencies is called the strength of the relaxation. The Cole-Cole equation is a dielectric relaxation model that constitutes a special case of Havriliak-Negami relaxation when the symmetry parameter (β) is equal to 1 - that is, when the relaxation peaks are symmetric:

$$\varepsilon^*(\omega) - \varepsilon_\infty = \frac{\varepsilon_S - \varepsilon_\infty}{1 + (i\omega\tau)^{1-\alpha}} \qquad 2.36$$

Where ε^* is the complex dielectric constant, ε_s and ε_∞ are the "static" and "infinite frequency" dielectric constants, ω is the angular frequency and τ is a relaxation constant. The parameter α, which takes a value between 0 and 1, is an experimentally determined correction factor. When $\alpha = 0$, the Cole-Cole model reduces to the Debye model. The dielectric behavior of a material is usually described by using Debye dispersion equation [95-97]

$$\varepsilon = \varepsilon' - i\varepsilon'' = \varepsilon_\infty + \frac{\varepsilon_0 - \varepsilon_\infty}{1 + (\omega\tau)^2} \qquad 2.37$$

where ε_0 is the static or relaxed dielectric constant at ($\omega = 0$), ε_∞ is the high frequency or unrelaxed dielectric constant and the quantity τ is a characteristic time constant, usually called the dielectric relaxation time. For distribution of relaxation time, the complex permittivity can be represented by Cole and Cole law

$$\varepsilon^* = \varepsilon_\infty + \frac{(\varepsilon_0 - \varepsilon_\infty)}{1 + (i\omega\tau_0)^\beta} \qquad 2.38$$

The parameter β is the representative of relaxation-time distribution. The Cole-Cole curve is useful to understand the degree of the distribution of the relaxation times. The variation of real and imaginary parts of ε for a PPTMA thin film as functions of temperature and frequency in the form of Cole-Cole plots. In general, a full, or a partial or no arc is observed depending on relaxation strength in the sample with in experimentally available frequency range. When the angle between the two radii of the Cole-Cole curve is defined as βπ, the factor β indicates the degree of distribution of the relaxation time.

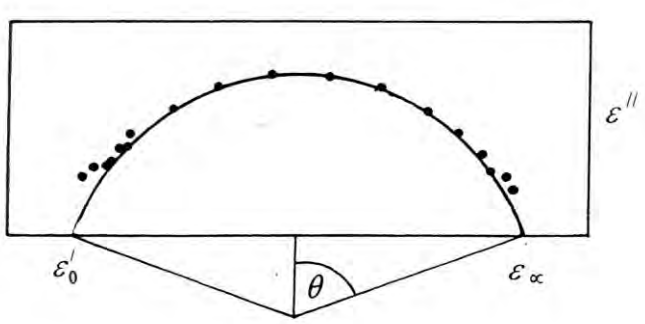

Fig: 2.21 Cole-Cole circular plot.

2.6.3.3 Temperature dependent relaxation

Since the relaxation times are found to be temperature dependent, a complete study of the dielectric properties might be represented by contour maps of ε and ε'' against frequency f and temperature T. The frequency f_{max}, at which ε'' is maximum, is determined and is treated as analogous to rate constant. Thus, a convenient summary of the effect of temperature on the relaxation process is a plot of $\log f_{max}$ versus 1/T or relaxation map [97, 98]. If the characteristic of a specimen is the principal goal, the loss verse temperature plot is required. For this, a number of relaxation curves $\log f_{max}$ versus $1/T$ are to be presented, and then the activation energy can be calculated.

The various dielectric relaxation may be observed in the scan of dielectric loss at constant frequency as presented in Fig.2.22. With the increase in temperature, the molecular mobility"s of various kinds of a material become successively energized and available for dipolar orientation. By convention, the dielectric relaxation processes are labeled as α,β,γ and so on, beginning at the high temperature end. The same relaxation processes were generally responsible for dispersions in mechanical properties too, although a particular molecular rearrangement process may produce stronger dielectric than mechanical effect or vice versa. In case of amorphous solid polymer, there is always a high temperature α-relaxation associated with the micro-Brownian motion of the whole chains and in addition, at least, one low temperature (β, γ etc.) auxiliary relaxation may occur.

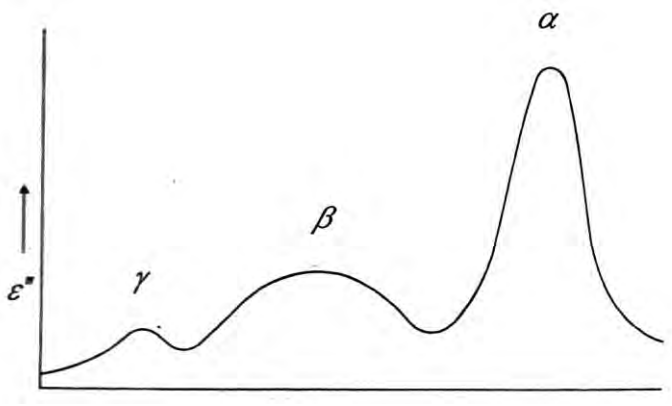

Fig: 2.22 The various dielectric relaxations in the scan of dielectric loss with temperature at constant frequency.

The relative strength of α and β relaxations depends on how much orientation of the tail groups can occur through the limited mobility allowed by the β process before the more difficult but more extensive mobility of the α process comes into play; there is a partitioning of the total dipolar alignment among the molecular rearrangement processes.

The high frequency β, γ auxiliary peaks in amorphous polymers are characteristically very broad with half height width of several decades, although, a good linear Arrhenius plot is usually obtained suggesting a non-cooperative mechanism.

CHAPTER 3

Experimental Details

3.1 Introduction

This chapter describes the details of the monomer, substrates materials, capacitively coupled plasma polymerization set up for thin film deposition, modification of the system, generation of glow discharge plasma, thickness measurement, experimental procedure on EA, IR, SEM, DTA/TGA, UV-Visible, electrical formation and electrode deposition of PPTMA thin films.

3.2 The Monomer

N,N,3,5 tetramethylaniline (TMA) was used as a organic precursor (Aldrich-Chemie D-7924, Steinheim, Germany). Its chemical formula is $(CH_3)_2C_6H_3N(CH_3)_2$. It is a colored (orange) liquid with boiling point 499 ± 2 K. Its density is 0.913 ml and refractive index is 1.5443. It was used without further purification. TMA contains four methyl groups where two groups are attached to the nitrogen atom. The chemical structure of the monomer is shown in Fig.3.1. The ionic form of TMA was dissolved in the organic phase after formation of a salt soluble.

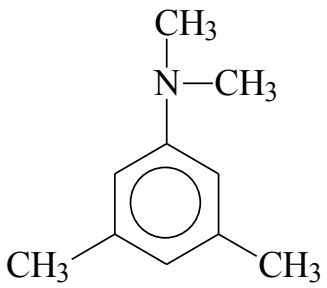

Fig 3.1 The structure of N,N,3,5 tetramethylaniline

3.3 Substrate Materials

Glass (Clear Glass, Sail Brand, China) was used as substrates. The substrates used were pre-cleaned glass slides (25.4mm × 76.2mm × 1.2mm) purchased from local market. Electrodes and PPTMA thin films were deposited onto them.

Before depositing the films, each substrate was chemically cleaned. For chemical cleaning, the substrates were kept in concentrated nitric acid for an hour and then cleaned with distilled water. After rinsing with distilled water the substrates were put in concentrated sodium hydroxide solution for more than half an hour and then washed with distilled water. The substrates were then kept in potassium dichromate solution for more than half an hour and

then rinsed with distilled water. Finally, the cleaned substrates were rinsed with carbon tetrachloride and distilled water. Then the substrates were dried in the vacuum oven for 10 min at 453 K and were preserved in desiccator for use.

3.4 Capacitively Coupled Plasma Polymerization Set-up

Plasma polymerization takes place in a glow discharge excited in a monomer gas or vapor, or their mixture with argon, providing thus the dielectric (polymeric) component of the composite.

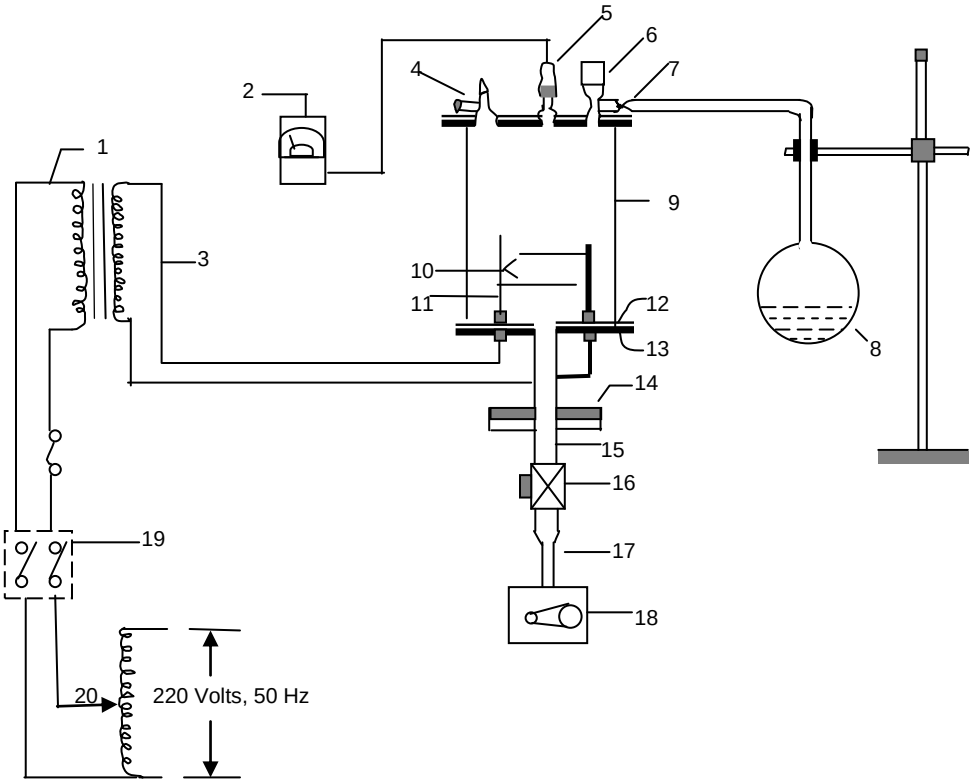

Fig.3.2 Schematic diagram of the plasma polymerization system (1 high voltage power supply, 2 pirani gage, 3 high tension leads, 4 gas inlet valve, 5 guage head, 6 monomer injection valve, 7 flowmeter, 8 monomer container, 9 Pyrex glass dome, 10 metal electrodes, 11 electrode stands, 12 gasket, 13, lower flange, 14 bottom flange, 15 brass tube, 16 valve, 17 liquid nitrogen trap, 18 rotary pump, 19 switch and 20 variac).

Plasma reaction chamber

A cylindrical Pyrex glass bell-jar having 0.15m in inner diameter and 0.18 m in length was used as a plasma chamber. The top and bottom edges of the glass bell-jar are covered with two rubber L-shaped (height and base 0.015m, thickness, 0.001 m) gaskets. The cylindrical

glass bell jar is placed on the lower flange. The lower flange is well fitted with the diffusion pump by a I joint. The upper flange is placed on the top edge of the bell-jar. The flange is made up of brass having 0.01 m in thickness and 0.25 m in diameter. On the upper flange a laybold pressure gauge head, Edwards high vacuum gas inlet valve and a monomer injection valve are fitted. In the lower flange two highly insulated high voltage feed-through are attached housing screwed copper connectors of 0.01m high and 0.004 m in diameter via Teflon^{TM} insulation.

Electrode system

In the present set-up capacitively coupled electrode system was used. Two circular stainless steel plates of diameter 0.09 m and thickness of 0.001 m are connected to the high voltage copper connectors. The inter-electrode separation can be changed by moving the electrodes through the electrode stands. After adjusting the distance between the electrodes they are fixed with the stands by means of screws. The substrates are usually kept on either of the electrodes for plasma deposition.

Pumping unit

For creating laboratory plasma, first step is pumping out the air/gas from the plasma chamber. In this system a rotary pump of vacumbrand (Vacumbrand GMBH & Co: Germany) is used.

Vacuum pressure gauge

A vacuum pressure gauge head (Laybold AG) and a meter (ThermotronTM 120) of Laybold, Germany, are used to measure inside pressure of the plasma deposition chamber.

Input power for plasma generation

The input power supply for plasma excitation comprises of a step-up high-tension transformer and a variac. The voltage ratio at the output of the high-tension transformer is about 16 times that of the output of the variac. The maximum output of the variac is 220 V and that of the transformer is about 3.5 KV with a maximum current of 100 mA. The deposition rate increases with power at first and then becomes independent of power at high power values at constant pressure and flow rate.

Monomer injecting system

The monomer injecting system consists of a conical flask of 25 ml capacity and a pyrex glass tube with capillarity at the end portion. The capillary portion is well fitted with metallic tube

of the nozzle of the high vacuum needle valve. The conical flask with its components is fixed by stand-clamp arrangement.

Fig.3.3 Plasma polymerization system.

Supporting frame

A metal frame of dimension 1.15mX0.76mX0.09m is fabricated with iron angle rods, which can hold the components described above. The upper and lower bases of the frame are made with polished wooden sheets. The wooden parts of the frame are varnished and the metallic parts are painted to keep it rust free. The pumping unit is placed on the lowed base of the frame. On the upper base a suitable hole is made in the wooden sheet so that the bottom flange can be fitted with nut and bolts.

Flowmeter

The system pressure of a gas flow is determined by the feed in rate of a gas and the pumping out rate of a vacuum system. The monomer flow rate is determined by a flowmeter. So flowmeters are used in plasma polymerization system to control the monomer deposition rate. In the plasma polymerization set up a flowmeter (Glass Precision Engineering LTD, Meterate, England) is attached between the needle valve and the monomer bottle.

Liquid nitrogen trap

Cold trap, particularly a liquid N_2 trap, acts as a trap pump for different type gas. The liquid N_2 trap system is placed in the fore line of the reactor chamber before the pumping unit in the

plasma deposition system. It consists of a cylindrical shape chamber having 6.4 cm diameter and 11.5 cm in length using brass material. The cross-sectional view of the liquid N_2 chamber is shown in Fig 3.4.

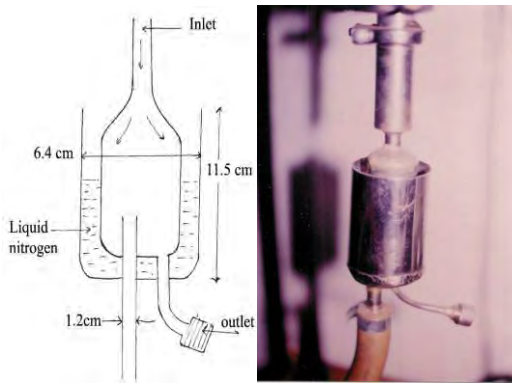

Fig. 3.4 The cross-sectional view and photograph of liquid nitrogen trap.

3.5 Generation of Glow Discharge Plasma

Glow discharges are produced by an applied static or oscillating electric field where energy is transferred to free electrons in vacuum. Inelastic collisions of the energetic free electrons with the gas molecules generate free radicals, ions, and species in electronically excited states. This process also generates more free electrons, which is necessary for a self-sustaining glow [5, 6, 96]. The excited species produced are very active and can react with the surfaces of the reactors as well as themselves in the gas phase.

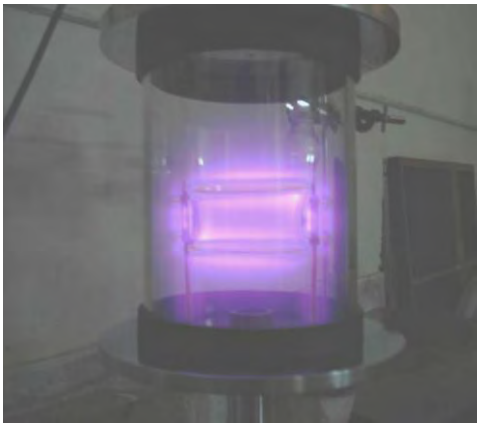

Fig.3.5 Glow discharge plasma during deposition.

The important feature of glow discharge plasma is the non-equilibrium state of the overall system. In the plasmas considered for the purpose of plasma polymerization, most of the

negative charges are electrons and most of the positive charges are ions. Due to large mass difference between electrons and ions, the electrons are very mobile as compared to the nearly stationary positive ions and carry most of the current. Energetic electrons as well as ions, free radicals, and vacuum ultraviolet light can possess energies well in excess of the energy sufficient to break the bonds of typical organic monomer molecules which range from approximately 3 to 10 eV. Some typical energy of plasma species available in glow discharge as well as bond energies encountered of approximately 0 .133 Pa.

The chamber of the plasma polymerization unit and monomer container is evacuated to about 0.13 Pa. The monomer vapor is then injected to the chamber slowly for some time. A high-tension transformer along with a variac is connected to the feed-through attached to the lower flange. While increasing the applied voltage, light bluish colors monomer plasma is produced across the electrodes about 13.3 Pa. Fig. 3.3 shows the photograph of plasma deposition set-up and Fig. 3.5 is the photograph of glow discharge plasma across the electrodes in the capacitively coupled parallel plate discharge chamber.

3.6 Plasma Polymer Thin Film Formation

The electric field, when applied to the gaseous monomers at low pressures (0.01 to 1 mbar), produces active species that may react to form cross-linked polymer films. In this experiments, air was used as the primary plasma, and the monomer TMA vapor was injected downstream of the primary air glow discharge. In laboratory PPTMA thin films were prepared using a bell-jar type capacitively coupled glow discharge system described earlier. The boiling point of TMA is about 499 K. So in order to deposit good PPTMA films the natural flow of monomer gas during deposition is not suitable. To increase the flow rate the container filled with TMA liquid is heated using a heating mantle. The conditions to prepare PPTMA thin films were 40W rf power, 0.15 mbar system pressure, and the monomer flow rate was kept 20cm^3/min. The deposition times for these films were varied from 30 minute to 120 minute in order to get films of different thicknesses.

3.7 Measurement of Thickness of the Thin Films

Thickness is the single most significant film parameter. Any physical quantity related to film thickness can in principle be used to measure the film thickness. It may be measured either by several methods with varying degrees of accuracy. The methods chosen on the basis of their

convenience, simplicity and reliability. Several of the common methods are i) During Evaporation, ii) Multiple-Beam Interferometry, iii) Using a Hysteresisgraph and other methods used in film-thickness determination with particular reference to their relative merits and accuracies. Multiple-beam interferometry technique was employed for the measurement of thickness of the thin films. This technique described below.

Multiple-Beam Inferferometry [103]

This method utilizes the resulting interference effects when two silvered surfaces are brought close together and are subjected to optical radiation.

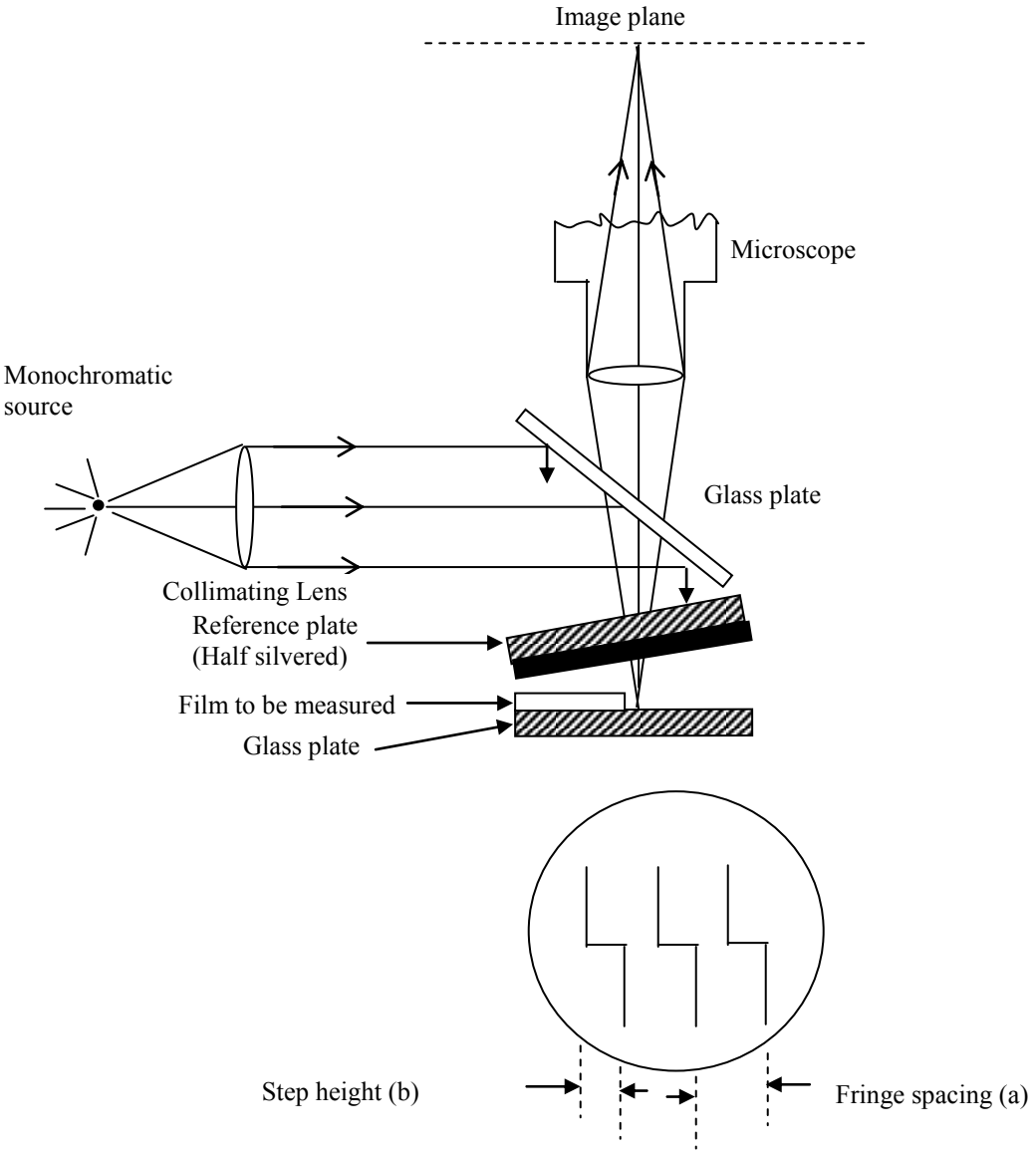

Fig 3.6 The schematic diagram of multiple-beam interferometer.

This interference technique, which is of great value in studying surface topology in general, may be applied simply and directly to film-thickness determination. When a wedge of small angle is formed between unsilvered glass plates, which are illuminated by monochromatic light, broad fringes are seen arising from interference between the light beams reflected from the glass on the two sides of the air wedge. Where the path difference is an integral and odd number of wavelengths, bright and dark fringes occur. If the glass surfaces of the plates are coated with highly reflecting layers, one of which is partially transparent, then the reflected fringe system consists of very fine dark lines against a bright background. A schematic diagram of the multiple-beam interferometer along with a typical pattern of Fizeau fringes from a film step is shown in Fig 3.6.

As shown in this figure, the film whose thickness is to be measured is over coated with a silver layer to give a good reflecting surface and a half-silvered microscope slide is laid on top of the film whose thickness is to be determined. A traveling microscope measures the step height and width of the Fizeau fringes that are formed due to the interference of light reflected from the glass and the thin film surfaces having path difference an integral or odd number multiple of wavelength. A monochromatic sodium light source of wavelength, λ=589.3 nm was used for this purpose and the thickness of the film "d" can be determined by the relation

$$d = \frac{\lambda b}{2a}$$

where b= step height of the fringes and a= fringe width. In practice, several half-silvered slides of varying thickness and therefore of varying transmission are prepared, and one of these is selected for maximum resolution. Accurate determinations of fringe spacings are difficult and time consuming; but a method of image comparison, which considerably improves the ease, and rapidity of measurement has recently been developed. In conclusion, it might be mentioned that the Tolansky method of film-thickness measurement is the most widely used and in many respects also the most accurate and satisfactory one.

3.8 Experimental Procedure

3.8.1 Differential thermal analysis and thermogravimetric analysis

The PPTMA films were scrapped off from the substrate to use as the sample for the DTA/TGA investigations. The DTA/TGA scans of PPTMA thin films were taken using a computer controlled TG/DTA 6300 system connected to an EXSTAR 6000 station, Seiko

Instruments Inc., Japan. The TG/DTA module uses a horizontal system balance mechanism. The specifications of the instrument are: sample weight ≤ 200mg, Temperature range; 300 K to 1573 K, Heating rate; 0.01°K/min. to 100.00 °K/min., TGA Measuring Range; ± 200 mg(0.2 μg), DTA Measuring Range; ± 1000 μV(0.06 μV), Gas flow; ≤ 1000m/min.

Fig 3.7 The photograph of a DTA/TGA instrument.

3.8.2 Scanning electron microscopy

Small pieces (1 cm× 1 cm) of glass were cut at first for thin film deposition. To avoid the charging effect, before SEM recording the sample surface was coated with a thin layer of gold by sputtering (AGAR Auto Sputter Coater). As deposited, heat treated (at 573 and 673 K for 1 hour) and iodine doped PPTMA thin films were used in this investigation. Scanning electron micrographs of PPTMA thin film surfaces were obtained by using a scanning electron microscope. (S-3400N Hitachi, Japan).

Energy dispersive X-ray (EDX) analysis

The PPTMA thins films were deposited onto small pieces of chemically cleaned glass substrates. Two samples of as deposited and iodine doped were sorted out of the analysis. To avoid the charging effect the PPTMA films were coated with a thin layer of gold by gold sputtering (AGAR Auto Sputter Coater). The EDX also were performed by a scanning electron microscope (S-3400 N Hitachi, Japan).

3.8.3 Elemental analysis

The PPTMA powder was collected from the monomer deposited substrates by scrapping process. The scrapped PPTMA was then made fine powder using agate mortar and pastle. The

C, H and N contents of PPTMA films were determined by an elemental analyzer EA 1180 of Carlo Erba Instruments, TYCHN, Milan, Italy. The analyzed has the following specification: Measuring range 100 ppm; accuracy<0.3% absolute; repeatability<0.20%; sample required 0.1 to 100 mg.; analysis time CHNS<12 min.; CHN<7 min.

3.8.4 Infrared spectroscopy

IR spectra of the monomer liquid and plasma polymerized thin films of as deposited, heat treated (at 573 and 673 K for 1 hour) and iodine doped TMA thin films were recorded at room temperature using a double-beam IR spectrometer Shimadzu-IR 470 (Shimadzu Corporation, Tokyo, Japan). A drop of each of the respective liquid monomer was placed between two thin KBr pellets to record the IR spectrum of the monomers. Plasma polymerized films of different precursors prepared on glass substrates were used for the IR analysis. Specimens were scraped off from the substrates and a little amount of sample was taken to prepare pallets after mixing with potassium bromide (KBr). The strength of an IR absorption spectrum is dependant on the number of molecules in the beam. With a KBr disk the strength will be dependant on the amount and homogeneity of the sample dispersed in the KBr powder. The spectrometer has its repeatability of the transmittance, 0.5%, except the wavenumber range, where the absorption bands of the water vapor exist. Its wavenumber range is 4000-400 cm^{-1}.

3.8.5 X-ray photoelectron spectroscopic (XPS)

The XPS of PPTMA was done with a soft X-ray absorption spectroscopy beamline BL13 in Hiroshima, Japan. The UHV chamber was equipped with a semispherical XPS analyzer (Omicron ,Germany). For XPS measurements the MgK_α (1253.6 eV) sources was used. After degassing the MgK_α –X ray sources all the parameters can be controlled by using a PC running with Ph/PC explorer software.

3.8.6 Ultraviolet Visible spectroscopy

Instrumentation

When A beam of light from a visible and/or UV light source (colored red) is separated into its component wavelengths by a prism or diffraction grating. Each monochromatic (single wavelength) beam in turn is split into two equal intensity beams by a half-mirrored device.

One beam, the sample beam (colored magenta), passes through a small transparent container (cuvette) containing a solution of the compound being studied in a transparent solvent. The other beam, the reference (colored blue), passes through an identical cuvette containing only the solvent. The intensities of these light beams are then measured by electronic detectors and compared. The intensity of the reference beam, which should have suffered little or no light absorption, is defined as I_0. The intensity of the sample beam is defined as I. Over a short period of time, the spectrometer automatically scans all the component wavelengths in the manner described. The ultraviolet (UV) region scanned is normally from 200 to 400 nm, and the visible portion is from 400 to 800 nm. If the sample compound does not absorb light of a given wavelength, $I = I_0$.

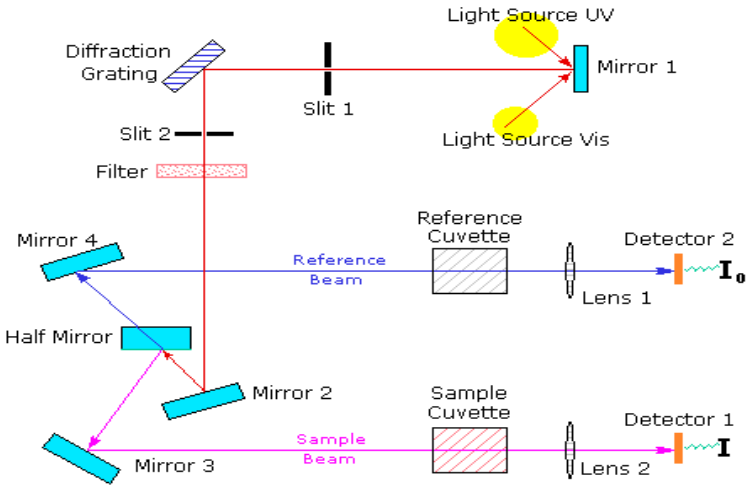

Fig 3.8 Diagram of the components of a spectrometer

However, if the sample compound absorbs light then I is less than I_0, and this difference may be plotted on a graph versus wavelength. Absorption may be presented as transmittance or absorbance. If no absorption has occurred, T = 1.0 and A= 0. Most spectrometers display absorbance on the vertical axis, and the commonly observed range is from 0 (100% transmittance) to 2 (1% transmittance). The wavelength of maximum absorbance is a characteristic value, designated as λ_{max}. Different compounds may have very different absorption maxima and absorbance. Intensely absorbing compounds must be examined in dilute solution, so that significant light energy is received by the detector, and this requires the use of completely transparent (non-absorbing) solvents. The most commonly used solvents are water, ethanol, hexane and cyclohexane.

For UV-Vis measurements, the samples were deposited on to cover glass slide. UV-Vis spectra of TMA, PPTMA as deposited, heat treated (at 473, 573 and 673 K for 1 hour) and iodine doped PPTMA thin films were obtained in absorption mode with a Shimadzu UV-160A spectrophotometer (Shimadzu Corporation, Tokyo, Japan) in the wavelength range 200 to 1100 nm at room temperature. The optical absorption was measured in the above wavelength region for the PPTMA films on substrate against a blank cover glass slide as the reference.

Fig 3.9 The photograph of UV-Vis spectroscopic instrument.

3.8.7 Contact electrodes for electrical measurements

Electrode materials:

Aluminium(Al) (purity of 4N British Chemical Standard) was used for electrode deposition. Al has been reported to have good adhesion with glass slides. Al film has advantage of easy self-healing burn out of flaws in sandwich structure.

Electrode deposition:

Electrodes were deposited using an Edward coating unit E-306A (Edward, UK). The system was evacuated by an oil diffusion pump backed by an oil rotary pump. The chamber could be evacuated to a pressure less than 1.33×10^{-3} Pa. The glass substrates were masked with 0.08m× 0.08m × 0.001m engraved brass sheet for the electrode deposition. The electrode assembly used in the study is shown in Fig.3.10. The glass substrates with mask were supported by a metal rod 0.1 m above the tungsten filament. For the electrode deposition Al was kept on the tungsten filament. The filament was heated by low-tension power supply of the coating unit. The low-tension power supply was able to produce 100 A current at a potential drop of 10 V.

During evacuation of the chamber by diffusion pump, the diffusion unit was cooled by the flow of chilled water and its outlet temperature was not allowed to rise above 305 K. When the penning gauge reads about 1.33×10^{-3} Pa, the Al on tungsten filament was heated by low-tension power supply until it was melted [100, 101].

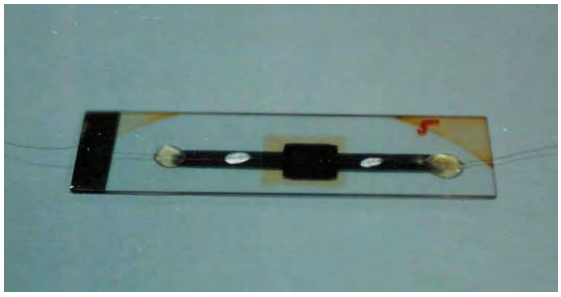

(a)

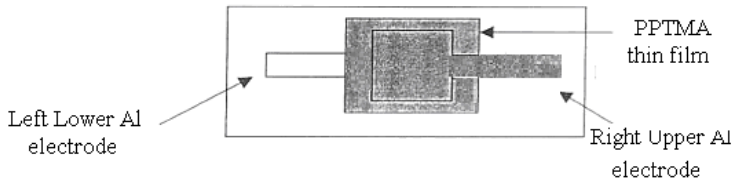

(b)

Fig.3.10 (a) Photograph of PPTMA thin film (b) the electrode assembly.

The Al was evaporated, and finally lower electrode onto the glass slide was deposited. Al coated glass substrates were taken out from the vacuum coating unit and were placed on the middle of the lower electrode of the plasma deposition chamber for TMA thin film deposition under optimum condition. The top Al electrode was also prepared on the PPTMA film as described above.

3.8.8 Direct current electrical measurements

The current across the Al/PPTMA/Al thin film structures of different thicknesses was measured by a high impedance electrometer (Model: Keithley 614, Keithley Instruments Inc., USA) and the dc voltage was supplied by a stabilized dc power supply (Model: E 3610A, Hewlett Packard, England). The measurements were carried out under dynamic vacuum of about 1.33 Pa. Sample temperature was measured using a chromel-alumel thermocouple

attached to a digital microvoltmeter (Model: 197A, Keithley Instruments Inc., USA). The thermally activated current or the temperature dependence of current across the PPTMA thin films was measured at applied voltages 2.0 and 30 V using the above-mentioned electrometer. The measurements were performed from 300 to 450 K. In both measurements the samples were heated by heating the specimen chamber externally by a heating coil. To avoid oxidation, all the measurements were performed in a vacuum of about 1.33 Pa.

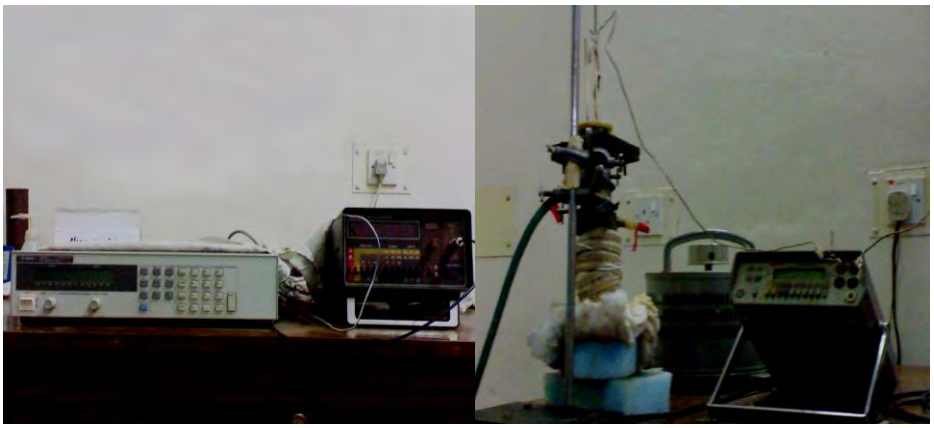

(a)

3.11(a) The photograph of dc measurement and (b) ac measurement.

3.8.9 Alternating current electrical measurements

The ac measurements were performed using a LF impedance analyzer Agilent, 4192 A (Agilent Technologies, Japan Ltd. Tokyo, Japan). The ac electrical conductivity (σ_{ac}), and dielectric constant (ε') of PPTMA thin films were calculated using the relations,

$$\sigma_{ac}(\omega) = G_p\, d/ A$$

$$\varepsilon' = C_p\, d / \varepsilon_o\, A$$

where G_p is the measured parallel conductance, C_p is the measured parallel capacitance, ε_o is the permittivity of free space, A is the effective electrode area of each of the electrodes and *d* is the thickness of the dielectric. The σ_{ac}, ε', and $tan\partial$ were calculated from the measured values of G_p and C_p.

3.9 Modification of PPTMA thin films by Iodine

Plasma polymerization of TMA was carried out in the presence of TMA monomer and then exposed to iodine for doping. Complex formation between PPTMA and iodine may happened by chamber method. Iodine doping of plasma polymerized TMA thin films of different thicknesses was affected by iodine vapor into the chamber. Iodine crystals are placed in a desiccator and the films to be doped were kept this chamber. The time of doping is 60 min. Due to doping, the color of the PPTMA thin film changes from light to dark brown.

CHAPTER 4

Results and Discussion

4.1 Introduction

This chapter deals with the investigations of structural, thermal, optical, electrical behaviors and iodine modification of PPTMA thin films. The surface morphology, structural, thermal properties of PPTMA were investigated by Scanning electron microscopy (SEM), Infrared (IR) spectroscopy, X-ray photoelectron spectroscopy (XPS) and Differential thermal analysis (DTA) and Thermogravimetric analysis (TGA). The investigation of the composition and structure of PPTMA by Elemental analysis (EA) and IR spectroscopy respectively are discussed. The XPS measurements were carried out to determine the relative amounts of C, N and O on the PPTMA thin film surface. The DTA and TGA of PPTMA are also discussed. The optical energy gaps, the allowed direct transition and allowed indirect transitions have been determined from the UV-Vis spectroscopic studies and are discussed in this chapter. This chapter describes dc electrical conduction mechanisms which are followed by the measurements of current density-voltage (J-V) and thermally activated current in the successive sections. The ac electrical conductivity (σ_{ac}), dielectric constant (ε'), and loss tangent (tan∂) were investigated as functions of frequency and temperature. In this chapter the finding of the electrical studies in conjunction with the other observations is described and are tried to explain the relaxation behavior and ac conduction mechanism in PPTMA thin films.

4.2 Differential Thermal Analysis and Thermogravimetric Analysis

The DTA and TGA traces taken at 10 K/min for PPTMA are shown in Fig. 4.1(i). The DTA thermogram shows an exotherm, which reaches a maximum at around 571 K. The corresponding TGA trace of PPTMA has been taken from 303 to 1023 K and showed different stages of thermal decomposition, which divided in three regions (A, B, and C). Every region may be associated with a different rate of weight loss. The weight losses in A, B, and C regions are about 3 %, 3 %, and 28 %, respectively. In the first region A, the weight loss may be due to the removal of water content, which is not necessarily associated with any change in the structure. The 3% of weight loss in the region B may be attributed to the loss of non-constitutional or adsorbed water and unreacted monomer settled on PPTMA films surface and/ or due to evolution of hydrogen and low molecular mass hydrocarbons gases.

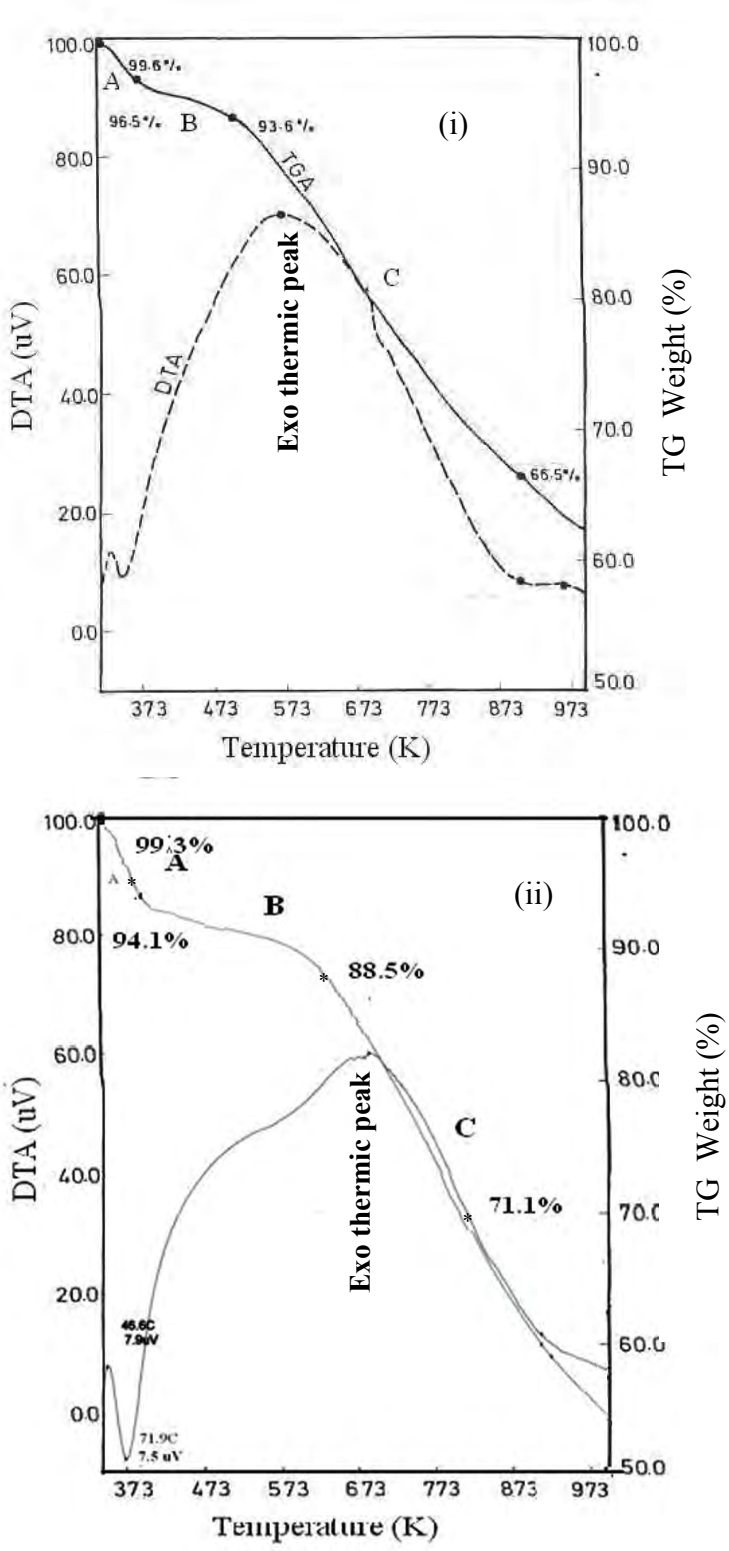

Fig 4.1 The DTA/TGA traces of (i) as deposited and (ii) heat treated PPTMA thin films.

The maximum change in the PPTMA structure has been occurred in the region C. The weight loss of 28% in this region is important because the DTA curve exhibits a wide peak. In region C the weight loss may be caused by the thermal breakdown of the PPTMA structure and expulsion of higher molecular mass hydrocarbons, oxygen containing compounds, etc. Thus, it may be attributed that PPTMA films are thermally stable up to about 505 K. A comparative study of as deposited PPTMA and heat treated PPTMA shows characteristics differences, which indicates that the monomer has undergone the re-organization during plasma polymerization.

It is observed by DTA and TGA in Fig. 4.1(ii) that heat treated PPTMA lose approximately 5.2%, 5.6% and 17.4% of their initial mass. The weight loss in PPTMA and heat treated PPTMA is much higher than that of its components even at relatively lower temperature. This behavior suggests that less breakdown thermal energy is needed for heat treated PPTMA samples than those of its components. The significant loss in the mass in heat treated PPTMA samples suggests that in the heat treated structure the bonds require more thermal energy to dissociate in comparison to the bonds formed in the PPTMA chains which need greater thermal energy to dissociate the bonds.

4.3 Scanning Electron Microscopy

4.3.1 SEM Micrographs as Deposited and Heat Treated PPTMA Thin Films

The SEM micrographs of as deposited and heat treated PPTMA thin films were recorded at various points at various magnifications (1k×, 10k×) at accelerating voltage of 10 kV are shown in Fig 4.2 - Fig 4.3. From the micrographs it can easily be visualized that the surface of the plasma polymerized thin films is smooth, flawless and pinhole free. The absence of pinholes was also demonstrated by the high electrical breakdown strengths of the sandwich cell (Al/PPTMA/Al) structure. A comparison between the micrographs of the as deposited and heat-treated films shows that no significant change is observed in the surface morphology upon heat treatment.

4.3.2 SEM Micrographs of Iodine Doped PPTMA Thin Films

The SEM photograph of the iodine doped PPTMA films shows that its surface is smoother with iodine, possibly indicating that closely connected blocks of polymer chains develop in the polymer when plasma polymerization is carried out in the presence of iodine.

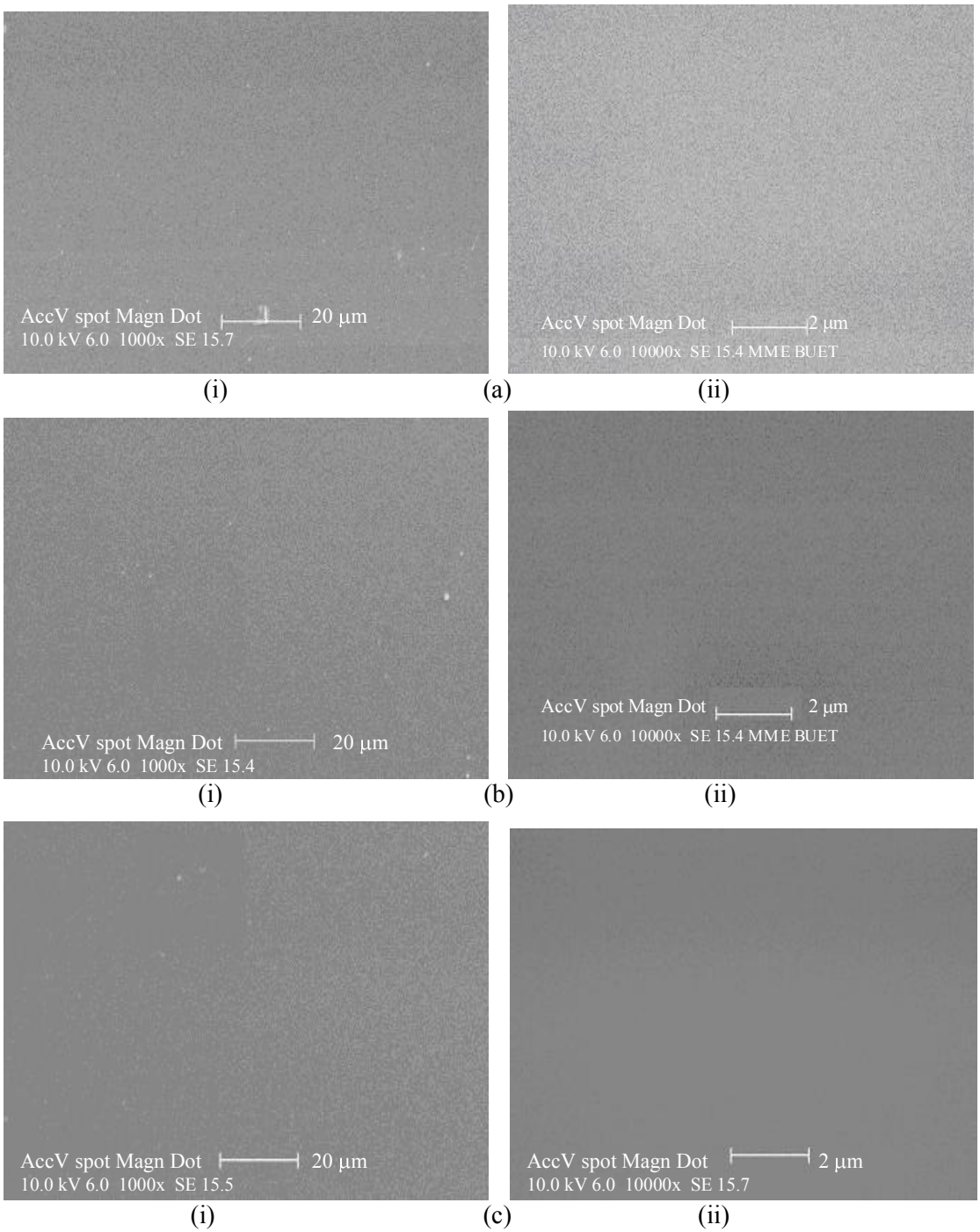

Fig 4.2 SEM Micrographs of (a) as deposited and heat treated at (b) 473 and (c) 573 K PPTMA thin films (i) magnification 1000×, (ii) magnification 10000×

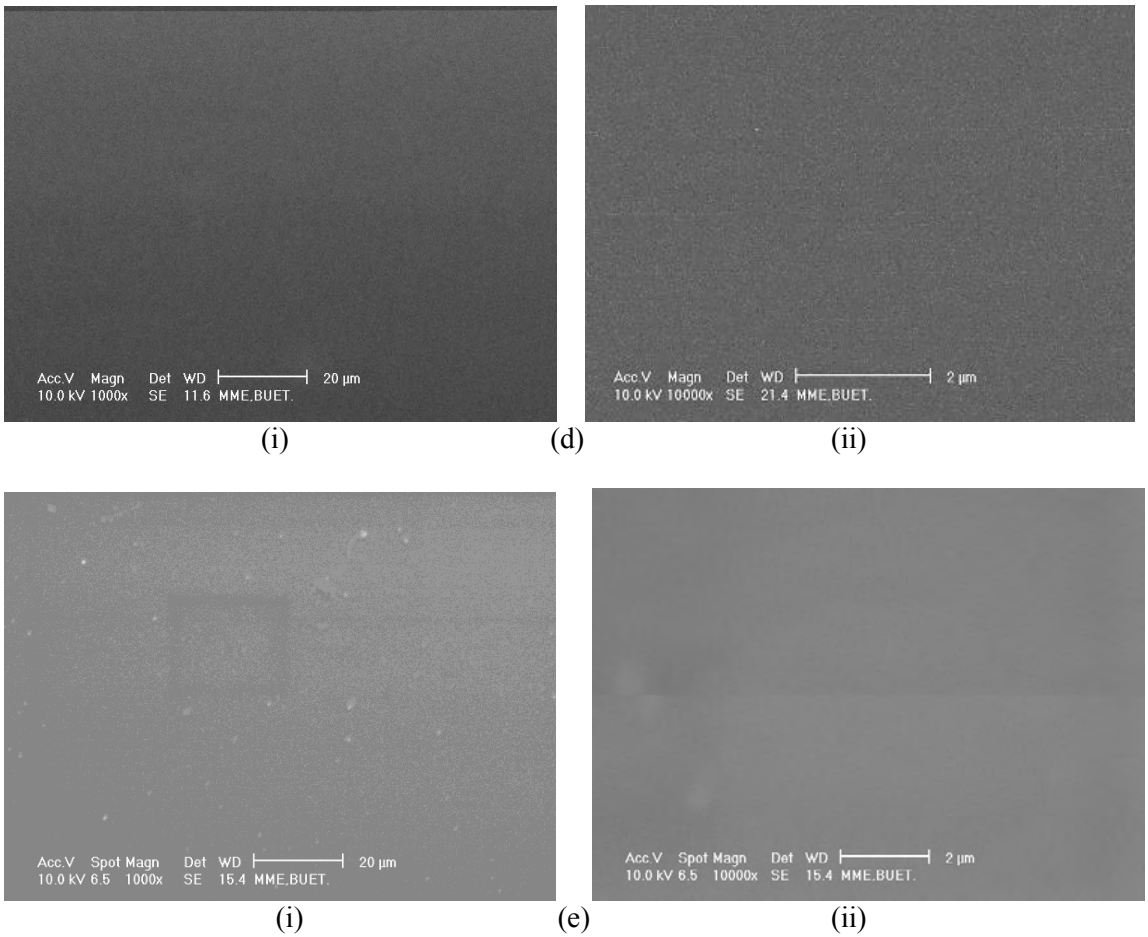

Fig 4.3 SEM Micrographs of PPTMA thin films (d) heat treated at 673 K and (e) iodine doped PPTMA thin films (i) magnification 1000×, (ii) magnification 10000×

4.4 Energy Dispersive X-ray Analysis

The compositional analysis was taken for the PPTMA thin films by Energy Dispersive X-ray (EDX), which is attached to the SEM. From EDX the weight percentages of monomer and as deposited samples are shown in table 4.1. The observations indicate the presence of C, N, O and I in the samples. The main obstacle of EDX is that it cannot detect the presence of H.

Table 4.1 Weight percentages of the elements for as deposited PPTMA and Iodine doped PPTMA obtained by EDX analysis.

Sample	Elements (wt %)				
	C	N	O	H	I
Monomer (TMA)*	80.53	9.39	-	10.07	-
PPTMA	47.62	18.89	33.49		
Iodine Doped PPTMA	34.29	12.39	27.92		25.41

*Calculated from Chemical formula

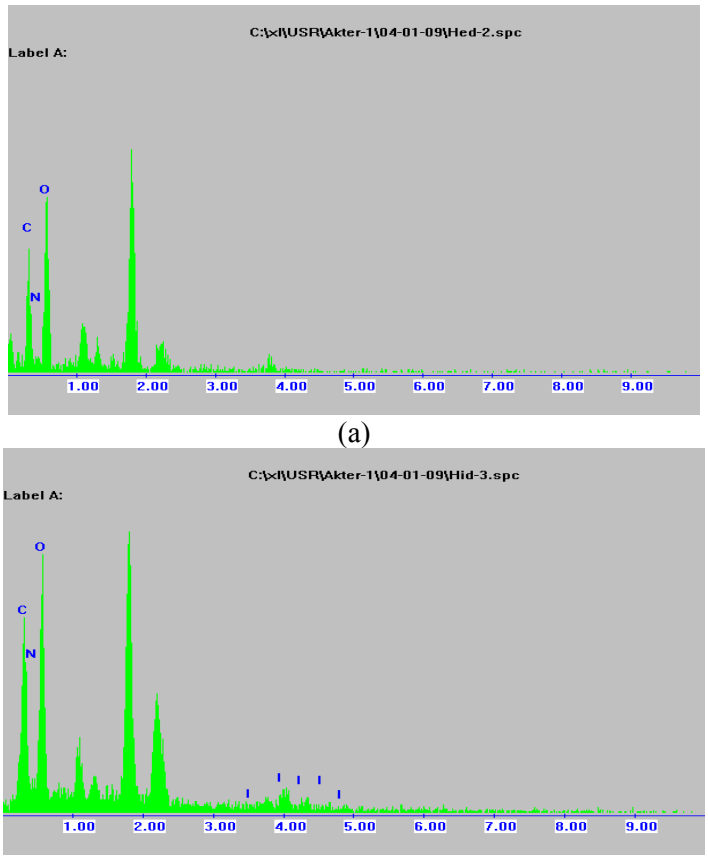

Fig. 4.4 EDX of (a) as deposited and (b) iodine doped PPTMA thin films.

The presence of O which was not present in TMA implies incorporation of carbonyl and hydroxyl groups in PPTMA through the reaction of the free radicals or due to the breakdown of bonds owing to the complex reaction during plasma polymerization. From the weight percentage of TMA, PPTMA and Iodine doped PPTMA, it is seen that the amount of C decreases due to the breakdown of bonds owing to the complex reaction during plasma polymerization. The incorporation of O and iodine in PPTMA and iodine doped PPTMA may be due to the post-deposition reaction of the PPTMA after exposure to air and iodine owing to complex reactions with radical species and dangling bonds in the structure and /or from the glow discharge chamber during polymerization and iodine vapor exposing iodine in desiccator.

4.5 Elemental Analysis

The chemical composition of PPTMA thin film was determined by elemental analysis, a useful technique for chemical investigation of organic inorganic materials. The weight

percentages (wt%) of carbon (C), hydrogen (H) and nitrogen (N) in PPTMA detected by EA and the percentage of O content calculated on subtraction from the wt (%) values of other elements [104] are presented in table 4.2.

Table 4.2 The weight percentages of C, H, N and O in as deposited PPTMA thin film

Sample	Elements detected (wt %)				Empirical formula
	C	H	N	O	
PPTMA	62.10	6.88	7.47	23.55	$C_{7.70}H_{10.30}N_{0.80}O_{1.50}$

It is seen from the table 4.2 that the amounts of C, N, and H in PPTMA are decreased relative to the amount of constituent elements in the monomer, $C_{10}H_{15}N$, TMA. From the EA the atomic ratio is found to be N/C=0.12 for PPTMA, which is just same to that of the monomer i.e. N/C=0.12. It is thus seen that there is no change of N/C ratio because N and C are decreased relative to the amount of constituent elements of TMA. The deficiency of C, N, and H contents in PPTMA may be due to the breakdown of bonds owing to the complex reaction during plasma polymerization. The incorporation of O and decrease in the amount of N in PPTMA may be due to the post-deposition reaction of the PPTMA after exposure to air owing to reactions with radical species and dangling bonds in the structure and /or from the glow discharge chamber during polymerization.

4.6 Infrared Spectroscopy

4.6.1 IR Spectroscopic Analysis of as Deposited and Heat Treat PPTMA

Fig. 4.5 shows the IR spectra of TMA, PPTMA as deposited and heat treated PPTMA in air at 473, 573 and 673 K which are represented by M, N, O, P and Q, respectively. The asymmetric N-H stretching band at 3475 cm^{-1} (A) and the symmetric N-H stretching band at 3340 cm^{-1} (B) are observed in the spectrum M of TMA. Relatively strong bands at 2935 (C) and 2793 cm^{-1} (D) correspond to the C-H stretching vibrations. The wide band at 1680-1645 cm^{-1} (E) and the absorption peaks at 1484 and 1595 cm^{-1} (F) may be attributable to C=C in aromatic ring stretching vibration of the benzenoid and quinoid rings, respectively.

Bands at1351 (G) and 1307 cm^{-1} (H) are observed due to conjugation of the electron pair of the nitrogen atom with the ring imparting double-bond character to the C-N bond and a lower frequency band at 1223-1030 cm^{-1} (I) may be due to aliphatic C-N stretching. The band character of tetra substituted benzene is present between 814-776 cm^{-1} (J) in the spectrum.

In spectrum N of the as deposited PPTMA film in Fig.4.5, the absorption bands at around 3435, 2935, 1850-1603, 1570, 1472 and 1340 cm^{-1} in the wide absorption envelope correspond to the regions A, C, E, F and G of TMA spectrum, which results from the N-H stretching vibration, C-H stretching vibration, an aromatic ring C=C stretching vibration in benzenoid and quinoid rings and C-N stretching vibration respectively. The wide band around 1850-1603 cm^{-1} may also include the contribution due to C=O stretching vibration which is typical for plasma polymers.

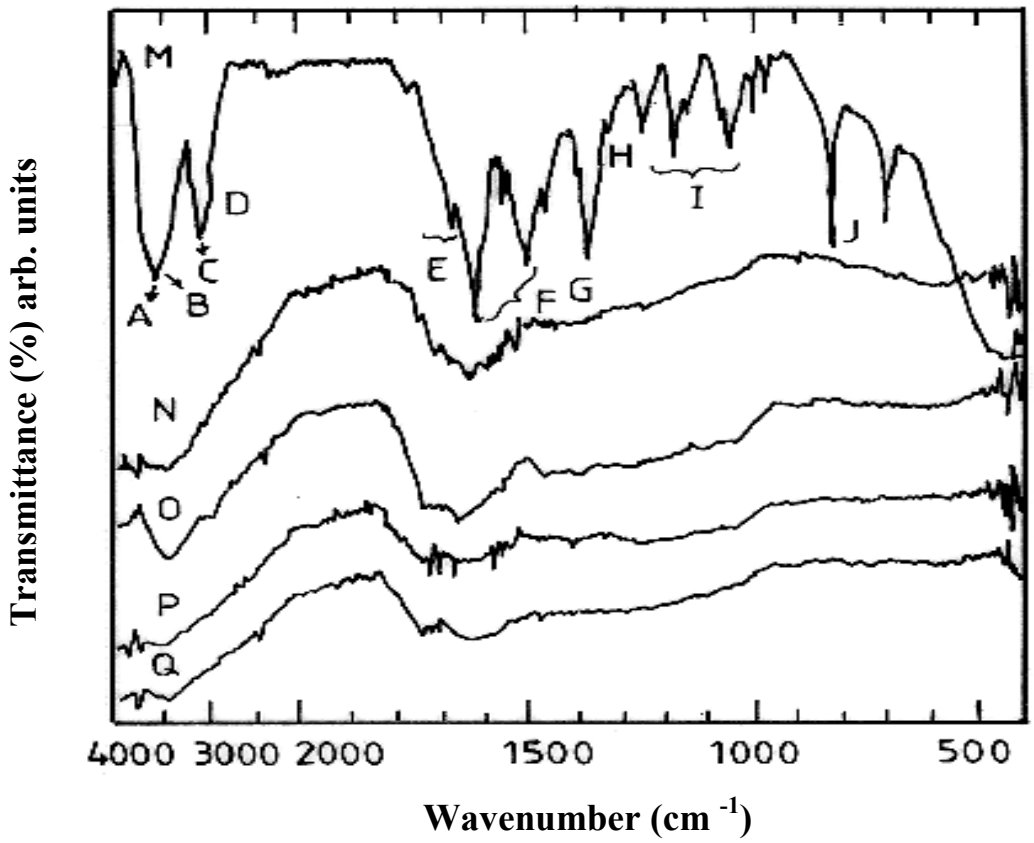

Fig 4.5 The IR spectra of TMA, as deposited PPTMA, PPTMA heat treated at 473, 573, and 673 K, which are represented by M, N, O, P, and Q, respectively (Curves are linearly shifted for convenience). The IR spectra were taken at room temperature.

The formation of carbonyl group is usually attributed to the oxidation of the hydrocarbon part of the PPTMA after exposure to air giving rise to oxygen reactions with radical species (dangling bonds) trapped in the structure of the plasma polymer. Cross-linking may also

occur between different carbons of the chains due to the loss of hydrogen, particularly in the plasma polymerized films, because of the impact of energetic particles within the plasma during deposition.

Table 4.3 Assignments of IR absorption peak for TMA and heat treated PPTMA samples

Vibrations	**Wavenumber (cm^{-1})**				
	Monomer	**PPTMA**	**473 K***	**573 K***	**673 K***
Asymmetric **N-H** stretching vibration (**A**)	3475	3435	3490	3510	3540
Symmetric **N-H** stretching vibration (**B**)	3340		3380	3390	3390
C-H. stretching vibration (**C, D**)	2935, 2793	2935	2950,2800	3005,2895	3030-2910
C=C stretching vibration (**E**)	1680-1645	1850-1603	1890-1645	1888-1645	1888-1645
C=C stretching vib. in benzenoid and quinoid (**F**)	1595, 1484	1570, 1472	1591,1483	1576, 1474	1572, 1475
C-N stretching vibration (**G, H**)	1351, 1307	1340	1358	1351	1357
C-N stretching vibration (**I**)	1223-1030		1231-1043	1229-1028	1223-1011
Tetra substituted Benzene (**J**)	814-776		824-787	829-781	808-784

*** heat treated for 1 hour in air.**

Here the PPTMA films show a widening of the band corresponding to the C=C stretching vibration of benzenoid and quinoid and slight down-shifting of C-N stretching vibrations, probably caused by cross-linking interactions intrinsically associated with plasma polymers. The above observations reveal that the PPTMA films contain an aromatic ring structure with NC and CH side groups.

It is seen that in the IR spectra of PPTMA heat treated at 473, 573 and 673 K represented by O, P and Q, respectively (Fig.4.5), the overall sharpness of the absorption bands decreases, because some of the bands are superimposed in the wide absorption bands. The peak area for N-H stretching of the sample heat treated at 473, 573 and 673 K decreases and shifts to higher wave number compared to those of the PPTMA. The overall peak intensity decreases slowly due to heat treatment up to 573 K. This means the bands are overlapped to each other and create a large band. Whereas the sharpness of these peaks reappear on heat treatment at about 673 K, which may be due to the structural rearrangement. It can be noticed in table 4.3 that the vibration positions are slightly shifted to lower or higher wave numbers corresponding to the PPTMA. Thus, further modification occurs in the PPTMA structure on heat treatment at higher temperatures by conjugation and cross-linking.

4.6.2 IR Spectroscopic Analysis of Iodine Doped PPTMA

The IR spectra of iodine doped PPTMA is shown in Fig. 4.6. The assignments of the IR absorption bands for as deposited PPTMA and iodine doped PPTMA are given in table 4.4. The sharpness of the absorption bands increases in the iodine doped IR compared to as deposited PPTMA. The structure corresponding to the iodine doped PPTMA shows absorption peaks at 1683 and 1577 cm^{-1}, which indicates the presence of aromatic ring stretching and C-C stretched vibration even after iodination of PPTMA thin film respectively. The presence of iodine in PPTMA increases the conductivity of plasma polymerized thin films [18, 19].

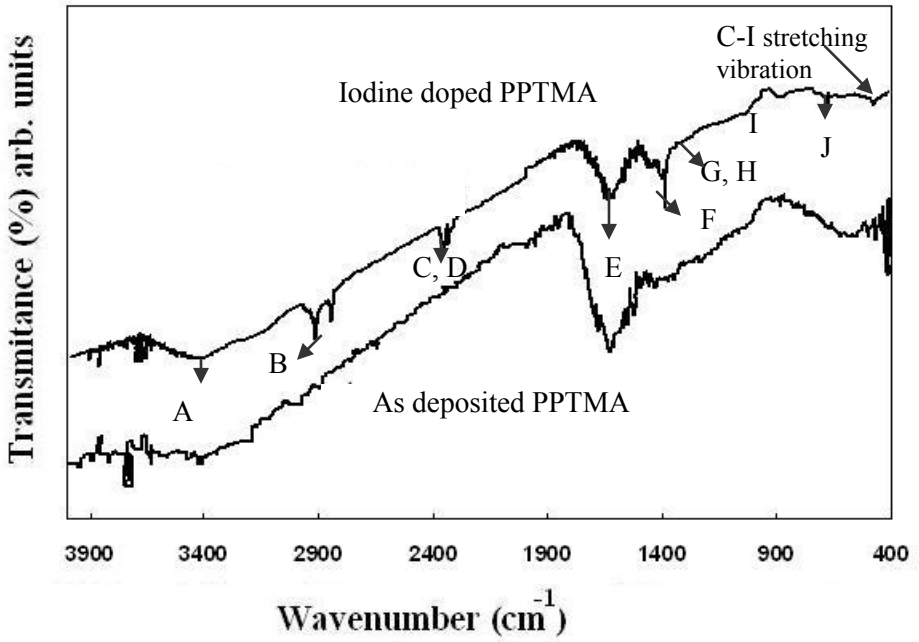

Fig 4.6 The IR spectra of PPTMA and iodine doped PPTMA thin film, taken at room temperature (Curves are linearly shifted for convenience).

From In table 4.4, it is seen that in the iodine doped PPTMA the N-H stretching shifts towards higher wave number 3384 cm^{-1} and C-N stretch at 1351 cm^{-1} for TMA shifts towards 1384 cm^{-1}. The shifts indicate that the iodine atoms might get attached to amine nitrogen site of TMA [16]. The bands corresponding to the aromatic rings and tetra-substituted benzene in the iodine doped PPTMA are found to be shifted to lower frequencies 1128, 877, 669 cm^{-1}. The band for C-I stretching of the sample appears at 500-470 cm^{-1}. This is an indication that iodine doping is affecting bond length and facilitates shifting of functional groups of PPTMA samples.

Table 4.4 Assignments of IR absorption peak for as deposited PPTMA and iodine doped PPTMA samples

Vibrations	Wavenumber (cm^{-1})	
	PPTMA	**Iodine doped PPTMA**
Asymmetric N-H stretching vibration (A)	3435	3384
Symmetric N-H stretching vibration (B)	2935	3263
C-H. stretching vibration (C, D)	1850-1603	2918, 2848
C=C stretching vibration (E)		1683-1610
C=C stretching vib. in benzenoid and quinoid (F)	1570, 1472	1577
C-N stretching vibration (G, H)	1340	1384
C-N stretching vibration (I)		1128
Tetra substituted Benzene (J)		877, 669
C-I stretching vibration		500- 470

4.7 X-ray Photoelectron Spectroscopy

4.7.1 XPS Analyses of as Deposited PPTMA Thin Films

The XPS measurements were carried out to determine the relative amounts of C, N and O on the PPTMA thin film surface. The C1s, N1s and O1s XPS spectra of the PPTMA thin films are shown in Figs. 4.7 (i,ii,iii), 4.8 (i,ii,iii) and 4.9 (i,ii,iii), respectively. The envelopes of all the spectra were analyzed by fitting Gaussian peaks. It has been reported that the full width at half maximum (FWHM) for plasma polymers is expected to be relatively large, about 1.8 eV due to their random assemblies of molecular fragments [79, 81, 82]. The C1s spectrum in Fig. 4.7(i) contains peaks those represent the presence of C, N, and O. The C1s spectrum for these films consists of peaks those are not only close together but also relatively broad, thus yielding significant overlapping the peaks associated with N and O, which are at higher binding energies than the C-C and C-H peaks. The XPS data of PPTMA thin films revealed that besides C and N there is also significant amount of O in PPTMA films. The presence of O in the PPTMA thin films is expected in the plasma-polymerized films owing to the existence of traces of oxygen and/or water vapor adsorbed on the walls of the reaction chamber, which would then be desorbed during the gas discharge. Another reason for the presence of oxygen is the reaction of long lived radicals in the deposited films with atmospheric oxygen and/or water after being exposed to the atmosphere.

The C1s spectrum of PPTMA film can be deconvoluated into three component peaks as indicated in Fig.4. 7(i). The binding energies (BE's) for aromatic C-H (285.0 eV) and C=C,

C-N and C-O, (286.1 eV) and C=O (288.0 eV) were assigned in the present material. The asymmetric region in the high BE side of the C1s spectrum could be attributed to the presence of the shake–up π - π^* structure arising from the transition from the aromatic rings in PPTMA film. This feature is also observed in the UV-Vis spectroscopic investigations [10]. The N1s XPS spectra for PPTMA samples are demonstrated in Fig. 4.8 (i). The N1s spectrum of PPTMA thin films may involve carbon and nitrogen bonds only. The spectra in Fig.4.8 (i). reveal that N1s shifted to form three separate peaks, which can be attributed to different groups. The peak at 398.6 eV represents N-H; the peak at 399.9 eV is assigned to N-C, N-O group; and the peak at 401.5 eV represents N=C. The O1s spectra for PPTMA films are shown in Fig.4.9 (i) which are quite similar with maxima at 530.8+1 eV. The O1s signal is the envelope of three components due to oxygenated structures such as O-N, O=C, O-C at about 529.0 eV, 530.9 eV and 532.0 eV, respectively.

The composition of the PPTMA thin films could be estimated from the XPS spectra. A generalized expression for the determination of the atomic fraction C_x of any contribution in a sample, utilizing peak area and sensitivity, can be written as

Atomic fraction, $$C_x = \frac{n_x}{\sum n_i} = \frac{I_x / \rho_x}{\sum I_i / \rho_i} \qquad (4.1)$$

where n is the number of atoms of an element, *I* is the area of the photoelectric peak and ρ is the corresponding photoionization cross section. The necessary photoionization cross-sections have been obtained from the article of Scofield [105]. The nitrogen-to-carbon atomic ratio, calculated using the eqn.(4.1), is found to be 0.20 for PPTMA thin films. From the XPS investigation, it is seen that plasma polymer of TMA prepared by glow discharge technique is elementally different from the monomer. The atomic concentration determined from elemental analysis is 0.12, which differs from value estimated by XPS analysis. It is suggested that on the film surface some carbon-nitrogen bonds in PPTMA were replaced by carbon-oxygen bonds. From the above observations, it is seen that there is quantitative variation in the surface and bulk compositions in the PPTMA thin films. On the surface of this film an increase of nitrogen content is observed with a drop of carbon concentration.

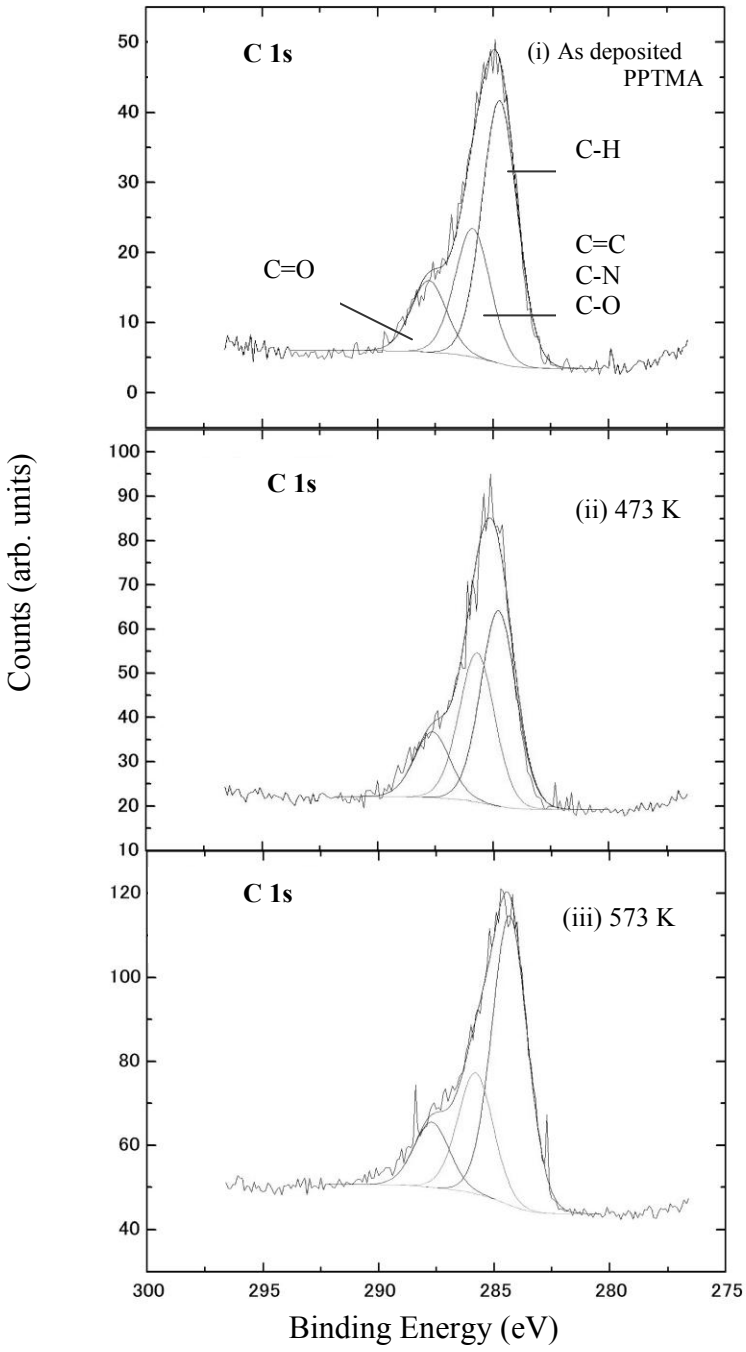

Fig.4.7 The C 1s XPS spectra of (i) as deposited PPTMA and PPTMA heat treated at (ii) 473 and (iii) 573 K. The measurements were recorded at room temperature.

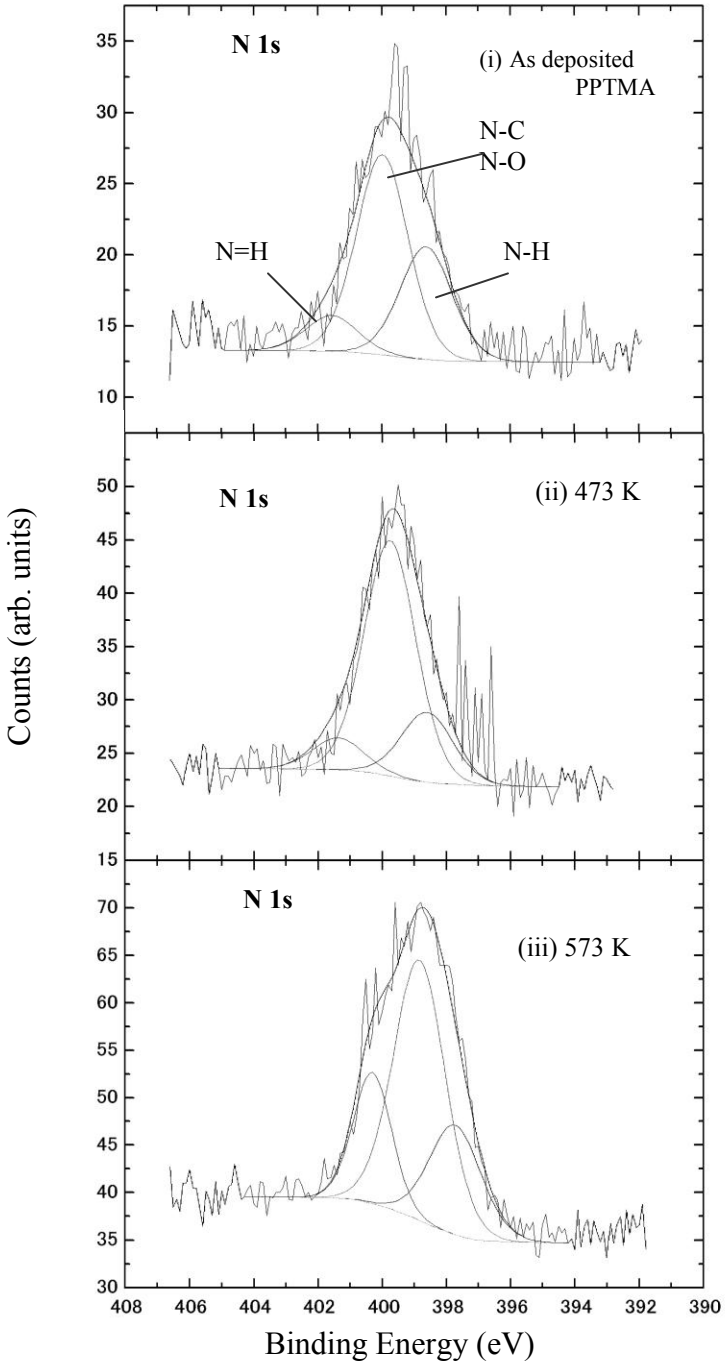

Fig.4.8 The N 1s XPS spectra of (i) as deposited PPTMA and PPTMA heat treated at (ii) 473 and (iii) 573 K. The measurements were recorded at room temperature.

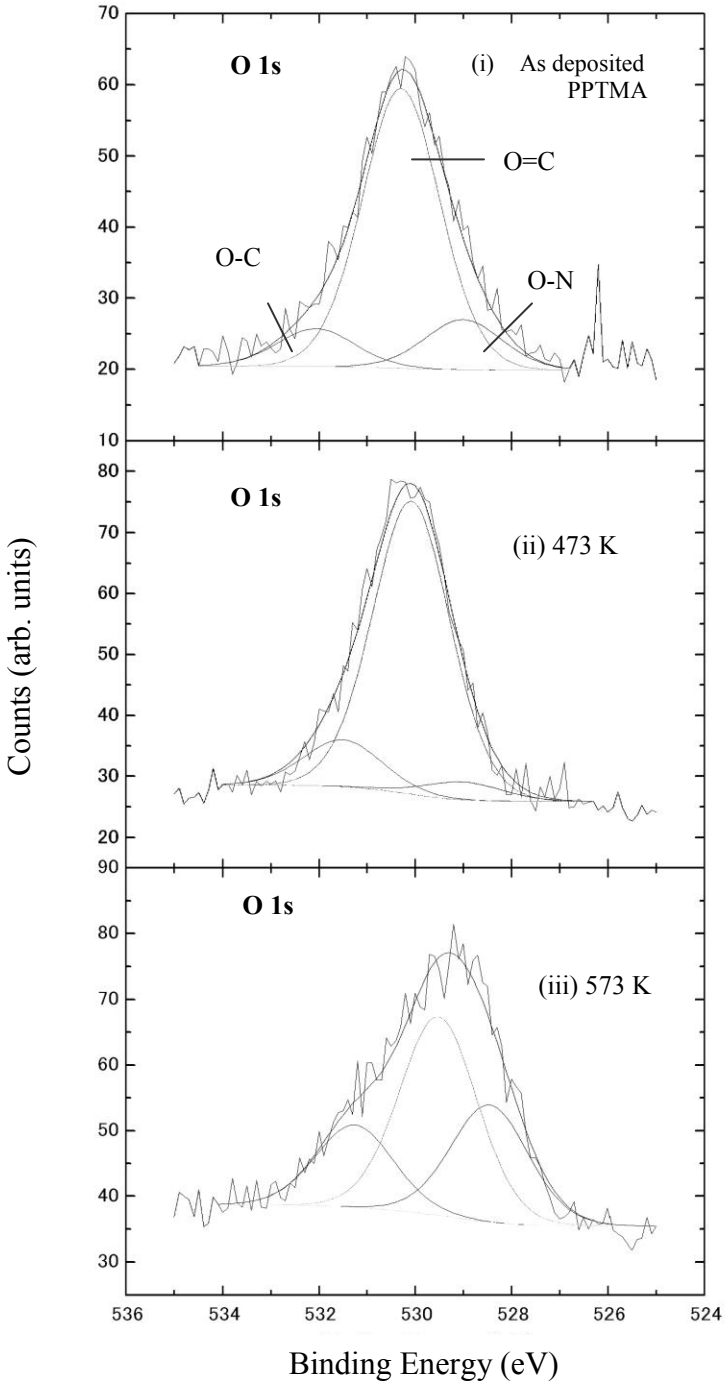

Fig.4.9 The O 1s XPS spectra of (i) as deposited PPTMA and PPTMA heat treated at (ii) 473 and (iii) 573 K. The measurements were recorded at room temperature.

4.7.2 XPS Analyses of Heat Treated PPTMA Thin Films

The C1s spectra of PPTMA thin films heat treated at 473 an 573 K have been recorded and are presented in Figs.4.7.(ii) and 4.7.(iii) respectively. The C1s spectrum of PPTMA in Fig.4.7(ii) is deconvoluated into three peak components. The three component envelopes have different BE's, peak height and peak areas. The contents of aromatic C=C and C=O components in PPTMA films are found to increase substantially compared with those in the as deposited PPTMA films. Meanwhile the relative contents for C-H, C-O, and C-N components were found to increase significantly, indicating more intensive monomer fragmentation process promoted during plasma polymerization. In Fig.4.7 the C1s spectra showed there peaks [C=C (284.3), C-H, C-O, C-N (285.8 eV) and C=O (287.7)] all of peaks has more intensity than as deposited and 473 K PPTMA thin films. The high intensity of PPTMA heat treated at a higher temperature may be due to the probable development of conjugation in the structure on heat treatment. The modifications on heat treatment were also observed in the IR and UV-Visible analyses of PPTMA.

Table 4.5 Peak position, peak area of C1s, N1s and O1s XPS spectra of PPTMA thin films.

Sample	C1s spectrum Peak (B.E eV)			N1s spectrum Peak (B.E eV)			O1s spectrum Peak (B.E eV)			FWHM
	1st C-H	2nd C=C, C-N, C-O	3rd C=O	1st N-H	2nd N-C, N-O	3rd N=C	1st O-N	2nd O=C	3rd O-C	
As deposited PPTMA	285.0	286.1	288.0	398.6	399.9	401.5	528.9	530.3	532.0	1.8 eV
Heat treatment temp. 473 K	284.7	285.7	287.6	398.6	399.8	401.4	528.8	529.9	532.6	1.8 eV
Heat treatment temp. 573 K	284.3	285.8	287.7	397.7	398.8	400.3	528.4	529.5	531.3	1.8 eV

The N1s XPS spectrum for PPTMA is demonstrated in Figs. 4.8 (i,ii,iii). After heat treatment there is no change in the 1st peak (N-H) in N 1s spectrum for 473 K and slightly shifting 397.7 eV for 573 K. It may be due to nitrogen decrease on the surface of the PPTMA film. In case of 2nd peak the BE 1.1 eV decrease for 473 K but no change for 573 K temperature. The O1s spectrum for PPTMA films is shown in Fig.4.9 (ii, iii), which has maximum at 530.8 eV. The O1s signal comprises the envelopes of three components due to oxygenated structures

such as O-N, O=C, O-C at about 529.0, 530.9 and 532.0 eV, respectively. The nitrogen-to-carbon atomic ratio, calculated using the eqn.4.1, is found to be 0.124, 0.087 and 0.098 for as deposited 473 and 573 K, respectively. The decrease of deviation may be indicative of either nitrogen contamination from unknown sources or deficit of nitrogen. It suggested that at the film surfaces some carbon-nitrogen bonds were replaced by carbon-oxygen bonds during plasma polymerization.

For N1s spectrum the nitrogen-to-carbon atomic ratio are 0.45, 0.39 and 0.56 for as deposited 473 and 573 K, respectively. Here the concentration of nitrogen was high on the surface of the PPTMA thin films increase of nitrogen content is observed with a tremendous drop of carbon concentration.

Table 4.6 N/C ration in XPS spectrum of PPTMA thin films

Sample	Peak number	N/C ratio	C1s spectra (N/C)/Total area
As deposited PPTMA	1st 2nd 3rd	0.12 0.45 0.14	0.20
Heat treatment temperature 473 K	1st 2nd 3rd	0.09 0.39 0.12	0.20
Heat treatment temperature 573 K	1st 2nd 3rd	0.10 0.56 0.39	0.26

4.8 Ultraviolet-Visible Optical Absorption Spectroscopic analysis

4.8.1 UV-Vis Spectroscopic Analyses of as deposited PPTMA of Different Thicknesses

The spectral behavior of absorbance in the wavelength range 200 to 800 nm of PPTMA thin films of thicknesses 300, 400 and 500 nm are shown in Fig.4.10(a). Here the absorbance increases with increasing thickness of the PPTMA thin films. In the absorption process, a photon excites an electron from a lower to a higher energy state, which is called an absorption edge. The absorption co-efficient was obtained from the absorbance spectra of the PPTMA thin films.

In the spectra, it is observed that there is a sharp rise in the absorption in the low wavelength side which rapidly decreases up to about 500 nm with a peak at around 370 nm; above 500 nm absorption decreases slowly.

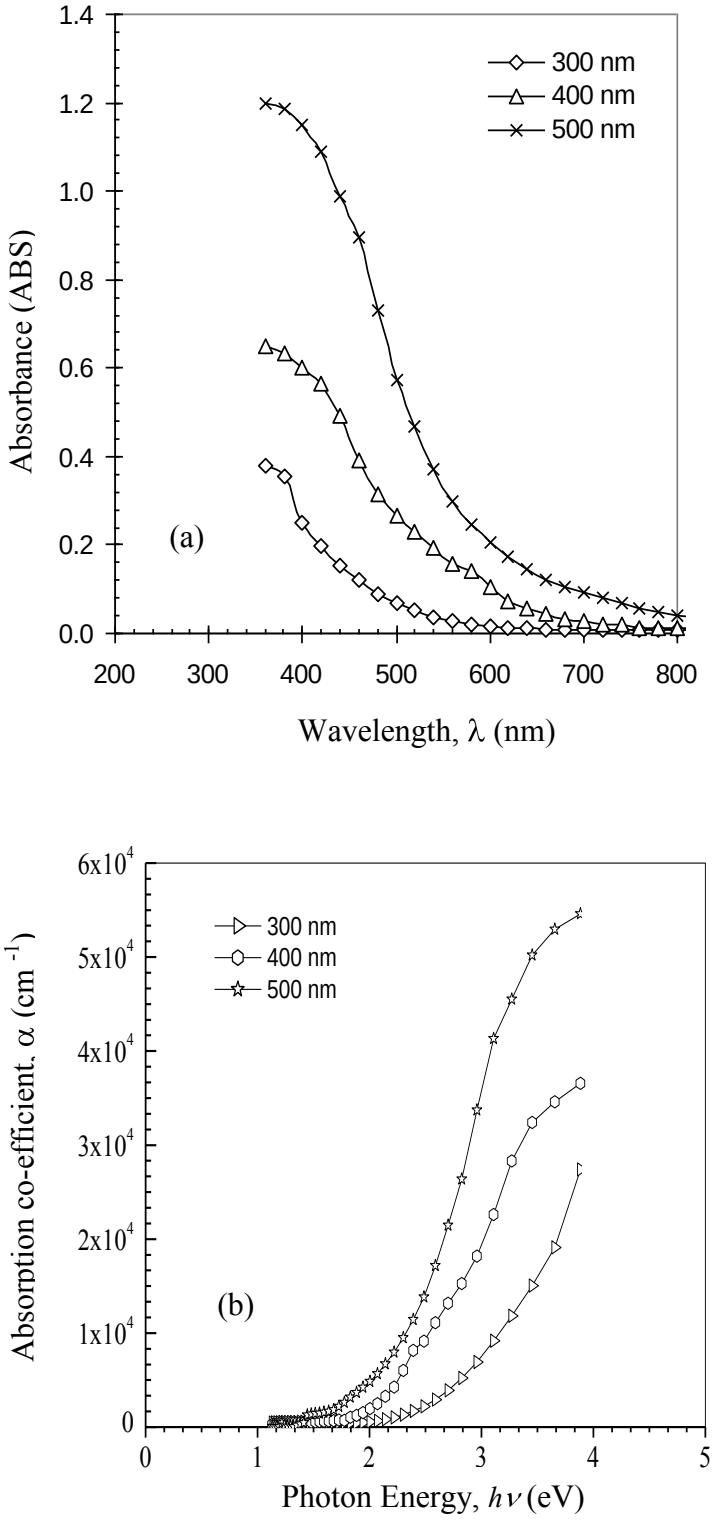

Fig. 4.10 (a) Variation of absorbance (ABS), with wavelength, for PPTMA thin films of different thicknesses (b) Plot of absorption co-efficient, α, as a function of photon energy (eV).

It is well known that increasing conjugation generally moves the absorption to longer wavelength [86, 104]. The absorption coefficient, α, is calculated from the absorbance data (Fig.4.10b) for samples of different thicknesses. It is found that in the low energy region follows an exponential fall for values of α below about 10,000 cm^{-1} for all the samples. These exponential falling edges may either be due to lack of long-range order or due to the presence of defects in the thin film.

One of the most significant optical parameters, which are related to the electronic structure, is the optical band gap. The optical band gap, E_{opt}, can be calculated between the bottom of the conduction band and the top of the valence band [86, 87]

$$\alpha h\nu = B(E_{opt} - h\nu)^n \qquad (4.2)$$

where B is the Tauc parameter, n is the parameter connected with distribution of the density of states which can assume values of 2, or 1/2 depending on the nature of the band to band electronic transitions (direct or indirect transition), h is the Planck constant, ν is the frequency of radiation and E_{opt} is the optical band gap obtained from the extrapolation of the linear part of the curve. Two different slopes could characterize all the curves in Fig. 4.10 (b). This may indicate the presence of direct and indirect transitions in PPTMA films. The E_{qd} can be evaluated from the plots of $(\alpha h\nu)^2$ as a function of $h\nu$ shown in Fig. 4.11(a). The E_{qd} was determined from the intercept of the linear part of the curves extrapolated to zero α in the photon energy axis. In Fig.4.11(b), $(\alpha h\nu)^{1/2}$ as a function of $h\nu$ was plotted to obtain the E_{qi}. The intercept of the linear part of the curves extrapolated to zero α in the photon energy axis was taken as the E_{qi}. It is evident from the Fig. 4.11(a) and Fig. 4.11(b) that there is a considerable reduction in the direct and indirect energy gap for PPTMA thin films at different thicknesses which shown in table 4.7. This means that the thickness affects the optical band gap due to the change of some of the bonds. The band gap change may also arise from the photon-lattice interaction.

Table 4.7 Allowed direct and indirect transition energy gaps for various PPTMA thin films.

Film thickness (nm)	Direct transition energy gap, E_{qd} (eV)	Indirect transition energy gap, E_{qi} (eV)
300	2.8	1.86
400	2.8	1.56
500	2.7	1.49

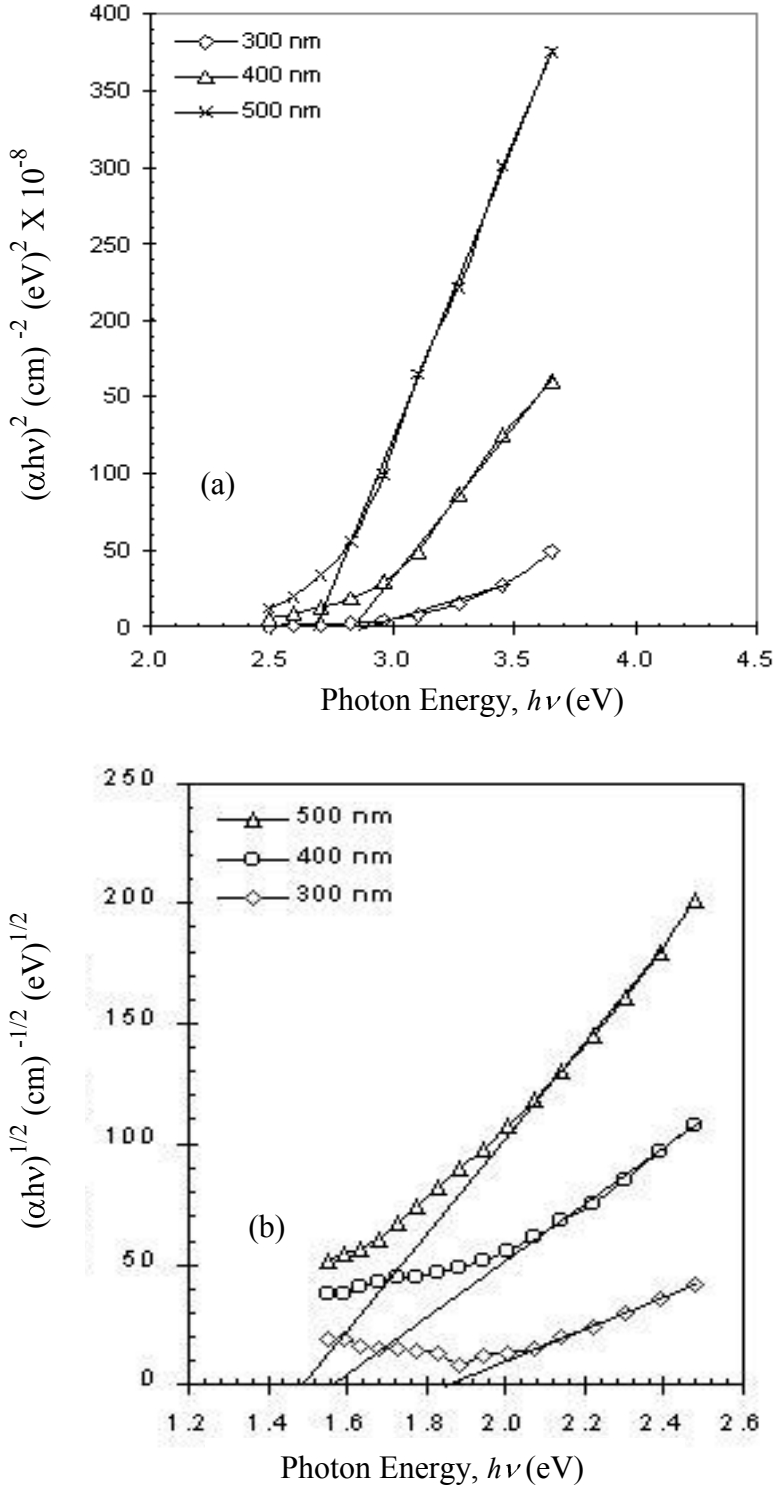

Fig 4.11 (a) $(\alpha h\nu)^2$ versus $h\nu$ curves of different PPTMA thin films. (b) $(\alpha h\nu)^{1/2}$ versus $h\nu$ curves of different PPTMA thin films.

4.8.2 PPTMA Thin Films Heat Treated at Different Temperatures

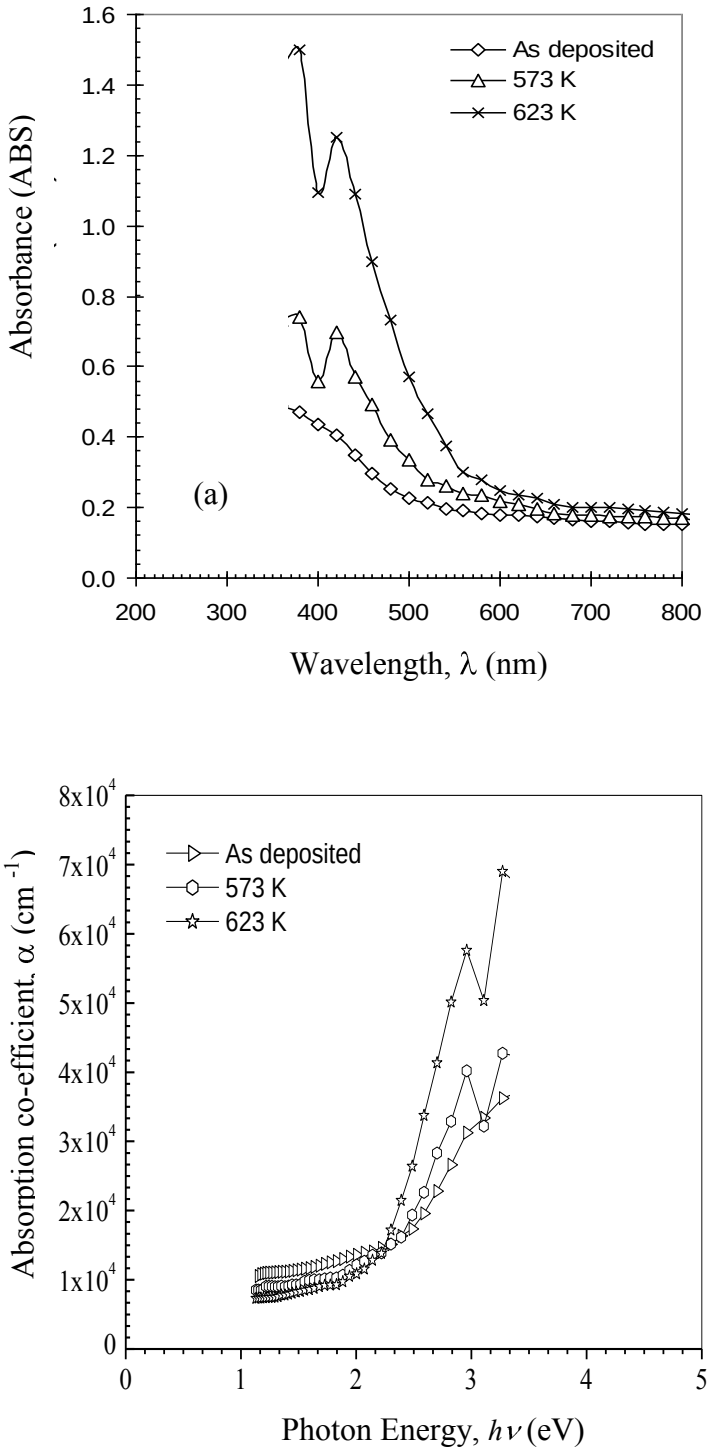

Fig. 4.12 (a) Variation of absorbance (ABS), with wavelength, for as deposited and heat treated PPTMA thin films of 300 nm (b) Plot of absorption co-efficient, α, as a function of photon energy (eV). Measurements were done at room temperature.

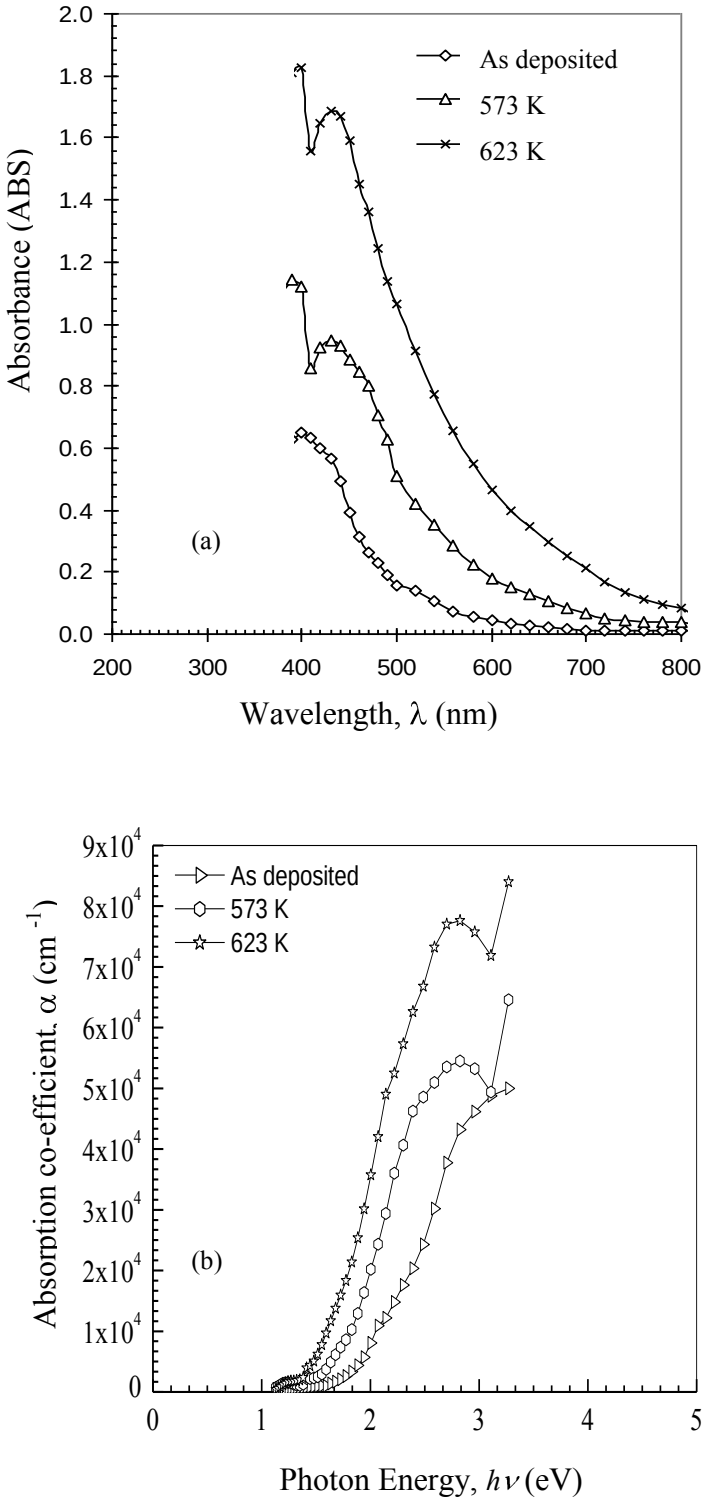

Fig. 4.13 (a) Variation of absorbance (ABS), with wavelength, for heat treated PPTMA thin films of 400 nm thick (b) Plot of absorption co-efficient, α, as a function of photon energy (eV). Measurements were done at room temperature.

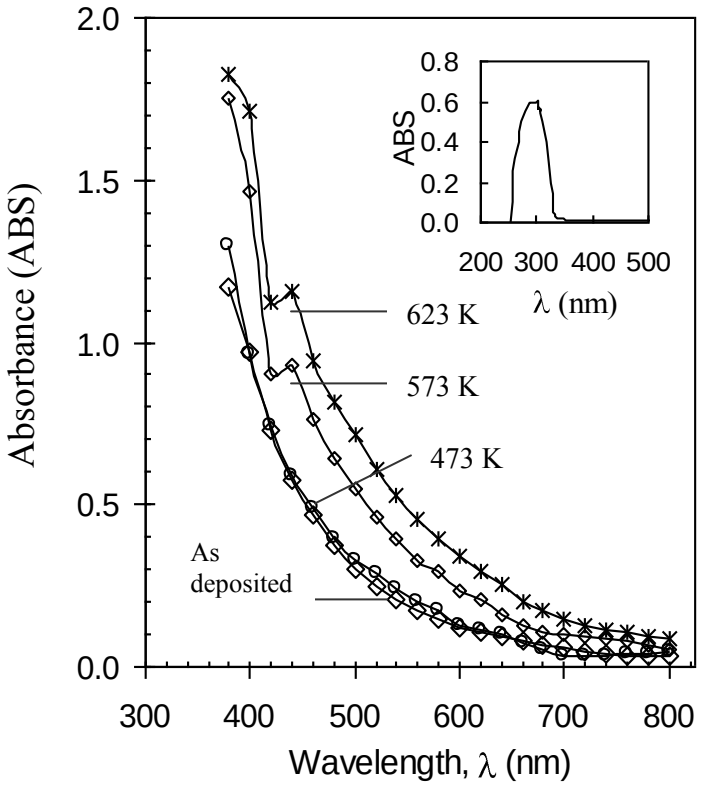

Fig 4.14 Variation of absorbance (ABS) with wavelength, λ, for as deposited and heat treated PPTMA thin films; measured at room temperature, thickness is about 500 nm (inset: Monomer).

The UV-Vis absorption spectra for TMA, as deposited and heat treated PPTMA thin films at 473, 573 and 623 K have been recorded at room temperature and are presented in Fig.4.12. 4.13 and 4.14, respectively. It is seen that the peak value shifts to the higher wavelength compared to the peak wavelength value, 300 nm of TMA. Thus, there is a red shift of about 79 nm in λ_{max} as compared to TMA peak. This red shift in PPTMA demonstrates an increased degree of conjugation present in the resulting films. It is observed that absorption of PPTMA does not much change on heat treatment up to 473 K. Whereas there is an overall increase in the absorption of the PPTMA heat treated above 473 K. It can be noticed that a small peak appears at around 420 nm (d=300 nm), 430 nm (d=400 nm), and 440 nm (d=500 nm), in the spectra of PPTMA heat treated at 573 and 623 K. The peaks are shifted to higher wavelength depending on thicknesses. An increase of the absorption intensity in the 380-600 nm region of PPTMA heat treated at higher temperature may indicate a structural rearrangement most probably by the removal of dangling bonds and/or formation of conjugation in the structure.

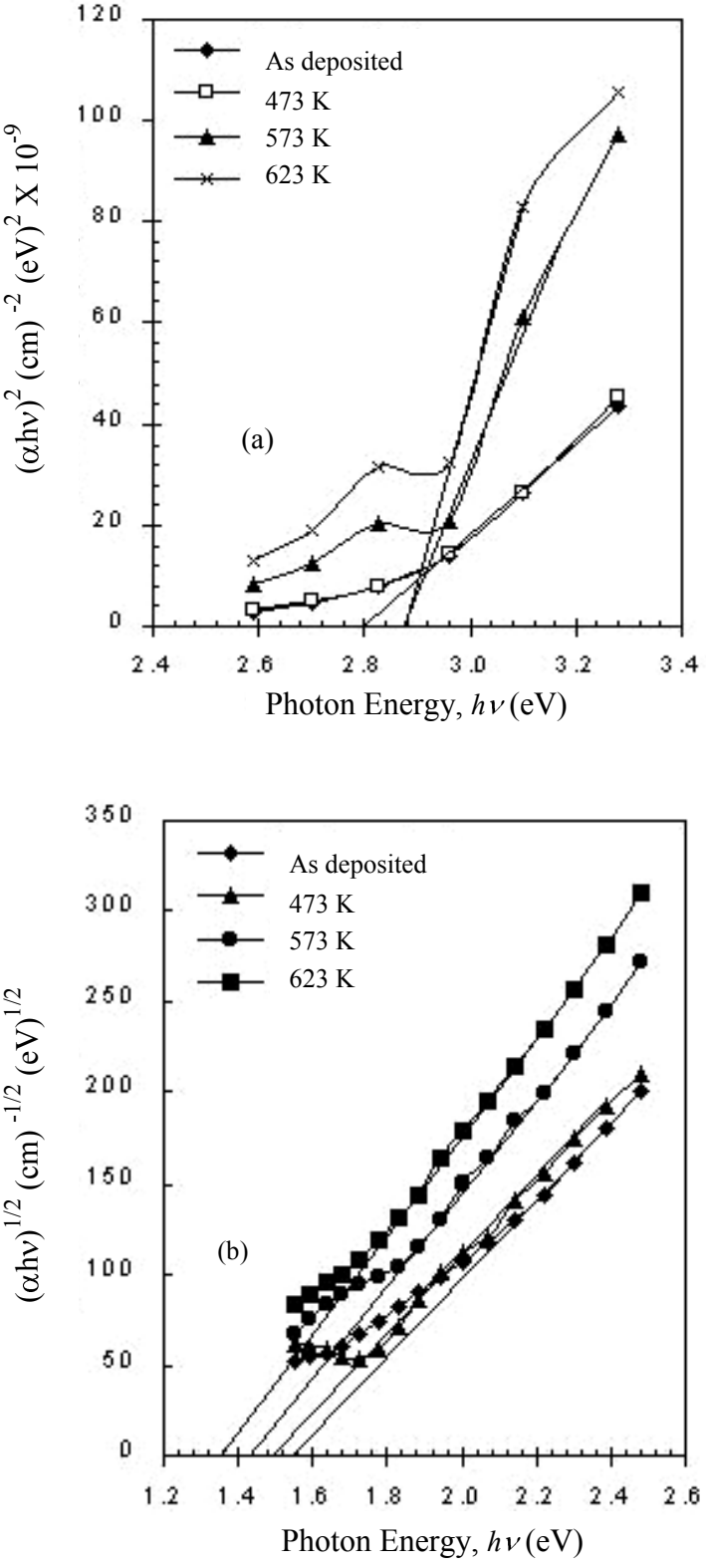

Fig 4.15 (a) $(\alpha h\nu)^2$ versus $h\nu$ curves and (b) $(\alpha h\nu)^{1/2}$ versus $h\nu$ curves of PPTMA thin films of 500 nm thick heat treated at different temperature.

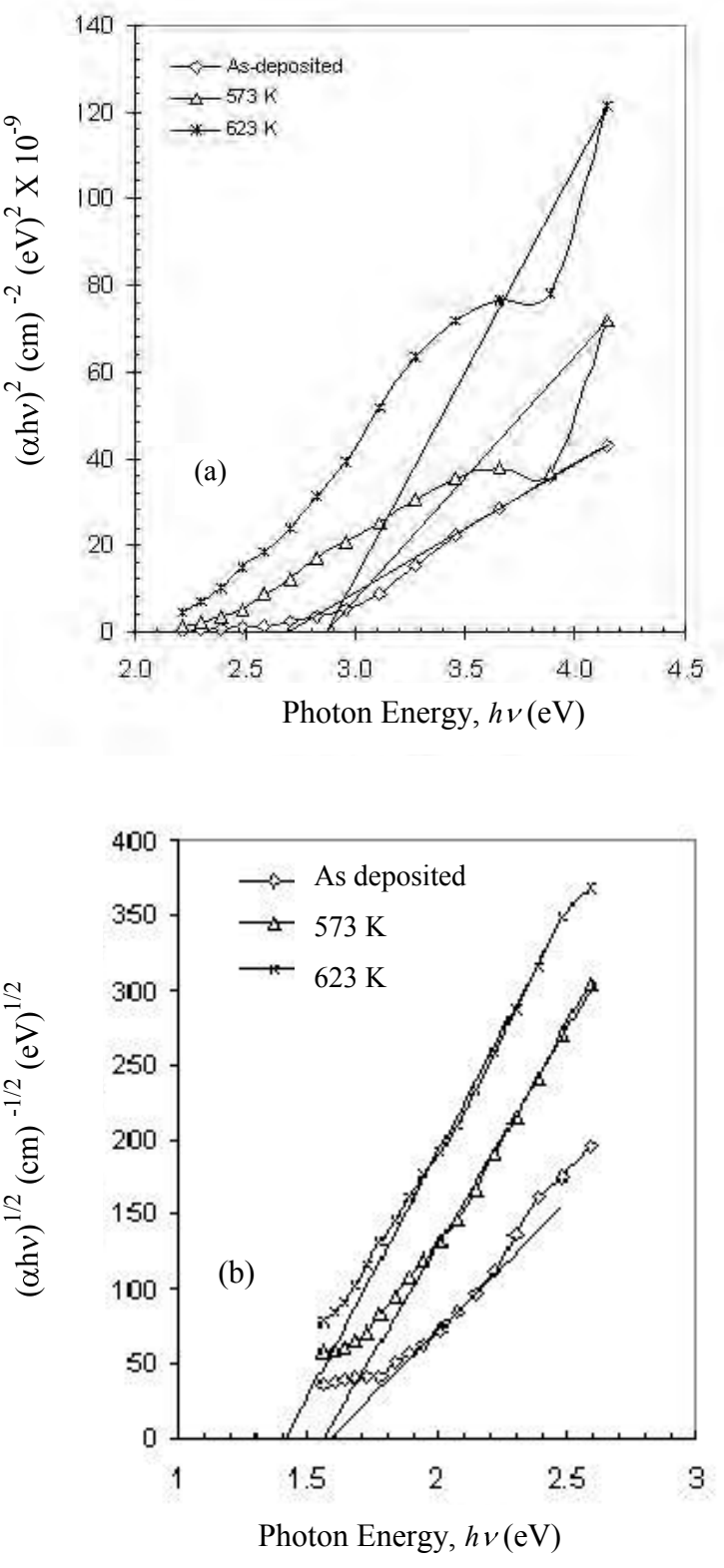

Fig 4.16 (a) $(\alpha h\nu)^2$ versus $h\nu$ curves and (b) $(\alpha h\nu)^{1/2}$ versus $h\nu$ curves of PPTMA thin films of 400 nm thick heat treated at different temperature.

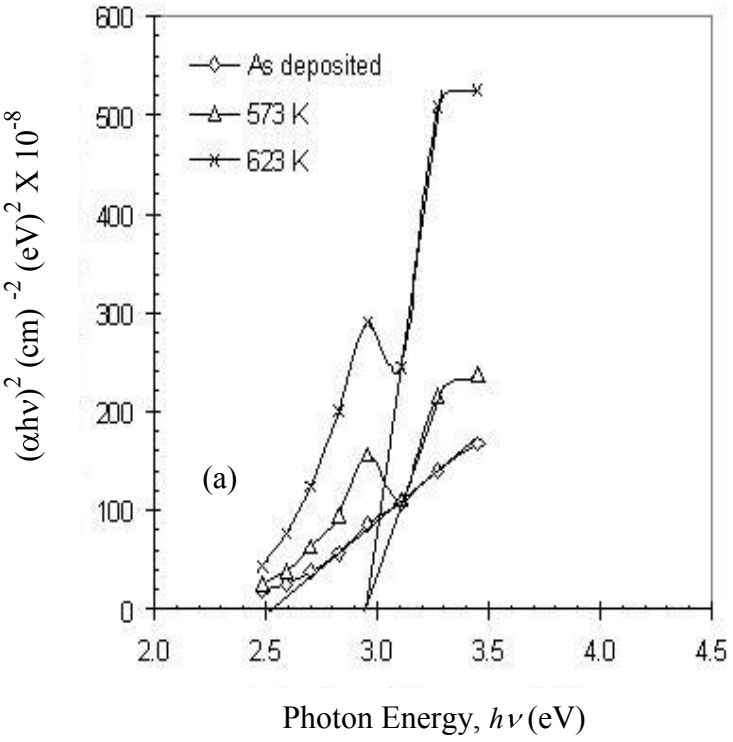

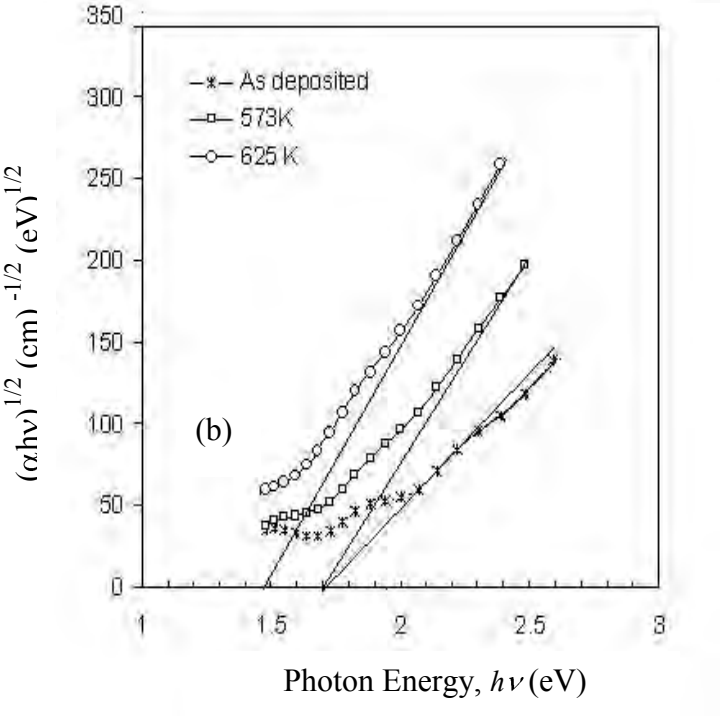

Fig 4.17 (a) $(\alpha h\nu)^2$ versus $h\nu$ curves and (b) $(\alpha h\nu)^{1/2}$ versus $h\nu$ curves of PPTMA thin films of 300 nm thick heat treated at different temperature.

The appearance of the absorption peak (d=500 nm) at around 440 nm in the PPTMA thin film heat treated at a higher temperature may be due to π-π^* transition because of the probable development of conjugation in the structure on heat treatment. The results of dependence of α on $h\nu$ indicate that in the films of lower thickness the intensity of light is reduced. The values of E_{qd} and E_{qi} obtained from the plots of Figs.4.15, 4.16 and 4.17 are documented in table 4.8. It is noticed that E_{qd} value is slightly increased when heat treated at 573 K and remains almost constant when heat treated above this temperature, whereas, E_{qi} gradually decreases with the increase of the heat treatment temperature. From table 4.8 it is seen that both the direct and indirect bands for 400 nm thick are higher than 300 nm and 500 nm thick. That means band gaps more than resistivity increase for the sample. So its conductivity is lower than other two samples. The effect for heat treatment it is seen that higher temperature the band gaps for all samples increases. Thus, it can be inferred from the variation of E_{qd} and E_{qi} that the bands in PPTMA become wider on heat treatment. From the comparative study of as deposited and heat treated PPTMA thin films of different thicknesses, it is observed that higher values for lower thick samples and opposite for higher thickness. That means high thickness samples give higher conductivity.

Table 4.8 Allowed direct and indirect band gaps for different thicknesses heat treated PPTMA thin films.

Temperature* (K)		As-deposited and heat treated PPTMA films	
Thickness		Direct transition energy gap (eV)	Indirect transition energy gap (eV)
500 nm	as deposited	2.80	1.56
	473*	2.80	1.50
	573*	2.88	1.44
	623*	2.88	1.36
400 nm	As deposited	2.70	1.70
	573*	2.88	1.70
	623*	2.88	1.49
300 nm	as deposited	2.80	1.86
	573*	2.94	1.58
	623*	2.94	1.60

* heat treated for 1 hour in air.

4.8.3 Iodine doped as deposited PPTMA

The UV-Vis absorption spectra in the range 200 to 800 nm of as deposited PPTMA thin films and PPTMA thin films doped with iodine of thicknesses 300, 400 and 500 nm are shown in Fig. 4.18(a). The spectra of the films exhibit a sharp absorption peaks at about 390 nm and there are no absorption peaks at the longer wavelengths. It is seen that the intensity of the absorption peak increases for the increase of PPTMA film thickness. UV-Vis spectra of PVDF films filled with iodine show new broad bands at 286 and 353 nm which are attributed to the formation of charge transfer complex [19]. After exposing the film to iodine doping process may be occurred due to the formation of iodine complex. In the PPTMA films doped with iodine also show a new broad band which can be attributed to the formation of charge transfer complex.

The absorption co efficient is plotted against the photon energy for as deposited PPTMA thin films and PPTMA thin films with iodine doped PPTMA thin films and is shown in Fig. 4.18(b). The optical transition energies corresponding to the films prepared under various deposition conditions are given table 4.9. The intercept of this plots on the photon energy axis give the direct band gap for all iodine doped PPTMA samples and one indirect band gap for one sample. It can be seen that the iodine doping decreases the direct transition energy gap from 2.6 eV to 2.4 eV (Fig.19a). The energy gap of as deposited PPTMA thin films is 2.8 eV and that of doped PPTMA thin films is 2.6 eV. The indirect transition energy gap is found 1.6 for 300 nm thick PPTMA (Fig.19b) but not get for 400 and 500 nm. The changes of energy gap indicate that there is a charge transfer complex arising between the as deposited PPTMA and the iodine.

Table 4.9 Allowed direct and indirect transition energy gaps for iodine doped PPTMA thin films.

Film thickness (nm)	Direct transition energy gap, E_{qd} (eV)	Indirect transition energy gap,E_{qi} (eV)
300	2.6	1.6
400	2.4	-
500	2.4	-

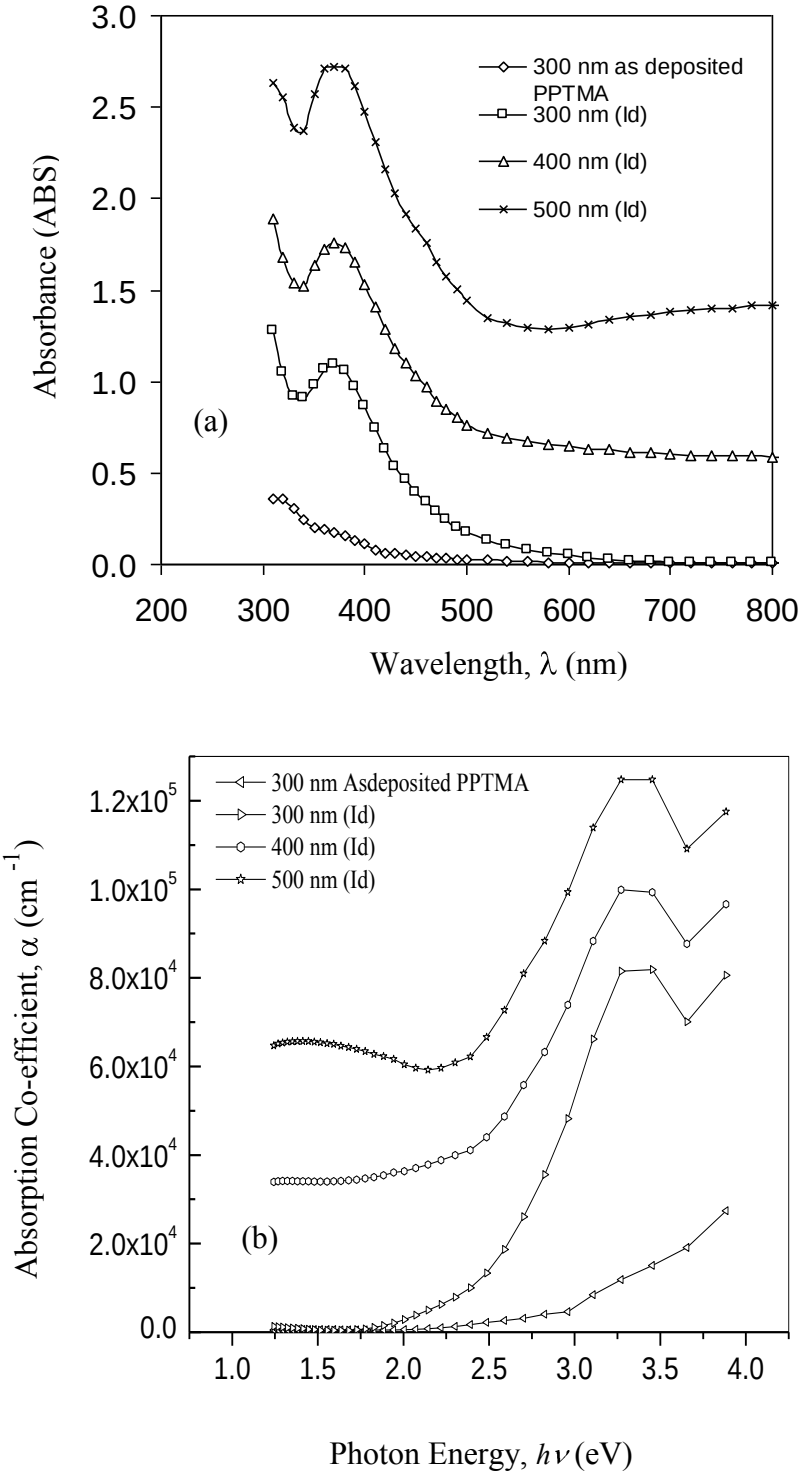

Fig 4.18(a) Variation of absorbance, ABS, with wavelength for as deposited PPTMA thin films and PPTMA thin films with iodine of different thicknesses (b) Plot of absorption co-efficient, α, as a function of photon energy (eV).

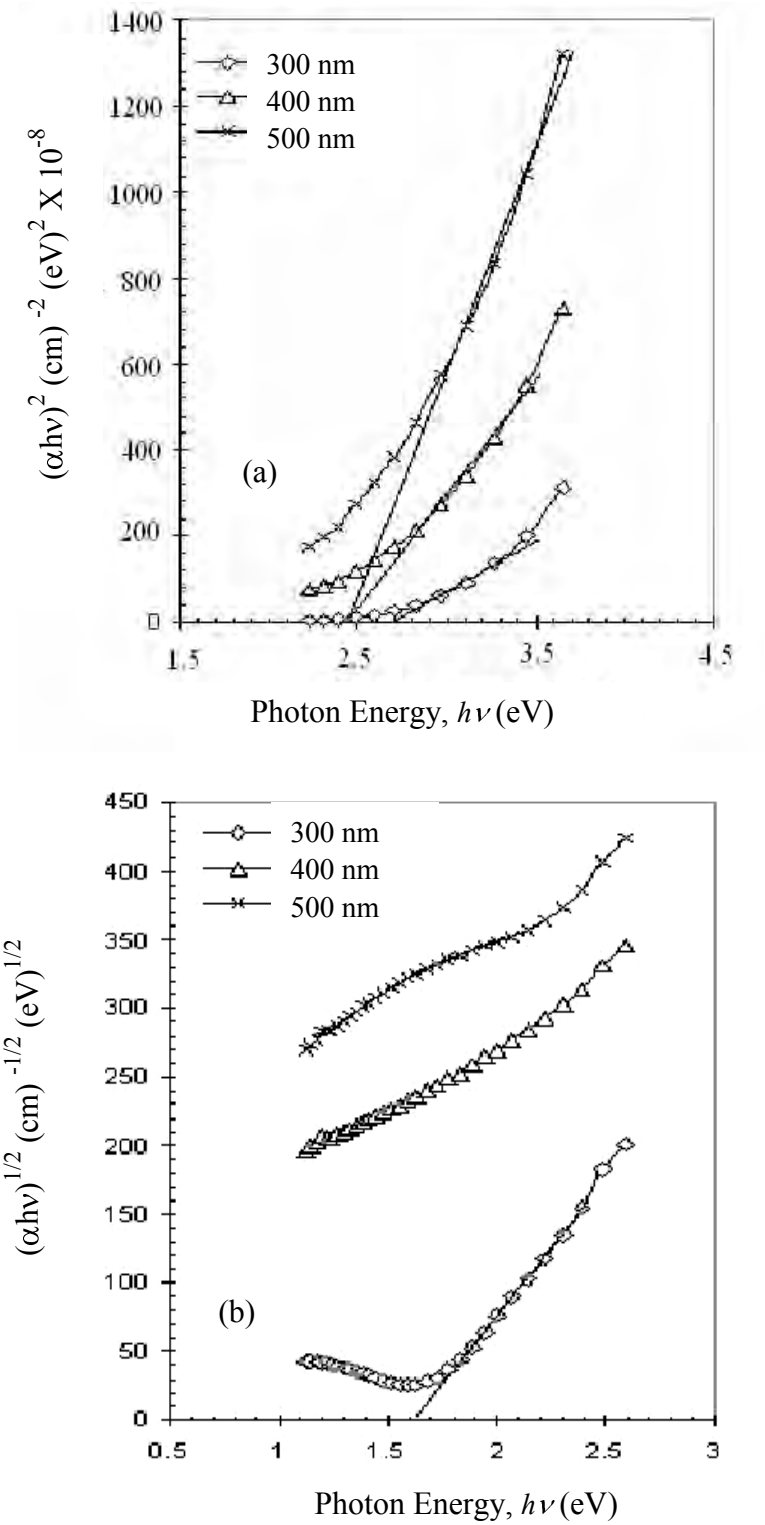

Fig 4.19 (a)$(\alpha h\nu)^2$ versus $h\nu$ curves of iodine doped PPTMA thin films and (b) $(\alpha h\nu)^{1/2}$ versus $h\nu$ curves of iodine doped PPTMA thin films.

4.9 Reaction of PPTMA with iodine

In a glass beaker the PPTMA thin film was exposed to iodine crystals. The reaction between PPTMA thin film and iodine takes place because the color of the PPTMA thin film changes from light to dark brown. After the reaction of PPTMA with iodine the iodination of benzene rings might be anticipated in Fig.4.20. During such a reaction, the iodine replaces the hydrogen atoms in the benzene rings, but not replaces the hydrogen in the methylgroup of PPTMA thin film. Hydrogen atoms recombine with iodine and produce hydriodic acid.

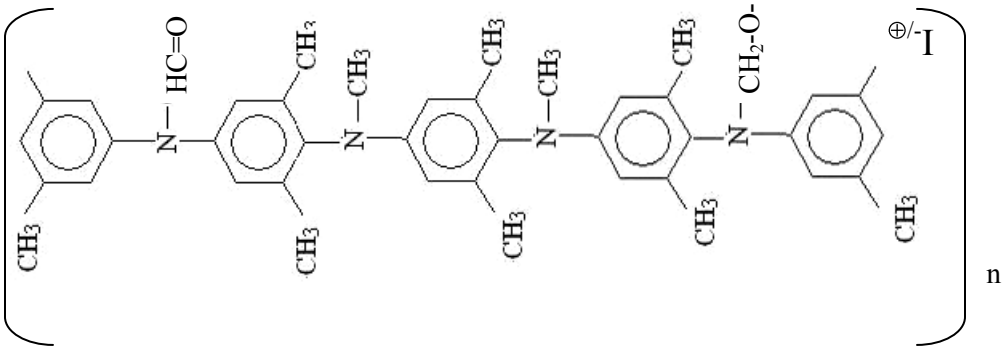

Fig 4.20 The proposed structure of PPTMA polymer with iodine.

4.10 Direct Current Electrical Conduction Mechanism in PPTMA Thin Films

4.10.1 Current density-Voltage characteristics of PPTMA thin films

J-V characteristics of PPTMA thin films of thicknesses 300, 350, 400 and 500 nm at temperatures 300, 373 and 423 K were recorded in the voltage region from 0.2 to 15.0 V. The observed room temperature J-V characteristics of the PPTMA thin films are presented in Fig. 4.21. The J-V curves follow a power law of the form $J \propto V^n$ with different slopes in the lower and higher voltage regions, where n is a power index. In the lower voltage region the values of slope are $0.80 < n < 1.26$, correspond to the ohmic region, whereas in the higher voltage region the values of slope lie between $1.70 < n < 2.20$, represent the non-ohmic region. Fig. 4.22 presents the representative J-V curves for one sample at three different temperatures. It is observed that the slopes of both the voltage regions are increased slightly with increasing temperature. This increase may be due to increased molecular motions in PPTMA at higher temperatures. The thickness and voltage dependence of current density at the higher voltage region suggest that the current may be due to SCLC, Schottky or PF mechanisms in PPTMA thin films. To differentiate the type of conduction mechanisms, the

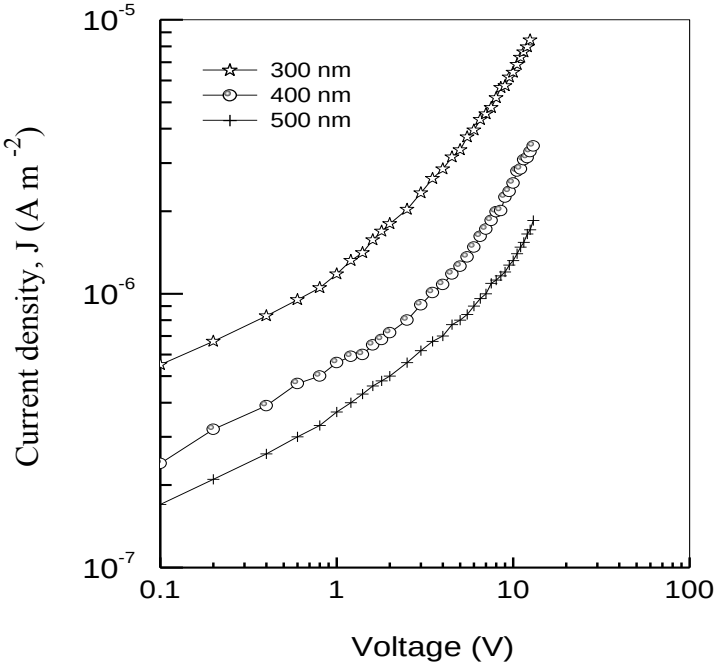

Fig 4.21 Plots of J-V for as deposited PPTMA thin films of different thicknesses recoded at room temperature

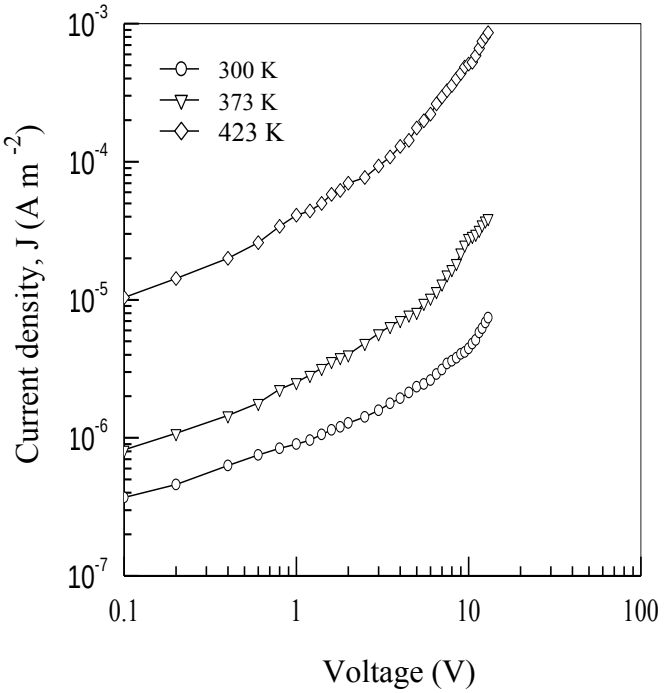

Fig 4.22 Plots of J-V for as deposited PPTMA thin film, measured at different temperatures, (Thickness: 300 nm).

dependence of J on film thickness, d, for the samples of different thicknesses at a constant voltage (10 V) is presented in Fig. 4.23. The thickness dependence of the current follows the relation, $J \propto d^{-l}$ where l is a parameter depending upon the trap distribution. A slope $l < 3$ suggests the possibility of Schottky or PF mechanism and $l \geq 3$ reveals the possibility of SCLC mechanism. The linear slope derived from these data has a value of about 3.5, which is much higher than that corresponding to Schottky and PF conduction mechanism. Thus the type of conduction mechanism in PPTMA most probably is SCLC. The current density for SCL conduction can be presented as

$$J = \frac{9}{8}\varepsilon'\varepsilon_o\mu\frac{V^2}{d^3} \qquad (4.3)$$

where μ is the mobility of charge carriers, ε' is the dielectric constant of the dielectric material, ε_o is the permittivity of free space, V is the applied voltage, d is the thickness. The analyses of J-V curves (Fig. 4.23) for PPTMA thin films yield the μ value to be about 1.3×10^{-13} m^2 $V^{-1}s^{-1}$ using the relation (4.3). The intrinsic free carrier density, n_o, can be determined by the relation

$$V_t = \frac{8}{9}\frac{n_o e d^2}{\varepsilon_o\varepsilon'} \qquad (4.4)$$

where V_t is the threshold voltage and e is the electronic charge. The ε' is required to calculate n_o. So the capacitance of the sample was measured at 30 KHz and the ε' was calculated out to be about 2.5. Using the values of the ε_o, ε', e, d (=350 nm) and V_t = 2.7 V (from Fig. 4.23), the n_o is calculated out to be about 2×10^{21} m^{-3}. The transition from the ohmic region to the SCLC region occurs at a threshold voltage, V_t, which may be derived from each J-V characteristics in Fig. 4.23. The values of V_t between ohmic and SCL conduction dependence on d is shown in Fig. 4.24. The slope of about 2 derived from the figure further supports the interpretation of SCLC dominated by an exponential trap distribution.

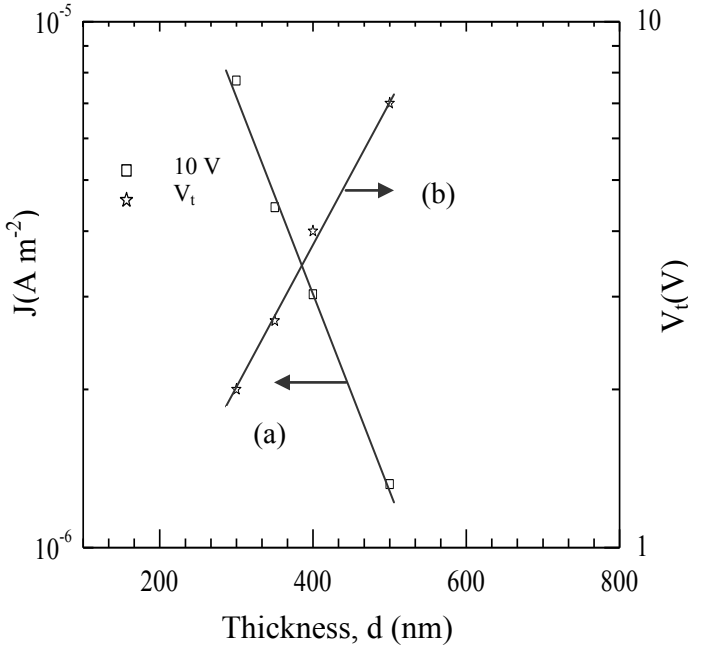

Fig 4.23 Plots of (a) current density (J) against different thicknesses (left hand scale) and (b) V_t against different thicknesses (right hand scale) for PPTMA thin film in the non-ohmic region.

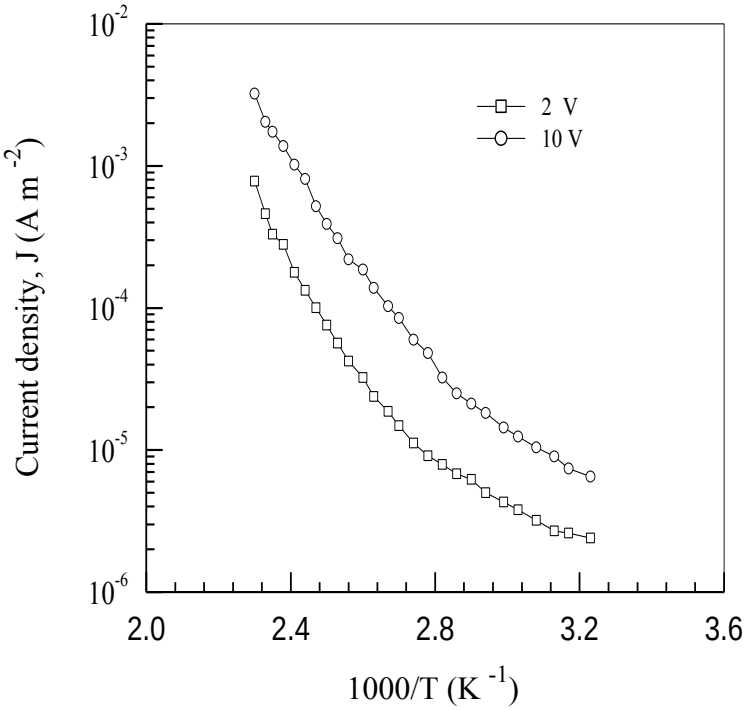

Fig 4.24 Plots of J -1/T for PPTMA thin film in the ohmic and non-ohmic regions (d = 300 nm).

Considering the linearity of curves in Fig. 4.24 at higher temperatures to results from an exponential trap distribution the total trap density, N_t may be determined from the intercept on the log J axis as described by Gould [106]. The value of $N_t = 4 \times 10^{30}$ m^{-3} was obtained assuming $N_c = 1 \times 10^{27}$ m^{-3}.

4.10.2 Current density-Voltage characteristics of iodine doped PPTMA thin films

The SEM, band gap energy, and literature studies mentioned in the chapter as before have indicated that the electrical conductivity of PPTMA would be enhanced upon iodine doping. Fig.4.25 shows J-V characteristics of the undoped and iodine doped PPTMA thin film. It may be noted that as a result of iodine doping, the current increases with the voltage and significantly similar behaviors were observed in films of different temperatures. Fig.4.26 presents the representative J-V curves of iodine doped PPTMA thin films of as deposited PPTMA 300, 400 and 500 nm. J-V characteristics of iodine doped PPTMA thin films of different thicknesses at temperatures 300, 373 and 423 K were recorded in the voltage region from 0.2 to 30.0 V. The value of current density is enhancing by iodine doping in PPTMA thin films. The observed J-V characteristics of the films are presented in Figs. 4.27 to 4.29. The J-V curves follow a power law, with different slopes in the lower and higher voltage regions. The values of the slopes are depicted in table 4.10.

Table 4.10 The slopes in the two voltage regions at different thicknesses and different temperatures.

Thickness of iodine doped PPTMA thin films d (nm)	Measurement temperature	Value of slopes	
		Low voltage region (ohmic)	High voltage region (non ohmic)
300	300	0.54	1.59
	373	1.03	1.55
	423	1.00	1.64
400	300	0.63	1.70
	373	0.80	2.08
	423	0.95	2.28
500	300	0.61	1.97
	373	1.00	2.10
	423	1.21	2.37

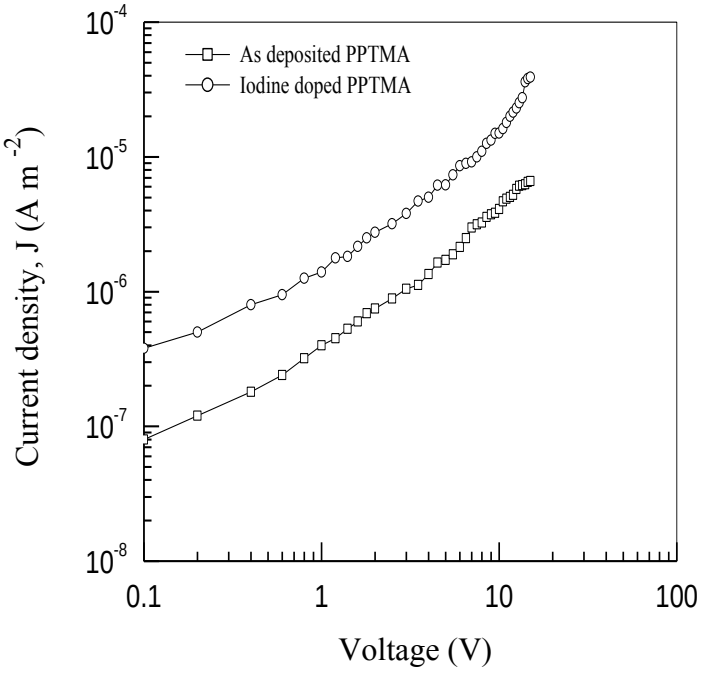

Fig 4.25 Plots of J-V for as deposited and iodine doped PPTMA thin films of 400 nm thick recorded at room temperature.

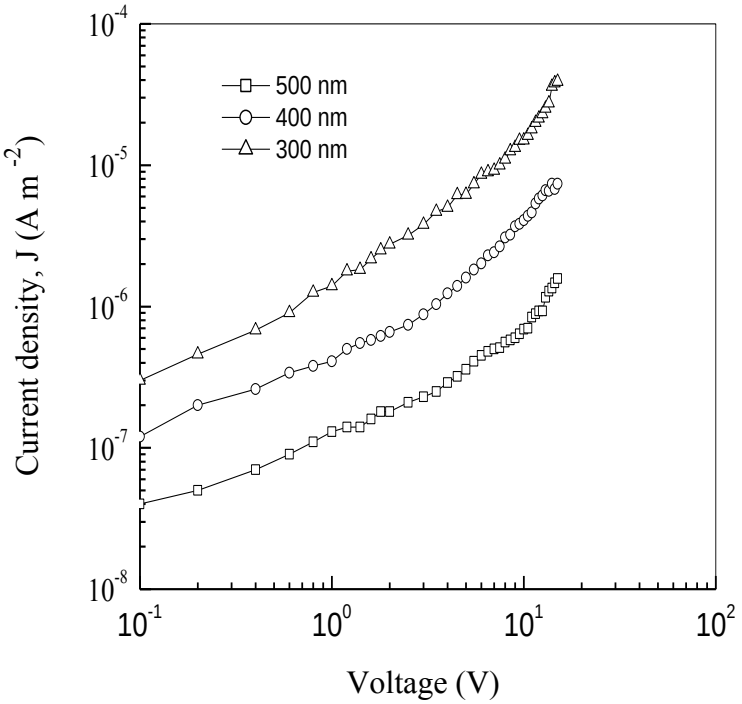

Fig 4.26 Plots of J-V for iodine doped PPTMA thin films of different thicknesses recorded at room temperature.

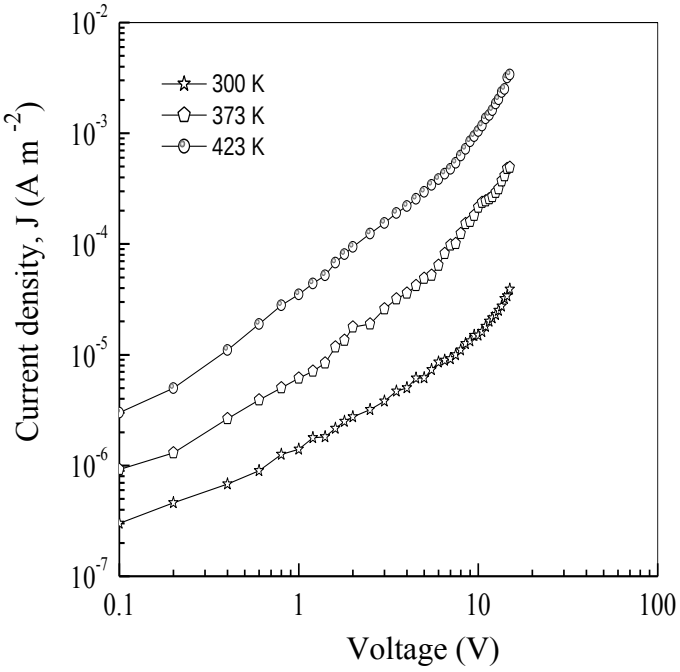

Fig 4.27 Plots of J-V for iodine doped PPTMA film, measured at different temperatures (Thickness ; 300 nm).

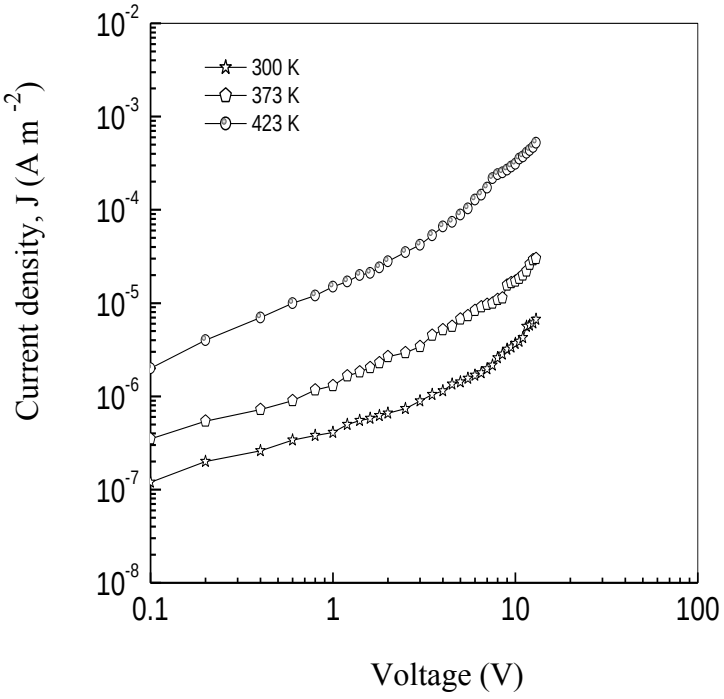

Fig 4.28 Plots of J-V for iodine doped PPTMA film, measured at different temperatures (Thickness ; 400 nm).

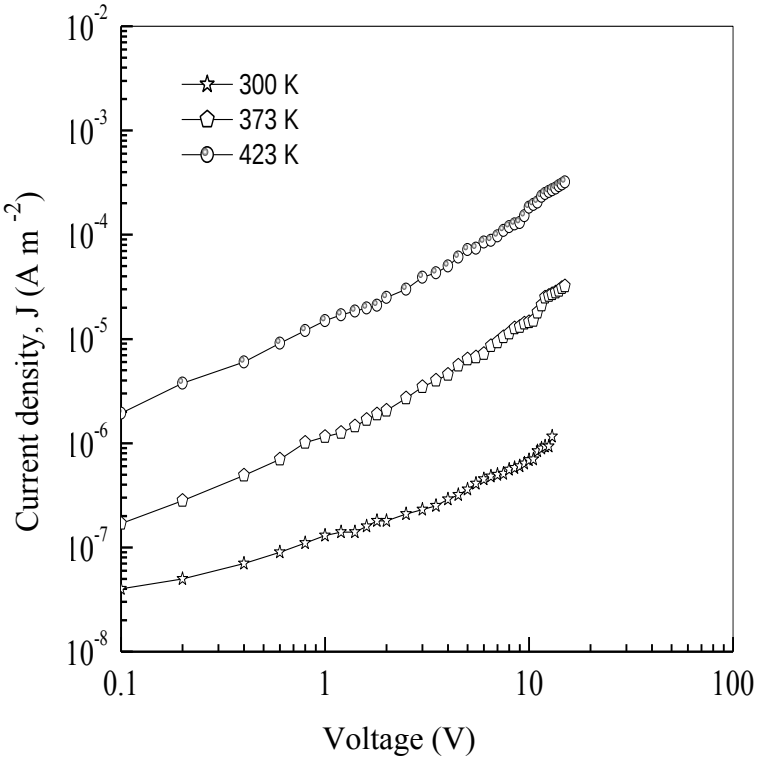

Fig 4.29 Plots of J-V for iodine doped PPTMA film measured at different temperatures (Thickness ; 500 nm).

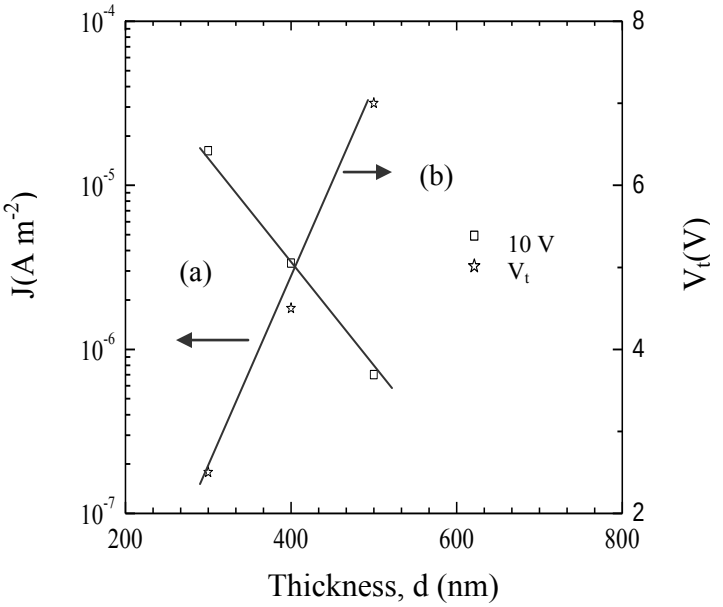

Fig 4.30 Plots of (a) current density (J) against different thicknesses (left hand scale) and (b) V_t against different thicknesses (right hand scale) for iodine doped PPTMA thin film

To ascertain the type of conduction mechanism, the dependence of J on film thickness d for a series of different samples at constant voltage (10V) is presented in Fig. 4.30. The linear slope derived from these data has a value of about 6.2. It is seen that in the non-ohmic region the slope is much higher than that corresponding to Schottky and PF conduction mechanism. This value satisfied the condition for SCLC mechanism as discussed in section 4.10.1 Thus, it is seen that the type of conduction mechanism in iodine doped PPTMA most probably be SCLC. The analyses of J-V curves (Fig.4.26) for iodine modified PPTMA thin films yield the μ value to be about 1.2×10^{-12} m^2 $V^{-1}s^{-1}$ using the relation (4.3).

4.10.3 Thermally activated current in PPTMA and iodine doped PPTMA thin films

Figs.4.31 to 4.33 show the dependence of J on inverse absolute temperature, 1/T, for iodine doped PPTMA thin films of different thicknesses. There are two curves, one in the ohmic region with an applied voltage, 2 V, and other in the SCLC region with an applied voltage, 10V. Each of the curves has two different slopes in the low temperature and the higher temperature regions. The intrinsic free carrier density, n_o, and the total trap density of iodine doped PPTMA are about 3.7×10^{21} m^{-3} and 1.2×10^{27} m^{-3}, respectively.

Table 4.11 Values of carrier mobility, free carrier density, total trap density and electrical conductivity for as deposited and iodine doped PPTMA thin films (d=400 nm).

Sample	Carrier mobility, μ, m^2 $V^{-1}s^{-1}$	Free carrier density, n_o, m^{-3}	Total trap density, N_t, m^{-3}	Conductivity, (ohm-m) $^{-1}$
As deposited PPTMA thin film	1.30×10^{-13}	2.00×10^{21}	4.00×10^{30}	7.80×10^{-14}
Iodine doped PPTMA thin film	1.50×10^{-12}	3.70×10^{22}	1.20×10^{27}	3.10×10^{-13}

The electrical conductivity measurements on as deposited and iodine doped PPTMA thin films of 400 nm thickness show a higher value of electrical conductivity in the case of iodine doped PPTMA thin film when compared to the as deposited PPTMA thin film. Also, it is found that the iodine doping enhance conductivity of the polymer thin films considerably [16].

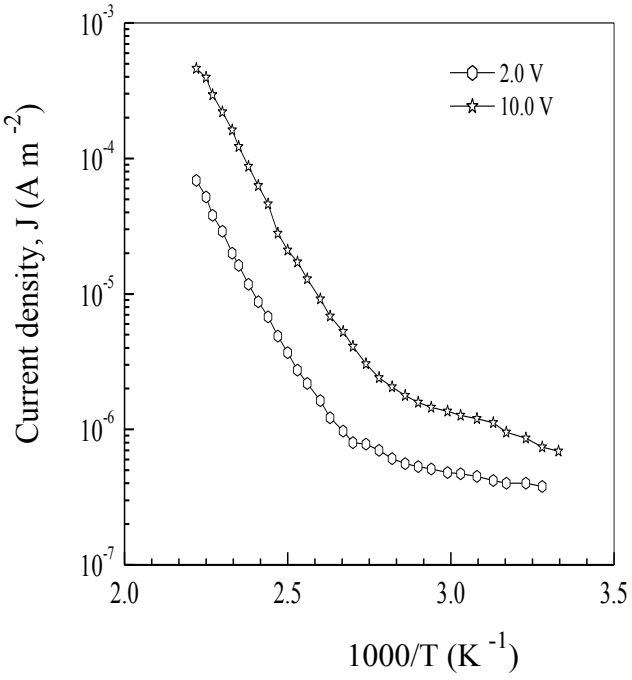

Fig 4.31 Plots of J-1/T for iodine doped PPTMA thin film the ohmic and non-ohmic regions (d = 300 nm).

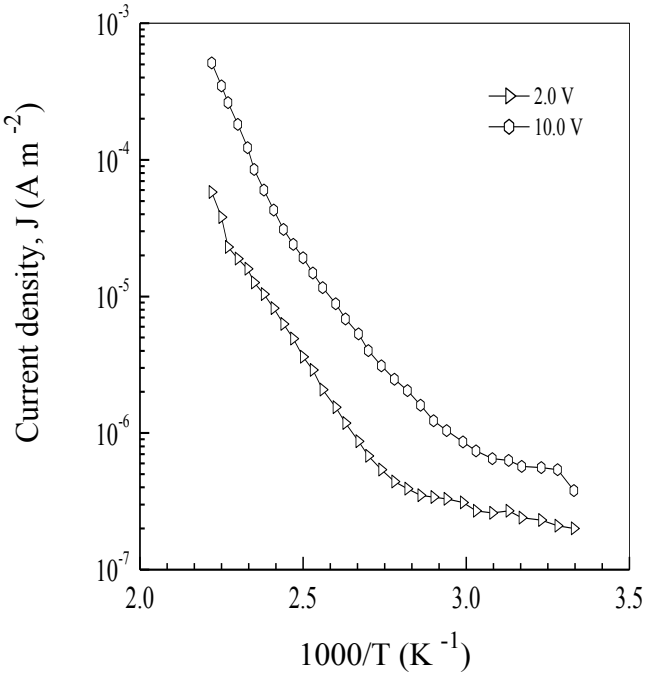

Fig 4.32 Plots of J-1/T for iodine doped PPTMA thin film the ohmic and non-ohmic regions (d = 400 nm).

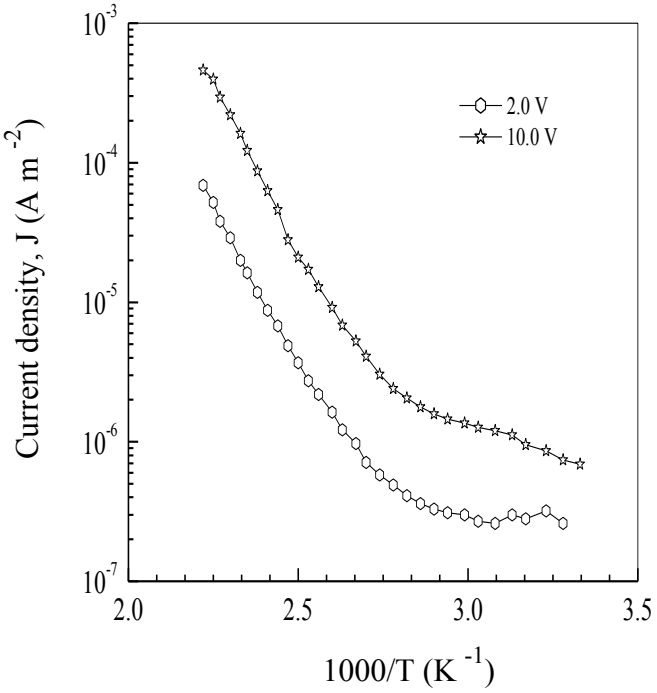

Fig 4.33 Plots of J-1/T for iodine doped PPTMA thin film the ohmic and non-ohmic regions (d = 500 nm).

4.10.4 Explanation of the Correlation between the Activation Energy and Optical Band Gap of the PPTMA Thin Film

The dependence of J on inverse absolute temperature, 1/T, for PPTMA thin films of different thicknesses (300, 400, and 500 nm) in the SCLC region with an applied voltage, 10 V, which studied in my M.Phil thesis. The activation energies are about 0.21 ± 0.05 eV at the lower temperature and 0.93 ± 0.08 eV at the higher temperature regions. The ΔE values of lower and higher temperature regions suggest that there may be a transition of the conduction process from a hopping regime to a regime dominated by distinct energy levels.

The band gap between the valence and conduction band can be explained in terms of the observed SCLC and optical absorption results. PPTMA thin films deposited using identical conditions have an indirect optical band gap of 1.86 eV of as deposited PPTMA thin films of 400 nm thickness discussed M.Phil thesis and activation energy for conduction of 0.93 eV. It

is seen that the activation energy is about half of the indirect band gap. It may be imagined that the energy gap may be filled up partially from top of the valence band and bottom of the conduction band where the Fermi level may be situated at the middle of the gap. Similar results have been reported by Silva and Amaratunga [42] for dimond like carbon and for disorder solids [40].

4.11 Alternating Current Electrical Conduction Mechanism

4.11.1 Variation of ac Electrical Conductivity with Frequency and Temperature

The σ_{ac} curves of PPTMA thin films against frequency from 100Hz to 100 kHz in the temperature range from 300 to 450 K are presented in Figs.4.34 –4.36. It is observed that the σ_{ac} increases as frequency increases and slightly change depending on thicknesses (300 to 450 nm). The σ_{ac} increases rapidly in the higher frequencies compared to that in the lower frequencies. This can be interpreted by the following empirical relation (1)

$$\sigma_{ac}(\omega)=A\omega^{n} \qquad (4.5)$$

where ω is the angular frequency and n the index that is used to understand the type of conduction mechanism in amorphous materials. The values of exponent for PPTMA are found to be 0.77-1.04 below 10^3 Hz and 1.79 - 1.83 above 10^3 Hz. The values of the slope n, is around 1 in the lower frequency region which corresponds to the ohmic region and in the higher frequency region the slope is around 2 for all samples corresponding to the non ohmic region. The values of n for PPTMA thin films at different temperatures are recorded in Table 4.12. The values of n in the lower frequency region are in accordance with the theory of Debye type loss mechanism and other mechanisms may be operative in the high frequency region.

Table 4.12 The values of n for different temperatures.

Sample	Measurement Temperature (K)	Values of 'n' in the frequency region	
		100 to 10^3 (Hz)	10^3 to 10^5 (Hz)
PPTMA	300	0.77	1.79
	350	0.85	1.84
	400	0.97	1.83
	450	1.08	1.79

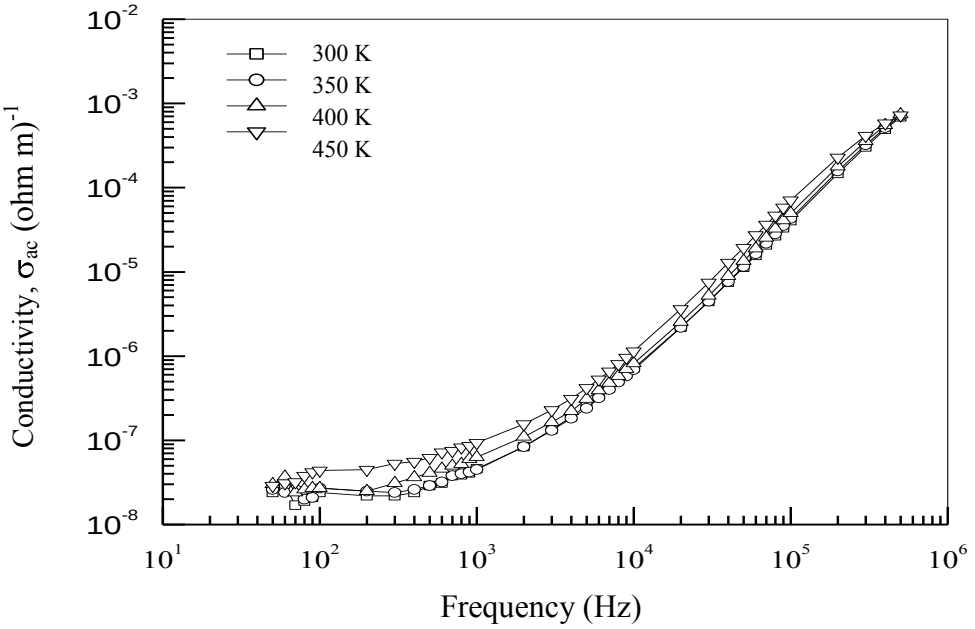

Fig 4.34 ac conductivity, σ_{ac}, as a function of frequency of the PPTMA films at different Temperatures (d= 300 nm)

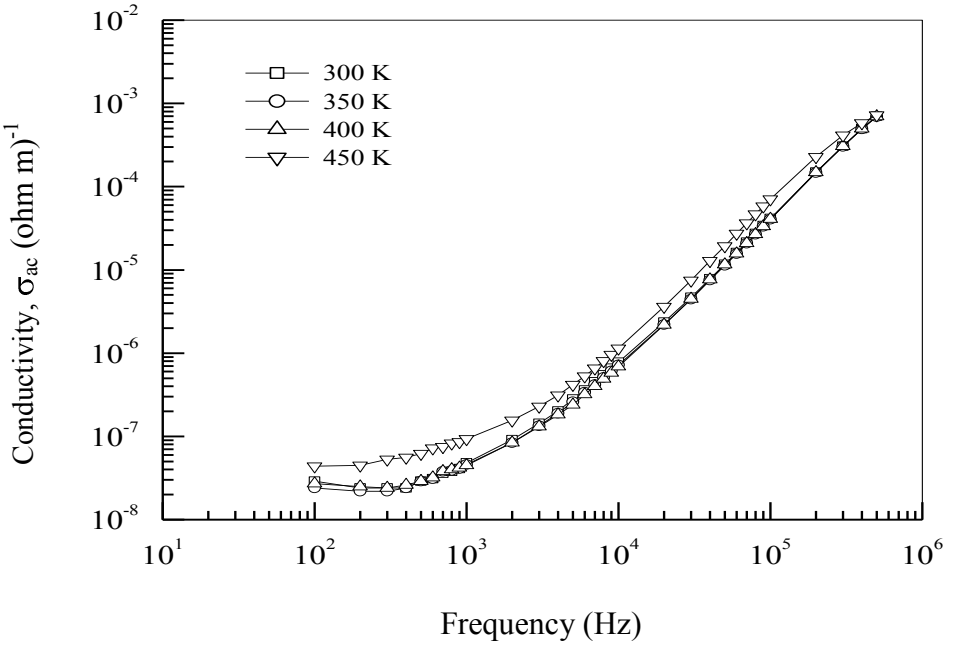

Fig 4.35 ac conductivity, σ_{ac}, as a function of frequency of the PPTMA films at different temperatures (d= 400 nm)

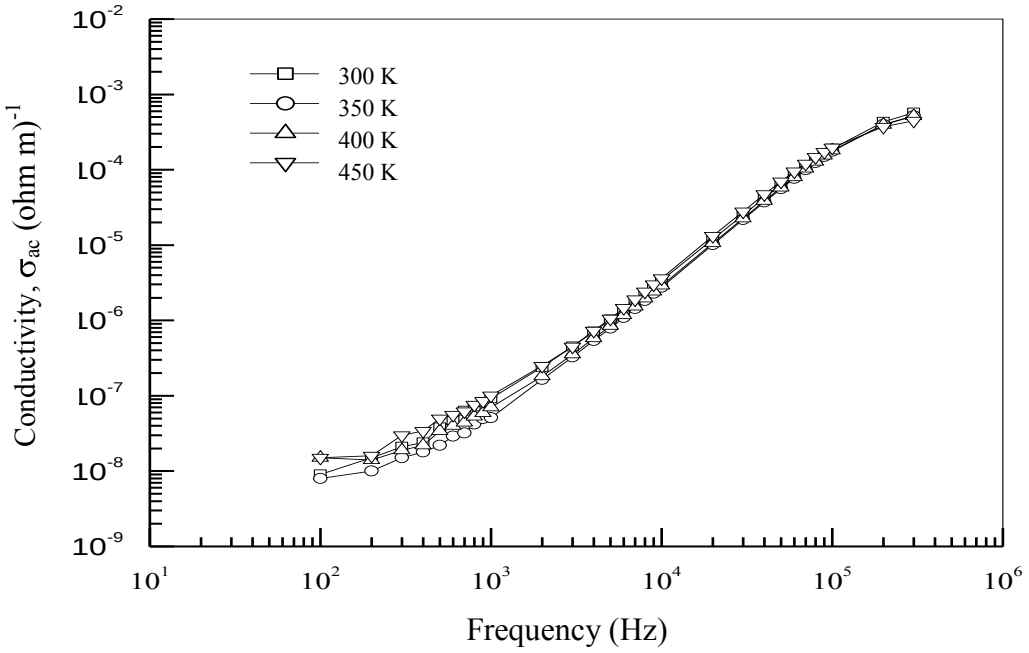

Fig 4.36 ac conductivity, σ_{ac}, as a function of frequency of the PPTMA films at different temperatures (d=450 nm)

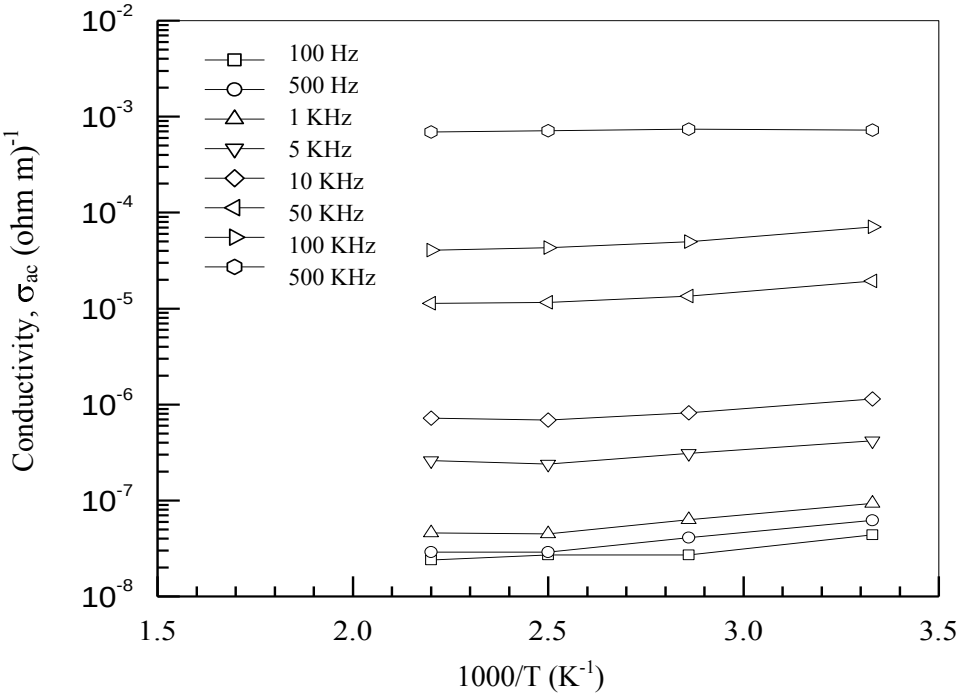

Fig 4.37 ac conductivity, σ_{ac}, as a function of inverse of absolute temperature of the PPTMA films at different frequencies (d= 300 nm)

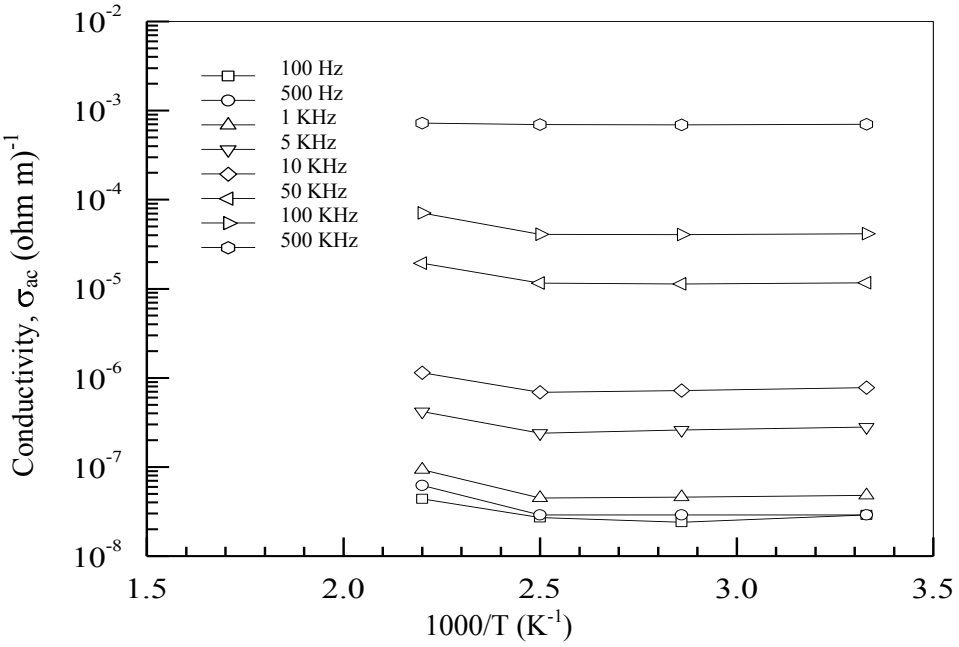

Fig 4.38 ac conductivity, σ_{ac}, as a function of inverse of absolute temperature of the PPTMA films at different frequencies (d= 400 nm)

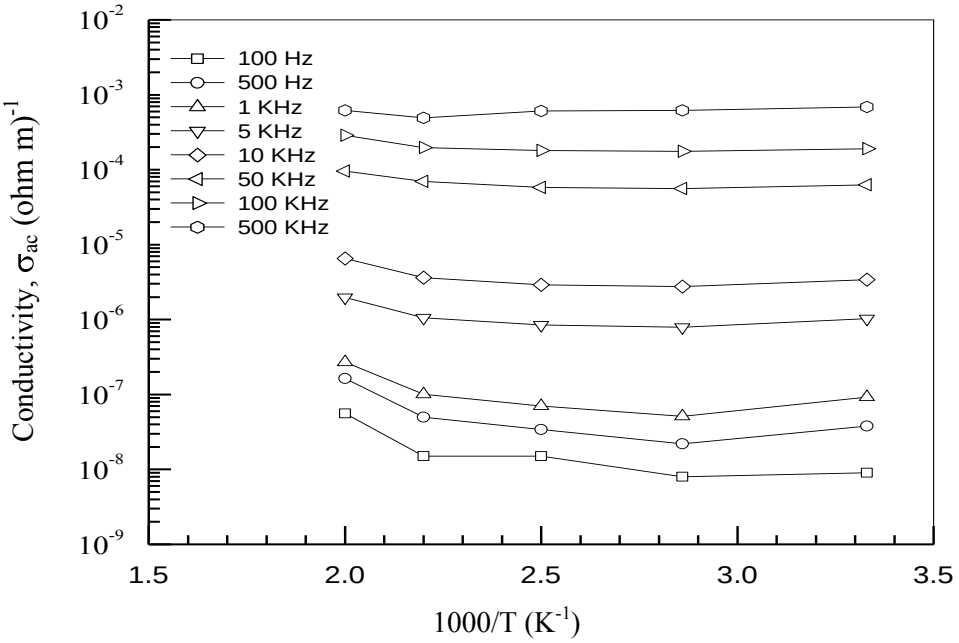

Fig 4.39 ac conductivity, σ_{ac}, as a function of inverse of absolute temperature of the PPTMA films at different frequencies (d= 450 nm)

To elucidate the temperature dependence of σ_{ac} behavior at different frequencies and different thicknesses (300 to 450 nm), the data of Fig. 4.34 to Fig 4.36 are plotted as σ_{ac} against inverse of absolute temperature in Figs. 4.37-4.39. It is seen that the σ_{ac} is weakly dependent on temperature below about 400 K and then gradually increases with temperature in the low frequencies. The temperature effect on the σ_{ac} of PPTMA thin films is weak in the higher frequencies. It is seen that the activation energy is about 0.05 eV in the low temperature at low frequencies and throughout the whole temperature range in the higher frequencies. This very low activation energy of the carriers in the low temperature and strong dependence of the σ_{ac} on frequency are indicative of a hopping conduction mechanism. The activation energy calculated for 100 Hz in the high temperature region is 0.23 eV for PPTMA thin films. These observations suggest that the conduction may be dominated by hopping of carrier between the localized states at low temperatures and movements of thermally excited carriers from energy levels within the band gap in the high temperature region. Saravanan et al. [56] studied rf plasma polymerized polyaniline thin films and activation energies were reported to be 0.356-0.1435 eV which indicated hopping conduction in these films. These values are close to the activation energies determined in the present investigation of ac electrical conduction in PPTMA.

4.11.2 Variation of Dielectric Constant with Frequency and Temperature

The variation of ε' with frequency at different temperatures is plotted in Figs. 4.40-4.42. The ε' decreases slowly with increasing frequency and ε' increases with increasing thickness. It is seen in Fig. 4.40 that the ε' decreases in the high frequencies. As the frequency increases, dipoles begin to lag behind the field, and as a result ε' decrease. It can be seen that in the whole frequency region there is a decrease in the ε' with an increase in frequency. This characteristic dependence of the ε' on frequency could be explained with space charge accumulation at the structural interface of the PPTMA thin films. The charges present in the PPTMA thin films can migrate under the influence of an electric field. It is possible that they get blocked at the electrode dielectric interface, which leads to space charge polarization. Such distortion causes an increase in ε' of PPTMA thin films at the low frequencies.

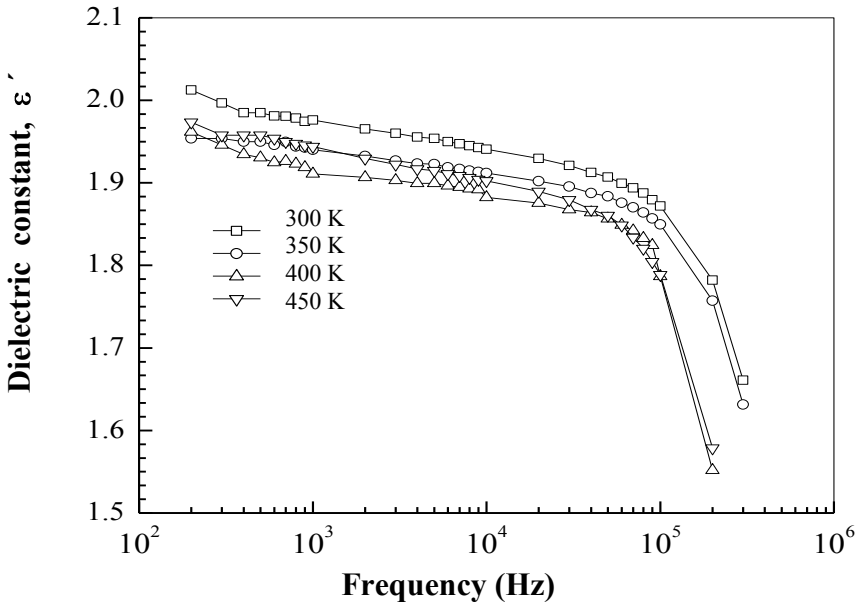

Fig. 4.40 Dielectric constant,ε', as a function of frequency of the PPTMA films at different temperatures (d=300 nm).

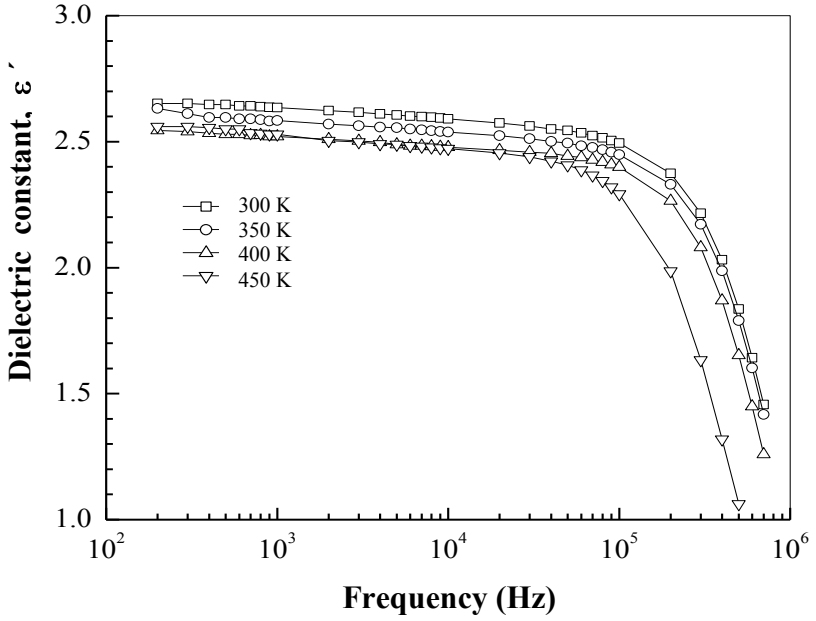

Fig 4.41 Dielectric constant,ε', as a function of frequency of the PPTMA films at different temperatures (d=400 nm).

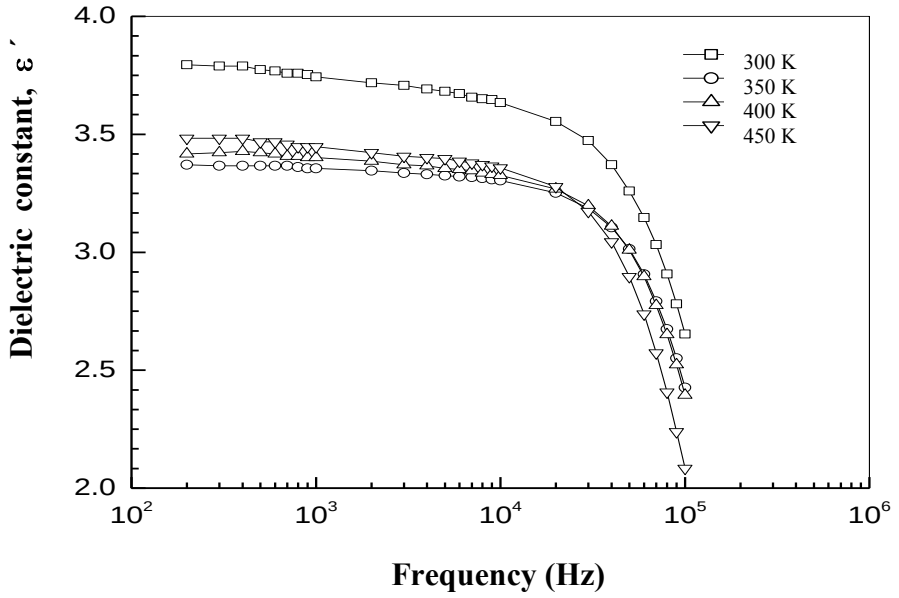

Fig 4.42 Dielectric constant,ε', as a function of frequency of the PPTMA films at different temperatures (d=450 nm).

The dielectric relaxation time refers to a gradual change in the polarization following an abrupt change in applied field. When frequency reaches the characteristic frequency (ω=$1/\tau$), the ε' drops means relaxation process. At very high frequency ($\omega \geq 1/\tau$) dipoles can no longer follow the field, $\varepsilon' \approx \varepsilon_{\infty}$. Relaxation may be occurred above 1 MHz ($1/\tau \geq 1MHz$). This is indicating of a fast polarization mechanism and the polarization process will be labelled the γ process. The γ process dominates the behavior of ε' from 100 Hz to 10^5 Hz. Figs.43-46 presents the ε' as a function of temperature of the PPTMA thin films. The general trend of ε' is to decreases with increasing temperature. In Fig.4.43 it is seen that the ε' decreases with temperature up to 350 K and above this temperature ε' tends to increase up to 10 kHz and above 10 kHz ε' decreases with temperature throughout. In case of thickness variation the ε' decreases up to 400 K and than increases but in higher thickness (450 nm) thin films the ε' decreases up to 350 K and above this temperature ε' increases. The variation of ε' with temperature is related to the charge carriers, which in most cases can not orient themselves with respect to the direction of applied field, therefore they posses a weak

contribution to the polarization and hence to the ε'. As the temperature increases, the space charge carriers get enough thermal excitation energy to be able to respond to the change in the conductivity. This conductivity change in turn decreases their contribution to the polarization leading to decrease of the ε' due to high dielectric loss.

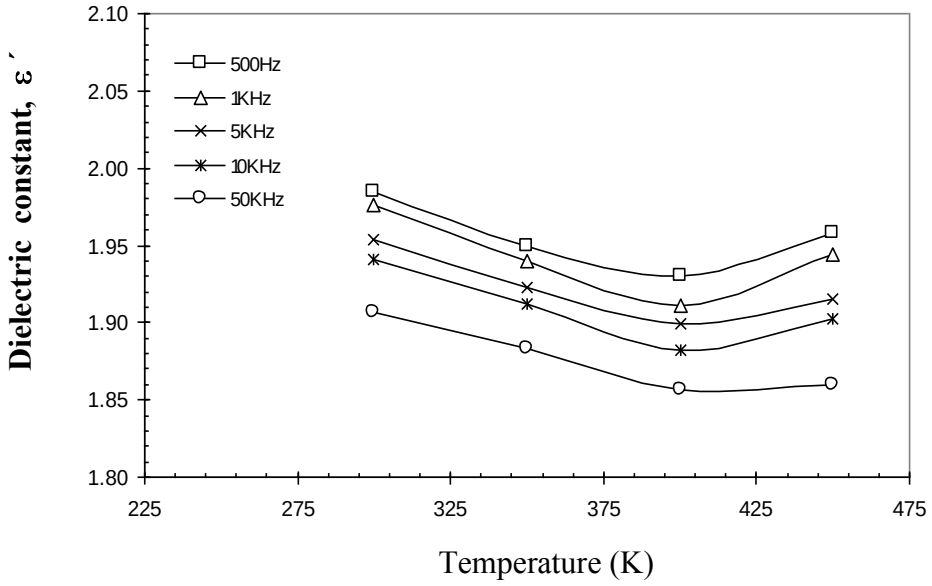

Fig 4.43 Dielectric constant,ε', as a function of temperature of the PPTMA films at different frequencies (d= 300 nm).

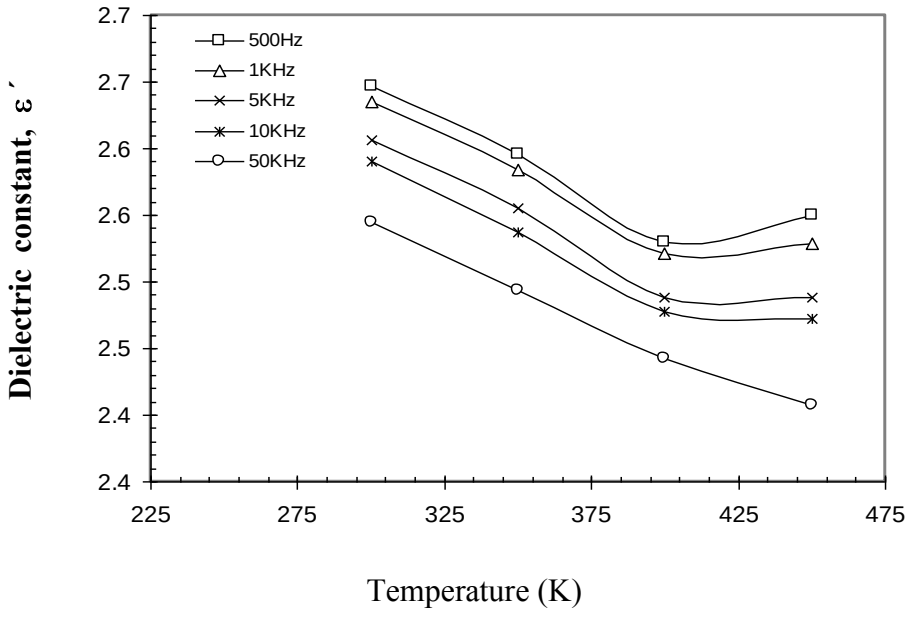

Fig 4.44 Dielectric constant,ε', as a function of temperature of the PPTMA films at different frequencies (d= 400 nm).

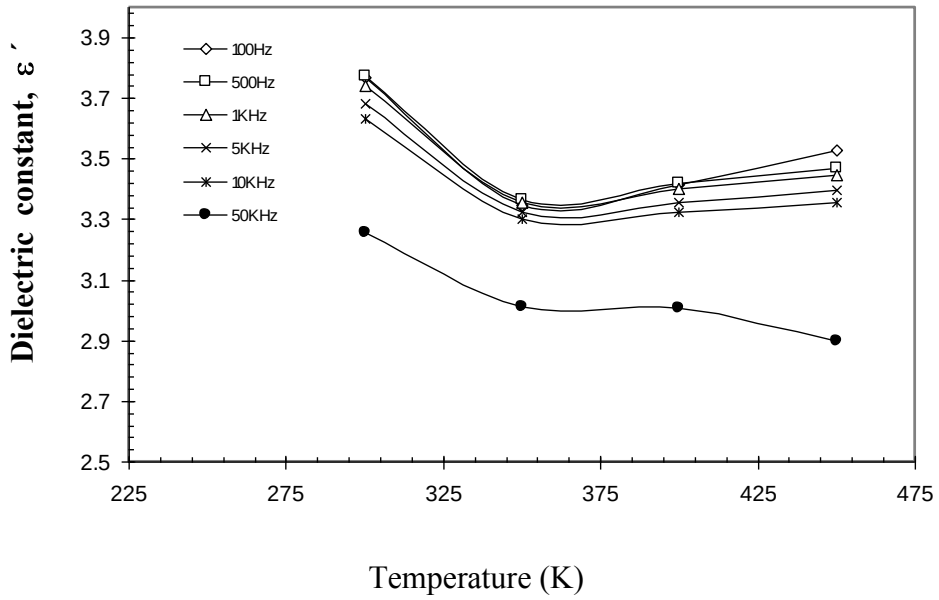

Fig 4.45 Dielectric constant,ε', as a function of temperature of the PPTMA films at different frequencies (d= 450 nm).

4.11.3 Variation of Dielectric Loss Tangent with Frequency and Temperature

A real capacitor can be represented with a capacitor and a resistor. The parameters such as angular frequency (ω) of the applied field, the parallel conductance G_p, parallel capacitance C_p are related to $tan\partial$ as

$$tan\partial = \frac{G_p}{2\pi f C_p} \qquad (4.6)$$

Where f is the linear frequency in Hz. The dependence of the $tan\partial$ on frequency at different temperatures (300 to 450 K) is shown in Fig.4.48 for a PPTMA thin film.

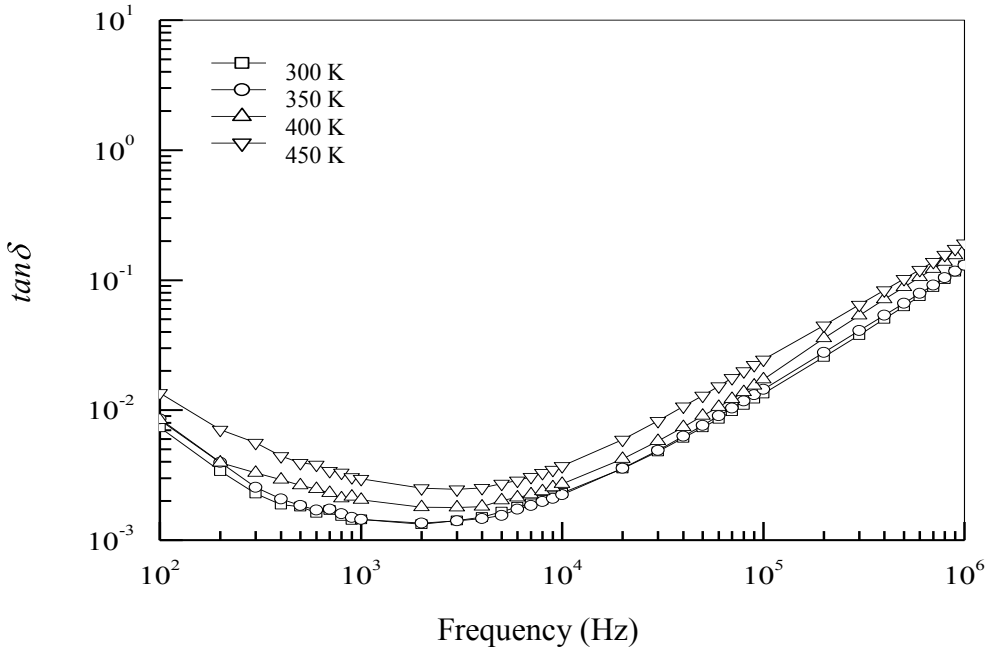

Fig.4.46 Dielectric loss tangent, as a function of frequency of the PPTMA at different temperature (thickness ; 300 nm).

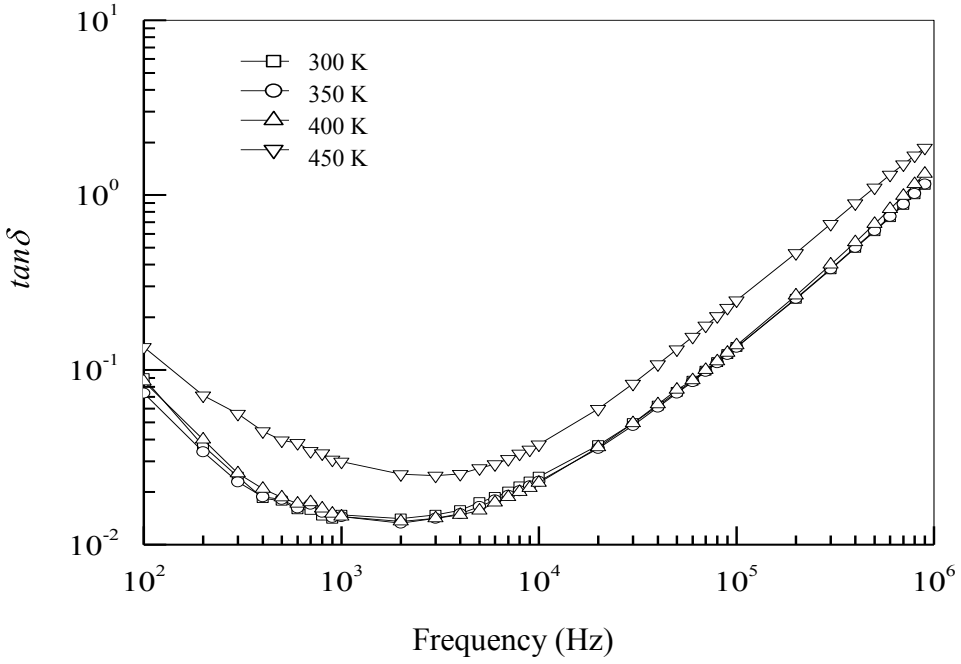

Fig 4.47 Dielectric loss tangent, as a function of frequency of the PPTMA at different temperature (thickness ; 400 nm).

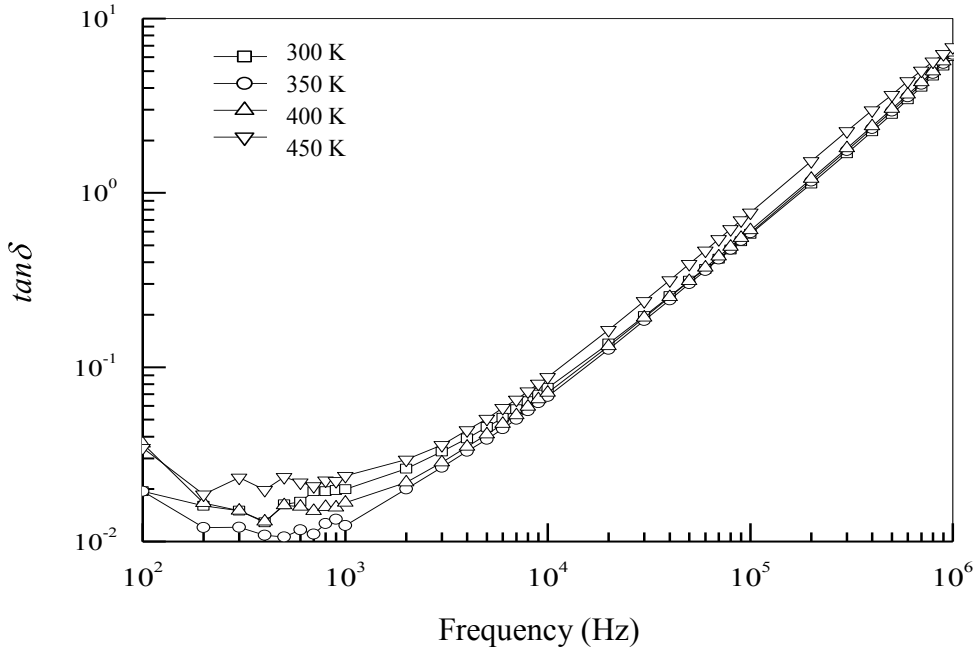

Fig 4.48 Dielectric loss tangent, as a function of frequency of the PPTMA films at different temperature (thickness ; 450 nm).

Eqn (4.6) shows that the loss has a peak at (ω=1/τ). The loss increase observed at high frequencies is the low-frequency tail of the loss peak associated with γ polarization. As temperature increases the γ loss peak shifts toward higher frequencies, so that the loss measured around 10^4-10^5 Hz decreases (low-frequency tail of the γ peak). The *tan∂* increases with frequency with a deep in the low frequency region. The relaxation peaks in the low frequency region are not clear and not progressively moving with increasing frequency. The relaxation peaks decreases in the higher frequencies with increasing thicknesses. These weak relaxation peaks may occur owing to the slow motion of molecular groups in the PPTMA thin film structure.

4.10.4 *Dependence of ε″on ε′ (Cole-Cole plot)*

The Cole-Cole curve is useful to understand the degree of the distribution of the relaxation times. Fig.4.49 shows the variation of real and imaginary parts of ε' for a PPTMA thin film as functions of temperature and frequency in the form of Cole-Cole plots. In general, a full,

or a partial or no arc is observed depending on relaxation strength in the sample with in experimentally available frequency range. When the angle between the two radii of the Cole-Cole curve is defined as $\beta\pi$, the factor β indicates the degree of distribution of the relaxation time.

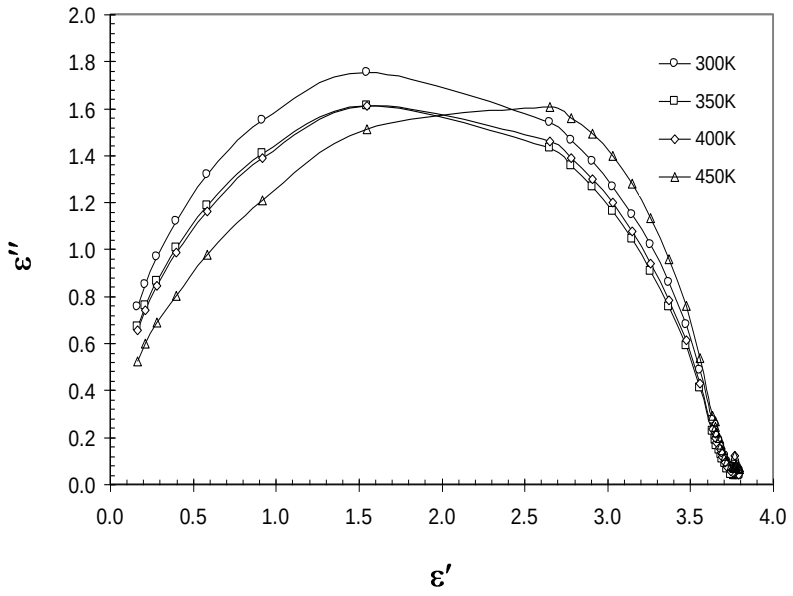

Fig 4.49 Cole-Cole plots of PPTMA films at different frequencies (thickness; 400 nm).

The values of β are found to be in the range 0.75 to 0.85 for PPTMA thin films. The values of β are thus found smaller than the value (unity) of the Debye model with a single relaxation, indicating the presence of distribution of relaxation times in this material. The full semicircles formed suggesting a distribution of relaxation times in the sample [101, 107]. It is evident from Cole Cole plots that there is a tendency of deformation of the semicircular shape with increase of temperature. This implies that the relaxation time distribution increase with temperature.

CHAPTER 5

Conclusions

5.1 Conclusions

Plasma polymerization technique was successfully used to prepare good and reproducible thin films of desired thickness from TMA. TMA is an aniline derivative with -N$(CH_3)_2$ group. Although studies on polyaniline have been reported, there are scanty of reports on experimental studies on aniline derivatives in thin film form. So TMA was chosen as a potential organic monomer for thin film preparation and study of its different properties. Here the main findings of the structural, thermal, optical and electrical properties of as deposited and iodine doped PPTMA produced from TMA are summarized.

The surfaces of the as deposited PPTMA thin films are observed to be smooth and pinhole free. A comparison between the SEM micrographs of the as deposited and heat treated films show that the surface morphology of the PPTMA heat treated at higher temperature becomes smoother. The surface is smoother with iodine, possibly indicating that closely connected blocks of polymer chains develop in the thin film. The energy dispersive x-ray observations indicate the presence of C, N, O and I in iodine doped PPTMA samples.

The empirical formula of the PPTMA film was determined to be $C_{7.70}H_{10.30}N_{0.80}O_{1.50}$ from the EA data. It is found that the N/C ratio is 0.12 for as deposited PPTMA, which is very close to N/C of TMA. Non-monomeric oxygen was incorporated into the PPTMA films due to the post-deposition reaction with radical species (danging bonds) trapped in the structure and from the glow discharge chamber during polymerization. The deficiency of carbon and hydrogen contents in PPTMA may be due to the breakdown of bonds owing to the complex reaction during plasma polymerization. The IR investigation shows that the as deposited PPTMA is structurally different from monomer and the PPTMA may contain an aromatic ring structure with NC and CH side groups. It is observed that definite structural modification occurs by further conjugation in the PPTMA structure on heat treatment. The IR spectra of iodine doped PPTMA indicate that the iodine atoms might form charge transfer complex to amine nitrogen site in PPTMA.

The XPS analyses of PPTMA thin films also show the presence of possible groups, C-H, C=C, C-N, C-O, C=O on PPTMA surface. The atomic ratio N/C of the PPTMA thin film bulk and surface are found to be 0.12 and 0.20 by EA and XPS respectively. It is suggested that on

the film surface some carbon-nitrogen bonds in PPTMA were replaced by carbon-oxygen bonds. From the above observations, it is seen that there is quantitative variation in the surface and bulk compositions in the PPTMA thin films. On the surface of this film an increase of nitrogen content is observed with a drop of carbon concentration. The peak height of PPTMA heat treated at 473 and 573 K may be due to the probable development of conjugation in the structure on heat treatment. The modifications on heat treatment of PPTMA are also observed in the IR and UV-Visible spectroscopic analyses. The maximum change in the PPTMA structure has been occurred in the temperature region 373-873 K, where the DTA curve exhibits the exothermic peak. In the TGA, the weight loss might occur by thermal breakdown of the PPTMA structure and expulsion of higher molecular mass hydrocarbons, oxygen containing compounds, etc. above 505 K. The weight loss in heat treated PPTMA is much higher than that of its components at relatively higher temperature.

The UV-Vis absorption spectra for TMA, as deposited and PPTMA thin films heat treated at 473, 573 and 623 K have been recorded at room temperature. It is seen that there is a red shift of about 79 nm in λ_{max} as compared to TMA peak. It can be noticed that a small peak appears at around 420 – 440 nm, in the spectra of PPTMA of different thicknesses heat treated at 573 and 623 K. This peak is shifted to higher wavelength with increasing film thickness. The E_{qd} and E_{qi} are found to be 2.80 and 1.56 eV, respectively for as deposited PPTMA. While E_{qd} increases a little, E_{qi} decreases, on heat treatment of PPTMA. It is concluded that PPTMA thin film with conjugation can be produced by plasma polymerization and the structural order can be improved by heat treatment. The direct band gap of iodine doped PPTMA thin films is 2.6 eV. The changes of energy gap indicate that there is a charge transfer complex formation between the host PPTMA thin films and the iodine.

The J-V characteristics of PPTMA thin films with Al contacts show ohmic behavior at the lower applied voltage region and SCLC dominated by exponential trap distribution at the higher voltage region. The μ value of the charge carriers is found to be about 1.3×10^{-13} m^2 $V^{-1}s^{-1}$. The values of n_o and N_t are calculated to be about 2.0×10^{21} m^{-3} and 4.0×10^{30} m^{-3}, respectively at room temperature for PPTMA thin films. The J-V curves of iodine doping also follow power law and is seen that in the non-ohmic region the slope is much higher than that corresponding to other conduction mechanism. The carrier mobility, the free carrier density,

and the total trap density of iodine doped PPTMA are about 1.5×10^{-12} m^2 $V^{-1}s^{-1}$, 3.7×10^{22} m^{-3} and 1.2×10^{27} m^{-3}, respectively. The activation energy indicate that there is a transition in the conduction process from a hopping process to a distinct energy level process from lower to higher temperature regions. The electrical conductivity shows a higher value, (7.8×10^{-14} ohm-m^{-1}) of iodine doped PPTMA thin film compared to that of the as deposited PPTMA thin film (3.1×10^{-13} ohm-m^{-1}).

The ac electrical conductivity is more dependent on temperature in the low frequency region than that in the high frequency region. It is found that the ac conduction may be dominated by hopping of carriers between the localized states at low temperature and thermally excited in the high temperature region. Dielectric constant increases with increasing film thickness and decreases with increasing frequency of the PPTMA films which may be due to the complex nature of the deposition process of thin films in glow discharge. The characteristic dependence of the ε' on frequency could be explained by space charge accumulation at the structural interface of the PPTMA thin films. The dielectric loss decreases up to a certain frequency and then increasing with frequency with a minimum in the low frequency region, the frequency minima shifts to lower frequency with film thickness. The temperature dependence of the Cole-Cole diagram reveals the existence of several types of dielectric relaxation distribution with respect to temperature and frequency.

The PPTMA has been modified by heat treatment and iodine doping. These modifications affect the structure of PPTMA and thereby there is optical and electrical properties change. The band gap decreases and the electrical conductivity increases to some extent. The conduction mechanism and relaxation processes are also evaluated. These results may help in searching for some application of this material.

5.2 Suggestions for Future work

The present work shows the investigation of the structural, optical and electrical behavior of PPTMA thin films. But more investigations on PPTMA thin films are required to know different characteristics, which will help finding suitable applications of these materials. The following investigations on PPTMA thin films may be carried out for further study. In this thesis iodine modification occurred by chamber method but it can be done in situ iodine

doping. Because in situ method of doping is more reliable and the change effected in the bandgap is permanent. For in situ iodine doping, an additional iodine container is incorporated in the plasma deposition chamber. Both monomer and dopant iodine are injected simultaneously into the plasma zone, so that the polymer films deposited on the substrates have iodine incorporated in the structure.

The conductivity of the PPTMA thin films increases after reaction with iodine can be used for the sensing of halogens in general and of iodine in particular. In general, the chemistry of the halogen interaction with PANI, although complex, could be used in the sensing of these elements, even though additional research would be needed to develop a sensor suitable for practical application.

The interesting properties of multi layer composite thin films played a vital role in determining the physical characteristics of the composite thin films. The probable inhomogeneities, irregularties and disorderness of the interface may be affected the optical band gaps as well as the electrical conductivity of the composite thin films.

References

1. Lindford R.G., “In applications of electroactive polymers’; Scrosati, B, Ed.; chapman and Hall: London (1993).
2. Reynods J.R., Baker C. K., Jolly C.A., Poropatic P.A., Ruiz J. P., “In conductive polymers and plastics”, Margolis J.M., Ed.; Chapmann and Hall: New York (1989).
3 Yasuda H., “Plasma Polymerization” Academic Press, New York, 1985.
4 Frank F. Shi, “Developments in plasma-polymerized organic thin films with novel mechanical, electrical, and optical properties”, J.M.S.-Rev. Macromol. Chem. Phys. 36(4) (1996) 795.
5 Agostino R. d’, Ed.; “Plasma deposition, treatment, and etching of polymers”, Academic Press: Boston, 1990.
6 Chowdhury F-U-Z and Bhuiyan A. H., “An investigation of the optical properties of plasma-polymerized Diphenyl thin films”, Thin Solid Films, 306 (2000) 69.
7 Bell A. T. and Shen M. (Eds.), “Plasma Polymerization”, Am. Chem. Soc., Washington, D.C. (1979).
8 Inagaki N., “Plasma surface modification and plasma polymerization”, Wiley, New York, 1996.
9 Fried J.R., “Polymer Science and Technology” Printic, Hall of India PV. LTD. New Delhi, 2002.
10 Bogaerts A., Neyts E., “Gas discharge plasma and their applications”, Spectrochimica Acta Part B 57(2002) 609.
11 Suhr H. and Bell A.T., “In Techniques and applications of plasma chemistry; Hollahan”, Ed.; John Wiley & Sons: New York, 1974.
12 Fang J., Chen H., Yu X., “Studies on plasma polymerization of Hexamethyldisiloxane in the presence of different carrier gases”, J. Appl. Polym. Sci, 88 (2001) 1434.
13 Biederman H. and Slavinska D., “Plasma polymer films and their future prospects” Surface and Coatings Technol., 125(1-3) (2000) 371.

14 Moser E.M., Faller Ch., Pietrzko S., Eggimann F., "Modeling the functional performance of plasma polymerized thin films", Thin Solid Films, 355-356 (1999) 49.

15 Mhin B.J. and Park B.H., "Relationship between charge transfer and the structural deformation in para-substituted aniline derivatives", Chem. Phys. Letters, 325 (2000) 61.

16 John R.K., Kumar D.S., "Structural, Electrical, and Optical Studies of Plasma polymerized and Iodine-Doped Poly Pyrrole" J. Appl. Polym Sci, 83 (2002) 1858.

17 Bhadra S., Khastgir D., Singha N.K., Lee J.H., "Progress in preparation, processing and applications of polyaniline", Progress in Polym. Sci., 34 (2009) 783.

18 Sajeev U.S., Joseph Mathai C., Saravanan S., Ashokan Rajeev R., Venkatachalam S., Anantharaman M.R., On the optical and electrical properties of rf and ac plasma polymerized aniline films", Bull. Mater. Sci., 29 (2006) 159.

19 Elashmawi I.S., Abdelrazek E.M., Ragab H.M., and Hakeem N.A., "Structural and optical behaviour of PVDF films with different concentrations of iodine", Physica B, 405(2010) 94.

20 Chowdhury F.-U.-Z and Bhuiyan A.H., "An investigation of the optical properties of plasma-polymerized Diphenyl thin films", Thin Solid Films, 306(1-2) (2000) 69.

21 Nakamura K., Watanabe M., Zhou M., Fujishima M., Tsuchiya M., Handa T., Ishii S., Noguchi H., Kashiwagi K. and Yoshida Y., "Plasma polymerization of cobalt tetraphenylporphyrin and the functionalities of the thin films produced" Thin Solid Films 345 (1999) 99.

22 Bazaka K., Jacob M.V., "Synthesis of radio frequency plasma polymerized non-synthetic Terpinen-4-ol thin films" Mater. Lett., 63 (2009) 1594.

23 Bae I.-S., Jung C. –K., Cho S. J., Song Y.-H., Boo J.-H., "A comparative study of plasma polymerized organic thin films on their electrical and optical properties", J. Alloys and Compounds, 449 (2008) 393.

24 Bhuiyan A.H., Bhoraskar S.V., Badrinarayanan S., "X ray photoelectron spectroscopic studies on pyrolysis of thin films of plasma-polymerized acrylonitrile" Thin Solid Films 240 (1994) 66.

25 Mitu B., Bauer-Gogonea S., Leonhartsberger H., Lindner M., Baver S. and Dinescu G., "Plasma-deposited parylene-like thin films: process and material properties", Surf. Coat. Technol. 174-175 (2003) 124.

26 Hu Xiao, Zhao Xiongyan, Uddin A., Lee C.B., "Preparation characterization and electronic and optical properties of plasma polymerized nitriles", Thin Solid Films, 477 (2005), 81.

27 Tamirisa Prabhakar A., Liddell KNona C., Pedrow Patric D., Osman. Mohammed A., "Pulsed-plasma-polymerized aniline thin films", J. Appl.Polym. Sci., 93, (2004)1317.

28 Zhao X. Y., Wang M. Z., Zhang B.Z., Mao L., "Synthesis, Characterization and nonlinear optical properties of plasma-prepared poly (4-biphenylcarbonotrile) thin films", Polym. Int., 56 (2007) 630.

29 Hosono K., Mastubaia I., Murayama N., Shin W. and Noriya I.; "Effects of discharge power on the structure and electrical properties of plasma polymerized polypyrrole films", Mater, Lett. 58, (2004)1374.

30 Silverstein M. S. and Visoly-Fisher I.,"Plasma polymerized thiophene: molecular structure and electrical properties" , Polymer 43 (2002)11.

31 Valaski R., Ayoub S., L. Micaroni, I.A. Hummelgen, " Influence of thin thickness on charge transport of electrode deposited polypyrrole thin films", Thin Solid Films, 415 (2002) 206.

32 Luo H.L., Sheng J.Wan Y.Z., "Plasma polymerization of styrene with carbon dioxide under glow discharge conditions", Appl. Surf. Sci., 253, (2007) 5203.

33 Zaman M., Bhuiyan A. H., " Study of Direct Current electrical conduction mechanism in plasma polymerized thin films of tetraethaylorthosilicate", Thin Solid Films 517, (2009) 5431.

34 Joseph John, Sajeev Sivraman, Jayalekhmy, S., Anantharaman, M. R., "Investigations on the mechanism of carrier transport in plasma polymerized pyrrole thin films", J. of Phys. and Chem. of Solids, 71, (2010) 935.

35 Sajeev U. S., Joseph Mathai C., Saravanan S., Ashokan Rajeev R., Venkatachalam S., Anantharaman M.R., "On the optical and electrical properties of rf and a.c. plasma polymerized aniline films", Bull. Mater. Sci. 29, (2006)159.

36 Kumar D.S., Nakamura K., Nishiyama S, Ishil S., Noguchi H., Kashiwagi K., Yoshida Y, "Optical and electrical characterization of plasma polymerized pyrrole films", J. Appl. Phys., 93(5) (2003) 2705.

37 Hegemann D. and Schutz U., "Activation energy of an asymmetrical radio frequency discharge with methane" Thin Solid Films, 491 (2005) 96.

38 Mathai C.J., Saravanan S., Jayalekshmi S., Venkitachalam S., Anantharaman M.R., "Conduction mechanism in plasma polymerized aniline thin films", Materials Letters 57 (2003) 2253.

39 Bae I.S., Cho S.H., Lee S.B., Kim Y. and Boo J.H., "Growth of plasma-polymerized thin films by PEVCD method and study on their surface and optical characteristics", Surf. Coat. Technol. 193 (2005) 142.

40 Shah Jalal A.B.M, Ahmed S., Bhuiyan A.H. and Ibrahim M., "On the conduction mechanism in plasma polymerized m-xylene thin films", Thin Solid Films, 295 (1997) 125.

41 Riad A.S., El-Shabasy M. and Abdel-Latif R.M., "D.C. electrical measurements and temperature dependence of the Schottky-barrier capacitance on thin films of β–MgPc dispersed in polycarbonate." Thin Solid Films, 235 (1993) 222.

42 Silva S.R.P., Amaratunga G.A.J., "Use of space-charge-limited current to evaluate the electronic density of states in diamond-like carbon thin films", Thin Solid Films, 253 (1994) 146.

43 Pradhan Dilip K., Choudhary R.N.P., Samantaray B.K., "Studies of dielectric relaxation and ac conductivity behavior of plasticized polymer nanocomposite electrolytes", Int. J. Electrochem. Sci. 3 (2008) 507.

44 Gong X., Dai L., Mau A.W.H., and Griesser H. J., " Plasma-polymerized polyaniline films: Synthesis and Characterization", J. Polym. Sci.: PartA: Polym. Chem., 36 (1998) 633.

45 Ma. G. Olayo, Guillermo J. Cruz, Salvador L., Morales J., and Olayo R., "Conductivity and activation energy in polymers synthesized by plasma of thiophene", J. Mex. Chem. Soc. 54 (2010) 18.

46 Sanchez V.M.E., Ortiz R.A., Alvarez J.R., Rivera M., "Molecular materials derived from MPc (M=Fe, Pb, Co) and 1,8-dihydroxiantraquinone thin film:

formation, electrical and optical properties", J. Phys. And Chem. Solids 69 (2008) 1.

47 Pandey S.S., Annapoorni S., Malhotra B.D., "Synthesis and Characterization of Poly(aniline-co-o-anisidine): A processable Conducting Copolymer", Macromolecules 26 (1993) 3190.

48 Ram M.K., Annapoorni S., Pandey S.S., Malthotra B.D., "Dielectric relaxation in thin conducting polyaniline films", Polym. 39(15) (1998) 3399.

49 Yamada K., Haraguchi T. and Kajiyama T., Polym."Surface modification of polyaniline film by plasma-graft polymerization and its effect on the redox reaction", J.polymer, 30(2) (1998) 133.

50 Valaski, R., Ayoub, S., Micaroni, L., Hummelgen, I. A., "Influence of electrode material on charge transport properties of polypyrrole thin films", Thin Sodid Films 388 (2001) 171.

51 K. Yamada, T. Haraguchi and T. Kajiyama, Polym."Surface modification of polyaniline film by plasma-graft polymerization and its effect on the redox reaction", J.polymer, 30(2) (1998) 133.

52 Saleh A. M., Abu-Hilal A. O. and Gould R. D., "DC conduction processes and electrical parameters of the organic semiconducting zinc phthalocyanine, ZnPc, thin films", Curr. Appl. Phys. 3 (2003) 345.

53 Bhuiyan A.H. and Bhoraskar S.V, "Electircal, optical and ESR study of thin films of plasma polymerized acrylonitrile", J. of Mater. Sci. 24 (1989) 3091-3095.

54 Jousseaume V., Morsli M., and Bonnet A., "Aging of electrical conductivity in conducting polymer films based on polyaniline", J. Appl. Phys., 88(2) (2000) 960.

55 Han M.G. and Im S.S., "Dielectric spectroscopy of conductive polyaniline salt films", J. Appl. Plyom. Sci., 82 (2001) 2760.

56 EI-Nahass M. M., Zeyada H. M., EI-Samanoudy M. M., EI-Menyawy E.M., "Electrical conduction mechanisms and dielectric properties of thermally evaporated N-(p-dimethylaminobenzyllidene)-p-nitroaniline thin films", J. Phys. Condens Mat., 18 (2006) 5163.

57 Saravanan, S., Joseph Mathai, C., Venkatachalam, S., and Anantharaman, M. R., "Low k thin films based on RF plasma-polymerized aniline", New J. Phys. 6 (2004) 64.

58 Huang, Q.F., Annapoorni S., Panday S.S., and Malhotra, B.D., "Dielectric relaxation in thin conduction polyaniline films", Polymer, 82(1998)3399.

59 Zhao X.Y., Wang M.Z., Wang Z., "Deposition of plasma polymerized 1-Cynoisoquinoline thin films and their dielectric properties", Plasma Process Polym., 4 (2007) 840.

60 Tai H. Jer, "Dielectric spectroscopy of poly(butylenes succinate) films", Polymer 48 (2007) 4558.

61 Sethi R.S., Goosey M.T., "In special polymers for electronics and optoelectronics" J.A. Chilton and M.T., Ed: Chapman and Hall: London (1995).

62 Cowie J.M.G., "Polymers: chemistry & physics of modern materials", Glasgow (1991).

63 Biederman H., Osada Y., "Plasma Chemistry of Polymers", Advance in Polymer Sci., Berlin (1990).

64 Lieberman M.A., Lichtenberg A.J., "Principles of plasma discharges and materials processing", Wiley, New York (1994).

65 Bogaerts A., Wilken L., Hoffmann V., Gijbels R., Wetzig K., " Comparison of modeling calculations with experimental results for rf glow discharge optical emission spectroscopy", Spectrochimi. Acta Part B, 57(2002) 109.

66 Levitskii S.M., "An investigation of the sparking potential of a HF dischage in a gas in the transition range of frequencies and pressure", Sov. Phys.-Tech. Phys. **2** (1957) 887.

67 Stark R.H., Schoenbach K.H., "Direct current high pressure glow discharges", J. Appl. Phys. 85 (1999) 2075.

68 Biederman H. and Slavinska D., "Plasma polymer films and their Future prospects" Surface and Coatings Technology, 125(1-3) (2000) 371-376.

69 Grill A., "Cold plasma in materials fabrication: from fundamentals to applications", IEEE press, New York (1994).

70 Vurzel F.B., Acad.Sci., Moscow, USSR, "Plasma chemistry, technology, application", Inst. Plasma Chem. And Technol., Carlsbad, CA (1983).

71 Bogaerts A., E Neyts “Gas discharge plasma and their applications”, spectrochimica Acta Part ,B 57(2002) 609.

72 Segui Y. and Bui Ai, “Microelectronic applications of plasma-polymerized films”, Thin Solid Films, 50 (1978) 321.

73 Bell A.T. and Hollahan R., “Techniques and applications of plasma chemistry”, Ed.; John Wiley & Sons: New York (1974).

74 Hammer T., “Applications of plasma technology in environmental techniques, contrib.”, Plasma phys. 3(1999) 441.

75 Danilatos G.D., “Foundation of environmental scanning electron microscopy”, Advances in Electronics and Electron Phys. 71 (1988) 109.

76 Goldstein G.I., Newbury D.E., Echlin P., Joy D.C., Fiori C., Lifshin E., “Scanning electron microcopy and X-ray microanalysis”, Plenum Press NY (1981).

77 Silverstein R.M., Bassler G.C., Morrill T.C., “Spectrometric identification of organic compounds”, John Willey & Sons, New York (1981).

78 Hatakeyama T. and Quinn F.X., “Fundamentals and applications to polymer science”, John Wiley & Sons Ltd, London (1997).

79 Moulder J.F., Stickle W.F., Sobol P.E., and Bomben K.D., “Handbook of X-ray Photoelectron Spectroscopy” Perkin-Elmer Corp., Eden Prairie, MN, USA (1992).

80 Grant J.T. and Briggs D., “Surface Analysis by Auger and X-ray Photoelectron Spectroscopy”, IM Publications, Chichester, UK (2003).

81 Wagner C.D., Riggs W.M., Davis L.E., Moulder J.F., and Mullenberg G.E., “Handbook of X-ray Photoelectron Spectroscopy”, Perkin-Elmer Corp., Eden Prairie, MN, USA (1979).

82 Seah M.P., and Briggs D., “Practical Surface Analysis by Auger and X-ray Photoelectron Spectroscopy”, 2nd edition, ed. Wiley & Sons, Chichester, UK (1992).

83 Katsikas L., Jeremic K., Jovanovic S., Velickovic J. S. and Popovic I.G., “The thermal degradation kinetics of dextran and pullulan”, J. Therm. Anal., 40 (1993) 511.

84 Erogla M. S., Akilli M.M. and Guven O., "Spectroscpic, Thermal and mechanical characterization of carboxyl terminated polybutadieno- based carbon black filled networks", J. Appl. Polym. Sci., 66(2) (1997) 355.

85 Gong X., Dai L., Mau A.W.H., and Griesser H. J., "Plasma-polymerized polyaniline films: Synthesis and Characterization", J. Polym. Sci.: PartA: Polym. Chem., 36 (1998) 633.

86 Lambert J. H., David A. Lightner, Shurvell H. F., and Graham Cooks R., "Introduction to organic spectroscopy", Macmillan Publishing Co., New York (1987).

87 Tauc J., "Optical properties of Solids", Abeles, F., Ed., North-Holland, Amsterdam, 1972.

88 Tauc J., Amorphous and liquid Semiconductor, Plenum, London, (1974).

89 Gould R.D. and Shafai T.S., "Condction in lead phthalocyanine films with aluminim electrodes", Thin Solid Films, 373(1-2) (2000) 89.

90 Gould R.D. and Lopez M.G., "Poole-Frenkel condctivity prior to electroforming in evaporated Au-SiO_x-Aubsandwich structures", Thin Solid Films, 342(1999) 94.

91 Amar N., Gould R.D. and Saleh A.M., "Space-charge-limited conductivity in evaporated α-form metal-free ohthalocyanine thin films", Vacuum, 50(1-2) (1998) 53.

92 Xiao H., Xiongyan Z., Uddin A., Lee C.B., "Preparation, characterization and electronic and optical properties of plasma polymerized nitrites", Thin Solid Films, 477 (2005) 51.

93 Von Hippel A. R., "Dielectric materials and applications", Technology Press of MIT and John Wiley, NY (1954).

94 Ramo S., Whinnery J.R., and Van Duzer T., "Fields and waves in communication electronics", John Wiley, NY (1994).

95 Davis E.A. and Mott N.F., "Electronic processes in non-crystalline materials", Clarendon Press, Oxford (1971)

96 Sayed W.M., Salem T.A.,"Preparation of polyaniline and studying its electrical conductivity", J. Appl. Polym. Science, **77** (2000) 1658.

97 Han M.G. and Im S.S., "Dielectric spectroscopy of conductive polyaniline salt films", J. Appl. Plyom. Sci., 82 (2001) 2760.

98 Blythe A.R., "Electrical properties of polymers", Cambridge University Press, Cambridge (1979) 69.

99 Lamb D.R., "Electrical conduction mechanisms in thin insulating films", Methuen and Co. Ltd., London (1967).

100 Chowdhury F.-U.-Z. and Bhuiyan A.H.., "Dielectric properties of plasma polymerized diphenyl thin films", Thin Solid Films, 370 (2000) 69.

101 Tai Horng-Jer, "Interfacial polarization phenomenon in the recrystallization of poly(butylenes succinate)", Polymer, 49 (2008) 2328.

102 Yasuda H., "Glow discharge polymerization in thin film processes", Academic, New York (1978).

103 Tolansky S., "Multiple Beam Interferometry of surfaces and films", Clarendon Press, Oxford (1948).

104 Sharma Y. R.,"Elementary Organic Spectroscopy: Principles and Chemical Applications", New Delhi: S Chand and Company, 1998.

105 Scofield J.H., J. Electr. Spectr. Relat. Phen. 8(1976) 129.

106 Gould R.D.,"The interpretation of space-charge-limited currents in semiconductors and insulators" J. Appl. Phys. 53 (1982) 3353.

107 Tai Horng-Jer, "Dielectric Spectroscopy of poly (butylene succinate)films", Polymer, 48 (2007) 4558.

APPENDIX I:

Publications and Presentations Based on this Work

Journals:

1. Akther H. and Bhuiyan A. H., "Infrared and ultraviolet-visible spectroscopic investigation of plasma polymerized N, N, 3, 5 tetramethylaniline thin films", Thin solid films 474 (2005) 14-18.
2. Akther H., Bhuiyan A. H., "Space charge limited conduction in plasma polymerized N, N, 3, 5, tetramethylaniline thin films", Thin Solid Films 488 (2005) 93-97.
3. Akther H and Bhuiyan A H, "Electrical and Optical properties of plasma-polymerized N, N, 3, 5 tetramethylaniline thin films", New J. Phys. 7 (2005) 173.
4. Akther H and Bhuiyan A H, "Dielectric properties of plasma-polymerized N, N, 3, 5 tetramethylaniline thin films", Surf. Review Lett., 18(1) (2011).
5. Akther H, Bhuiyan A H, Syed J. A. , Sumi R., and Yagi S., "Chemical Analysis of Plasma Polymerized N,N,3,5 tetramethylaniline by X-ray Photoelectron Spectroscopy and Elemental Analysis", Vacuum, Revised to be submitted, April 2011.
6. Akther H and Bhuiyan A H, "Physical properties of plasma-polymerized N, N, 3, 5 tetramethylaniline thin films doped with iodine", Thin Solid Films, Submitted, March 2011.

Presentations

1. Akther H and Bhuiyan A H, "AC electrical properties of plasma polymerized N, N, 3, 5 tetramethylaniline thin films", Regional physical conference, Bangladesh, Feb 11-13, 2006.
2. Akther H, Jamal. A. Syed and Bhuiyan A H, "X-ray Photoelectron analysis of plasma polymerized N, N, 3, 5 tetramethylaniline thin films", National conference cum workshop on material science and Technology, , Dec 02-04, 2007.
3. Akther H, and Bhuiyan A H, "Some Fundamental properties of plasma polymerized N, N, 3, 5 tetramethylaniline thin films", Bose Conference on Contemporary Physics-08, March 19-21, 2008.
4. Akther H, and Bhuiyan A H, "Effect of iodine doping on the thin films of plasma polymerized N, N, 3, 5 tetramethylaniline", National conference, Feb 10-11, 2011.